

# Chapter 4

## Multi-scale modelling of dry granular flows

### 4.1 Introduction

In nature, instabilities of slopes or cliffs are dramatic events involving sudden release of a large mass of soil. The prediction of these catastrophic events represents several challenges, one difficulty being our incomplete understanding of the granular flow dynamics (Rondon et al., 2011). Understanding the mechanics is of particular importance for risk assessment. Small scale laboratory experiments are usually unable to properly capture the dynamics of geophysical events. However, they can be useful to precisely study the physical mechanisms, which may play a crucial role in real flows (Iverson, 1997).

Conventionally, granular materials such as soils are modelled as a continuum. On a macroscopic scale, granular materials exhibit many collective phenomena and the use of continuum mechanics to describe the macroscopic behaviour can be justified. However on a grain scale, the granular materials exhibit complex solid-like and/or fluid-like behaviour depending on how the grains interact with each other. Numerical studies at grain scale allow a precise understanding of the internal flow structure. However, even in simplified geometries such as those investigated in the laboratory-scale experiments, DEM suffers from a serious short-coming in the number of grains that can be simulated in a reasonable time. This is a critical issue when more complex geometries or long-time granular processes are considered, or when particle size distributions are broad. For this reason, most numerical studies are performed in 2D or simple particles shapes and size distributions are considered.

Classical modelling strategies based on the finite element method (FEM) cannot be used for the simulation of very large deformations due to mesh distortion. In various application of FEM,

1 this problem is treated by means of technical tools such as re-meshing. These methods are,  
2 however, not robust and lead to round-off errors and mesh sensitivity. Recent works on granular  
3 materials also suggest that a continuum law may be incapable of revealing in-homogeneities  
4 at the grain-scale level, such as orientation of force chains, collapse of local void and grain  
5 rearrangements, which are purely due to micro-structural effects (Rycroft et al., 2009). Discrete  
6 element approaches are capable of simulating the granular material as a discontinuous system  
7 allowing one to probe into local variables such as position, velocities, contact forces, etc. The  
8 fundamental question is how to model granular materials which exhibit complex phenomenon.  
9 It is important to understand the mechanics of granular flows and the ability and limitations of  
10 continuum methods in capturing the flow dynamics.

## 11 4.2 Granular column collapse

12 The collapse of a granular column, which mimics the collapse of a cliff, has been extensively  
13 studied in the case of dry granular material (Hogg, 2007; Kerswell, 2005; Lajeunesse et al.,  
14 2004; Lo et al., 2009; Lube et al., 2005; Staron and Hinch, 2007; Zenit, 2005). The granular  
15 column collapse experiment involves filling a rectangular channel of height  $H_0$  and width  $L_0$   
16 with a granular material of mass ‘m’ (see figure 4.1). The granular column is then released  
17 *en masse* by quickly removing the gate, thus allowing the granular material to collapse onto  
18 the horizontal surface, forming a deposit having a final height  $H_f$  and length  $L_f$ . Despite  
19 the complexity of the intermediate flow dynamics, experimental investigations have shown  
20 that the flow evolution, the spreading velocity, the final extent of the deposit, and the energy  
21 dissipation can be scaled in a quantitative way independent of the substrate properties, grain  
22 size, density, and shape of the granular material and the released mass (Lajeunesse et al., 2005;  
23 Lube et al., 2005; Staron and Hinch, 2007). The granular collapse has also been studied using  
24 discrete element method, which allows precise measurement of the internal flow structure (Lo  
25 et al., 2009; Staron and Hinch, 2007; Staron et al., 2005; Utili et al., 2014). Power laws  
26 relating the final run-out and height to the initial aspect ratio ( $a = H_0/L_0$ ) of the column were  
27 observed. These findings immediately pose a question: are these simple scaling fortuitous, an  
28 oversimplification, or in fact indicative of a simple dynamical balance?

29 Granular flows are conventionally modelled as a frictional dissipation process in continuum  
30 mechanics but the lack of influence of inter-particle friction on the energy dissipation and  
31 spreading dynamics (Lube et al., 2005) is surprising. However, Kerswell (2005) showed  
32 the run-out behaviour has a clear material dependence. Although, the collapse of a granular  
33 column on a horizontal surface is a simple case of granular flow, a proper model that describes  
34 the flow dynamics is still lacking. Simple mathematical models based on conservation of

## 4.2 Granular column collapse

3

horizontal momentum capture the scaling laws of the final deposit, but fail to describe the initial transition regime. From a theoretical point of view, the spreading has been described using depth averaged equations (Kerswell, 2005; Larrieu et al., 2006). The depth-averaged and Saint-Venant equations, however, struggle to recover the precise dynamic behaviour of the system (Warnett et al., 2013) and only succeeds in predicting the scaling observed for aspect ratio less than one. Describing the behaviour of larger aspect ratio and capturing the initial stage of the collapse, when the grains experience a rapid change of direction from vertical to horizontal, remain an open challenge.

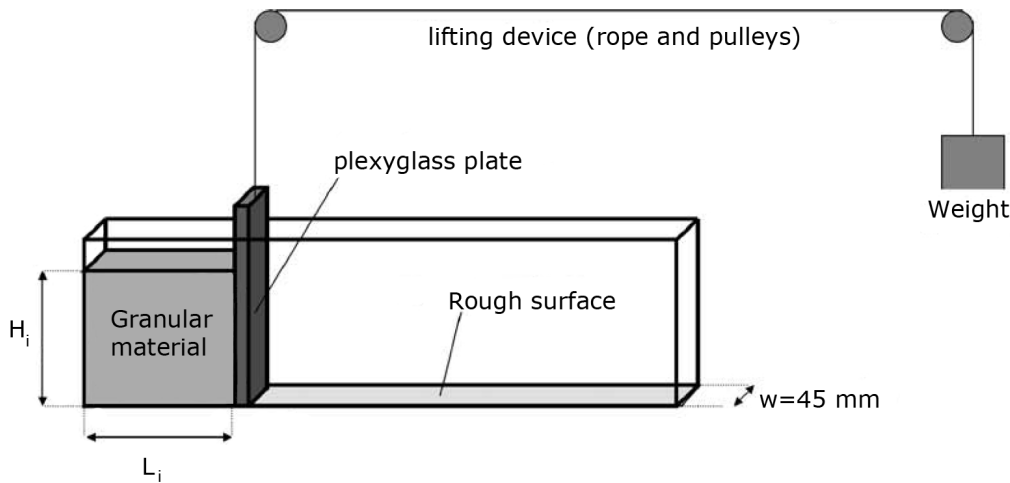


Figure 4.1 Schematic of experimental configuration for 2-D collapse in a rectangular channel, (Lajeunesse et al., 2004)

In the present study, multi-scale numerical modelling, i.e. grain-scale modelling and continuum analyses, of quasi-two dimensional collapse of granular columns are performed using Discrete Element (DEM) approach and Generalised Interpolation Material Point Method (GIMPM). GIMPM, a hybrid Eulerian – Lagrangian approach, with Mohr-Coloumb failure criterion is used to describe the continuum behaviour of the granular column collapse. While the micro-mechanics of the flow is captured using DEM simulations. Comparing the grain scale behaviour with the continuum simulations highlights the limitations of the continuum approach in modelling dense granular flows and their ability (or lack thereof) in capturing the complex micro-scale rheology.

### 4.2.1 Numerical set-up

In this study, numerical simulations of granular columns are analogous to the experimental investigation of column collapse performed by Lajeunesse et al. (2004). The experimental configuration of Lajeunesse et al. (2004) is shown in figure 4.1. Granular material of mass ‘ $M$ ’

1 was poured into a container to form a rectangular heap of length ' $L_0$ ', height ' $H_0$ ' and thickness  
 2 ' $W$ '. The internal friction angle and the wall friction between the wall and the glass beads  
 3 measured by Lajeunesse et al. (2004) are listed in table 4.1. The gate was then quickly removed  
 4 to release the granular mass that spreads in the horizontal channel until it comes to rest. The  
 5 final run-out distance ' $L_f$ ' and the collapsed height ' $H_f$ ' were measured. The run-out distance  
 6 and collapse height exhibit a power law relation with the initial aspect ratio ' $a$ ' ( $= H_0/L_0$ ) of  
 7 the column.

Table 4.1 Material properties of glass ballotini (Lajeunesse et al., 2004)

Parameter	Value
Mean diameter	1.15 mm
Repose angle	$22 \pm 0.5^\circ$
Avalanche angle	$27.4 \pm 0.5^\circ$
Wall friction angle	$24.8 \pm 0.2^\circ$

8 Granular materials when released suddenly on a horizontal surface exhibit transient flow.  
 9 In this study, the mechanism of flow initiation, spreading dynamics and energy dissipation are  
 10 studied for varying initial aspect ratios of the granular column. DEM soil grain characteristics  
 11 match that of the experiment. The particle size distribution (PSD) is one of the most impor-  
 12 tant factors controlling landslide initiation and soil permeability. Cumulative  $\beta$  distribution  
 13 (described in ??) is used to generate a graded sample with a mean grain diameter of 1.15mm  
 14 (see figure 4.2b). The DEM sample is composed of  $\sim 3000$  disks with a uniform distribution of  
 15 diameters by volume fractions in the range  $[d_{min}, d_{max}] = 0.92 - 1.38$  mm with polydispersity  
 16  $r = \frac{d_{max}}{d_{min}} = 1.5$ . The granular column is prepared by allowing the randomly placed grains to  
 17 undergo ballistic deposition with a constant potential head between layers of soil grains. A  
 18 snapshot of the sample generated is shown in figure 4.2a. A DEM sample with soil grains  
 19 arranged in a regular hexagonal lattice is also used to study the influence of crystallisation and  
 20 jamming on the run-out behaviour.

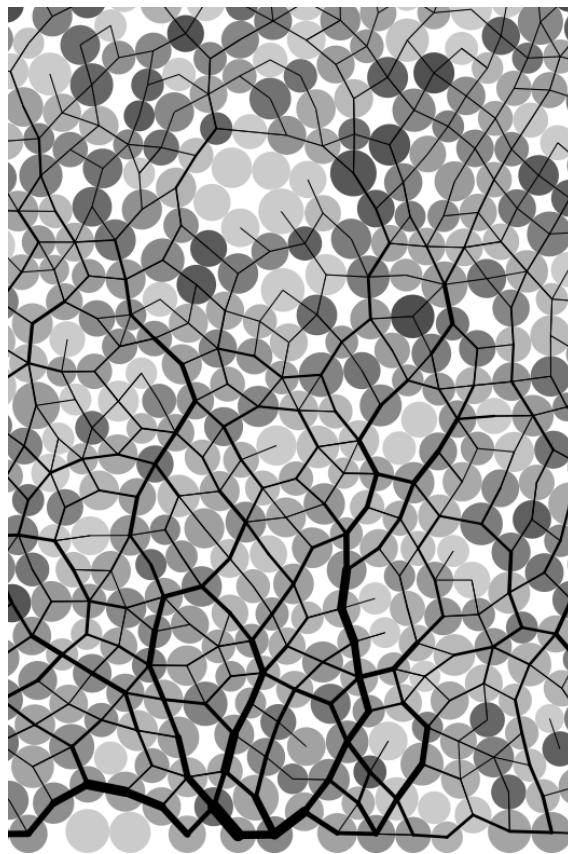
21 The overlap between grains are determined by the stiffness  $k_n$  of the spring in the normal  
 22 direction. Typically, an average overlap in the range 0.1 to 1.0% is desirable Zenit (2005) and  
 23 the spring constant is chosen to produce grain overlaps in this range. The stiffness is determined  
 24 as

$$25 \quad k_n = \frac{2\pi G}{(1-\nu)[2\ln(\frac{2r}{A}) - 1]} \quad (4.1)$$

$$26 \quad A = \left[ \frac{2r(1-\nu)f_n}{\pi G} \right]^{\frac{1}{2}}, \quad (4.2)$$

## 4.2 Granular column collapse

## 5



(a) DEM sample prepared using ballistic deposition

(b) DEM grains generated using the cumulative  $\beta$  distribution

Figure 4.2 DEM sample characteristics

1 where  $f_n$  is the normal contact force; G is the shear modulus; v is the Poisson's ratio and r is  
 2 the radius of the grain. A simpler form of stiffness for a spherical grain is defined as

3 
$$k_n = 4ER, \quad (4.3)$$

4 where E is the Young's modulus of the material and R is the radius of the grain. [Cambou et al. \(2009\)](#)  
 5 observed that the contact model has negligible influence on the run-out behaviour of  
 6 rapid granular flows. The granular collapse simulations performed using non-linear Hertz-  
 7 Mindlin contact model and the linear-elastic contact model showed no significant difference  
 8 on the granular flow behaviour [Utili et al. \(2014\)](#). Linear-elastic contact model is used in the  
 9 present study due to its simplicity and lower computation time requirement. The maximum  
 10 tangential force is limited by the Mohr-Coloumb criterion.

11 [Staron and Hinch \(2007\)](#) observed that the coefficient of restitution  $\varepsilon$  was dramatically  
 12 changing the behaviour of the systems for  $\varepsilon \rightarrow 1$ ; in particular, this dramatic change is  
 13 expected to become more important for increasing values of a. On the contrary, for  $\varepsilon \leq 0.8$ ,  
 14 the influence of the coefficient of restitution becomes negligible. In the present study, a value  
 15 of 0.75 is adopted as the coefficient of restitution, similar values of restitution coefficient  
 16 was adopted by [Girolami et al. \(2012\); Zenit \(2005\)](#). The normal damping coefficient  $C_n$  is  
 17 appropriately chosen to achieve the required coefficient of restitution  $\varepsilon$ :

18 
$$C_n = 2\gamma\sqrt{m_{ij}k_n} \quad (4.4)$$

19 where  $\gamma = -\frac{\ln(\varepsilon)}{\sqrt{\pi^2 + \ln^2(\varepsilon)}}, \quad \text{and} \quad m_{ij} = \frac{m_i m_j}{m_i + m_j}. \quad (4.5)$   
 20

21 The micro-mechanical parameters used in this study are presented in table 4.2. Due to the  
 22 unsteady nature of the flow, the grains get dispersed on the horizontal plane as discrete bodies  
 23 start to separate from the main mass, hence the run-out distance is calculated as the position of  
 24 the farthest grain which has at least one contact with the main mass.

25 GIMPM with Mohr-Coloumb constitutive model is used to simulate plane strain collapse  
 26 of granular columns. [Crosta et al. \(2009\)](#) observed that the Mohr-Coloumb with non-associate  
 27 flow rule is able to capture granular collapse dynamics and models the strong vertical motion  
 28 components, but it does not suffer the limitations of typical shallow water equation methods.  
 29 In order to understand the ability and limitations of continuum approaches in capturing the  
 30 local rheology, it is important to scale the grain scale properties, such as inter-particle friction  
 31 and stiffness, to the continuum scale (macroscopic friction and Young's modulus). [Crosta et al. \(2009\)](#)  
 32 observed that the friction angle plays a significant role on the run-out behaviour. In  
 33 MPM simulations, the granular flow is assumed to be in critical state and the critical state

Table 4.2 Micro-mechanical parameters used in DEM simulations

Parameter	Value
Young's modulus of glass bead	$70 \times 10^9 \text{ N m}^{-2}$
Poisson's ratio	0.22 - 0.24
Diameter of glass beads	0.92 to 1.38 mm
Normal and shear stiffness of grains	$1.6 \times 10^8 \text{ N m}^{-1}$
Normal and shear stiffness of wall	$4 \times 10^8 \text{ N m}^{-1}$
Inter-particle friction coefficient, $\mu$	0.53
Wall friction coefficient	0.466
Coefficient of restitution, $\epsilon$	0.755

friction angle is used in the Mohr-Coloumb model. In order to obtain the critical state friction angle of the granular sample, a shear test is performed using 1078 DEM grains. A bi-periodic boundary condition is adopted on the sides of the sample (see figure 4.3a). Two layers of fixed grains (shown in black) is placed at the top and the bottom of the shear sample. A normal pressure 'P' and a horizontal velocity  $v$  is applied to the fixed grains at the top of the shear sample. The normal effective stress is varied in the sample and the average shear stress of the sample is measured. The sample was sheared until critical state was reached. The slope of shear stress versus normal effective stress gives the critical state friction angle. A critical state friction angle of  $22.2^\circ$  is obtained. The macroscopic friction angle is in the range observed by [Estrada et al. \(2008\)](#); [Mitchell and Soga \(2005\)](#). The Young's modulus of the granular assembly is obtained as the initial slope of the stress-strain plot of a uni-axial compression of a granular column using DEM.

[Guilkey et al. \(2003\)](#) suggests using at least four material points per cell for large deformation problems. In the present study, 16 material points per cell is adopted. If the mesh is too fine and the number of particles is too large, the particle size  $2l/p$  decreases, and the GIMPM interpolation function tends to approach the original MPM function, as shown by [Bardenhagen and Kober \(2004\)](#). Hence GIMPM loses the merit that it reduces the numerical noise due to material points crossing the background mesh. In addition, the probability of particles crossing the background mesh increases with decrease in mesh size, hence, more noise can be produced [Abe et al. \(2013\)](#). The effect of number of material points per cell on the run-out behaviour is discussed in section 4.3.5. Each material point represents one-fourth of a DEM soil grain. The parameters used for the continuum analyses are presented in table 4.3.

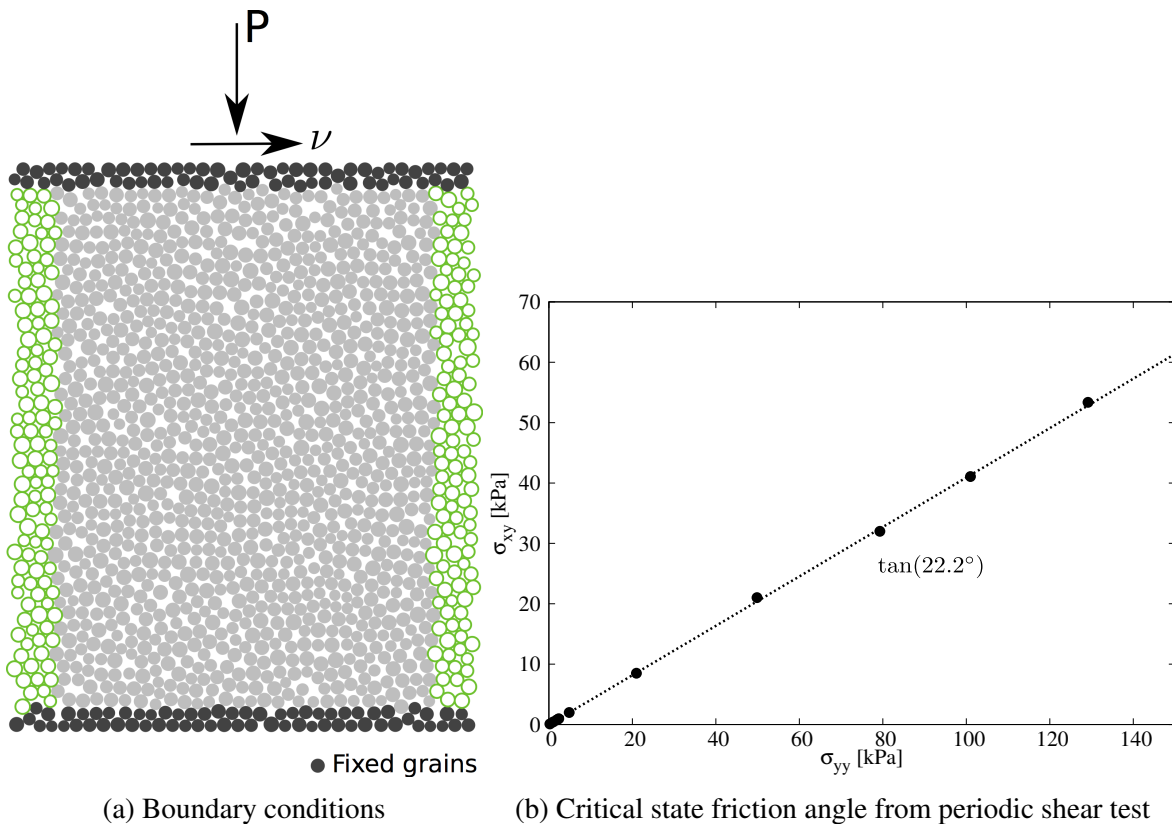


Figure 4.3 Periodic shear test

Table 4.3 Parameters used in continuum simulations

Parameter	Value
Material point spacing	0.575 mm
Number of material points per cell	16
Young's Modulus, E	$1.98 \times 10^6$ Pa
Poisson's ratio, $\nu$	0.22 to 0.24
Friction angle, $\phi$	$23.2 \pm 0.2^\circ$
Dilatancy angle, $\Phi$	$0^\circ$
Density, $\rho$	$1800 \text{ kg m}^{-3}$
Wall friction	0.466
Time step increment	$1.0 \times 10^{-6}$ s

### 4.2.2 Deposit morphology

MPM and DEM simulations of granular column collapse are performed by varying the initial aspect ratio of the column. The normalized final run-out distance,  $\Delta L = (L_f - L_0)/L_0$ , as a function of the initial aspect ratio ‘a’ of the column is presented in figure 4.4. Similar to the experimental behaviour a power law relation between the run-out and the initial aspect ratio of the column is observed. Two distinct flow regimes can be seen: (a) for ‘a’ < 1.7 a linear relation between the spread and aspect ratio can be observed, and (b) for ‘a’ > 1.7 a power-law relationship exists. In the present study, the following scaling law for the run-out (using DEM) is observed:

$$\frac{L_f - L_0}{L_0} \approx \begin{cases} 1.67a, & a \lesssim 2.3 \\ 2.5a^{2/3}, & a \gtrsim 2.3 \end{cases} \quad (4.6)$$

Both, MPM and DEM simulations are able to capture the linear relationship for ‘a’ < 1.7, and the simulation results agree with the experimental investigation [Lajeunesse et al. \(2005\)](#). This shows that a simple frictional dissipation model is able to capture the flow dynamics for columns with smaller aspect ratio. For ‘a’ < 1.7, the normalised run-out distance predicted using DEM simulations are very close to the run-out observed in the experiments. DEM simulations with hexagonal packing shows shorter run-out distances in comparison to randomly packed sample. This difference in the run-out behaviour might be due to the crystallisation and jamming effects in hexagonal packing. The small difference in the final run-out between DEM and experimental results can be attributed to the variation in the packing of grains. Also, the experimental data corresponds to granular column collapse in a rectangular channel, the collapse is not a pure two-dimensional collapse as in the case of numerical simulations.

Significant difference in the final run-out between MPM, which is based on a simple frictional model for dissipation of potential energy, and DEM simulations for ‘a’ > 1.7 indicates a change in the mechanism of energy dissipation for columns with large aspect ratios (‘a’ > 1.7). [Staron and Hinch \(2005\)](#) observed that a constant frictional dissipation model cannot describe a power-law relation observed at large aspect ratio. A transition in the run-out behaviour at an aspect ratio of 1.7 indicates a change in flow dynamics. Similar behaviour in the run-out distance was observed by [Bandara \(2013\)](#) for columns with large the aspect ratio  $\geq 2$ .

The longer run-out distance in MPM simulations at large aspect ratios might be influenced by the amount of material mobilised during the collapse. In tall columns, the entire column participates in the flow, in contrast to short columns where the collapse is due to avalanching of flanks, [Lajeunesse et al. \(2004\)](#). It is possible that MPM simulations collapses more resulting

in longer run-out distance. Figure 4.5 shows the normalized final height as a function of the initial aspect ratio of the column. Similar to the run-out behaviour, the normalised-height also shows two distinct regimes. The scaling of final height of the column with the initial aspect ratio of the column can be written as

$$\frac{H_f}{L_i} \propto \begin{cases} a, & a \lesssim 0.7 \\ a^{2/3}, & a \gtrsim 0.7 \end{cases} \quad (4.7)$$

The final height predicted by both DEM and MPM simulations match the experimental data for columns with smaller aspect ratio ( $a' \leq 0.7$ ). Linear relationship between the final height and the aspect ratio indicates that only a part of the granular column is mobilised during the collapse. For tall columns, both approaches predict similar normalised height. However, the normalised height observed in MPM is higher than in DEM simulations, which is in contrast to the idea of increase in the amount of material mobilised during the collapse in MPM simulations resulting in longer run-out distance. Hence, the longer run-out observed in MPM simulations is due a change in the flow dynamics at higher aspect ratios, which is not captured in MPM simulations. The final height of a column is controlled by the amount of static region in the granular column collapse, while the run-out distance is essentially a function of the flowing mass. Hence, it is essential to compare the evolution of flow and the internal flow structure in DEM and MPM simulations.

### 4.2.3 Flow evolution and internal flow structure

The normalised run-out and height as a function of the aspect ratio indicates that, for a given granular material and substrate properties, the flow dynamics and the final deposit morphology are independent of the volume of granular material released, but depend only on the geometry of the column. A power law relationship is observed between the run-out distance and the initial aspect ratio of the column. A transition in the run-out behaviour at an aspect ratio of 2.3 indicates a change in the flow dynamics.

For smaller aspect columns ( $a' < 2.3$ ), the flow is initiated by a failure at the edge of the pile along a well-defined fracture surface. The granular mass fails through avalanching of flanks producing a truncated cone-like deposit ( $a' < 0.7$ ) or conical deposit ( $a' > 0.7$ ). The grains located above the failure surface move “*en masse*” leaving a static region underneath the failure surface.

Dimensional analysis of granular column collapse reveals an intrinsic time defined as  $\sqrt{H_i/g}$ . This intrinsic time is a transient time of order  $\tau_c$ , at which the flow is fully developed, i.e., the potential energy available at the initiation of collapse is now fully converted to kinetic

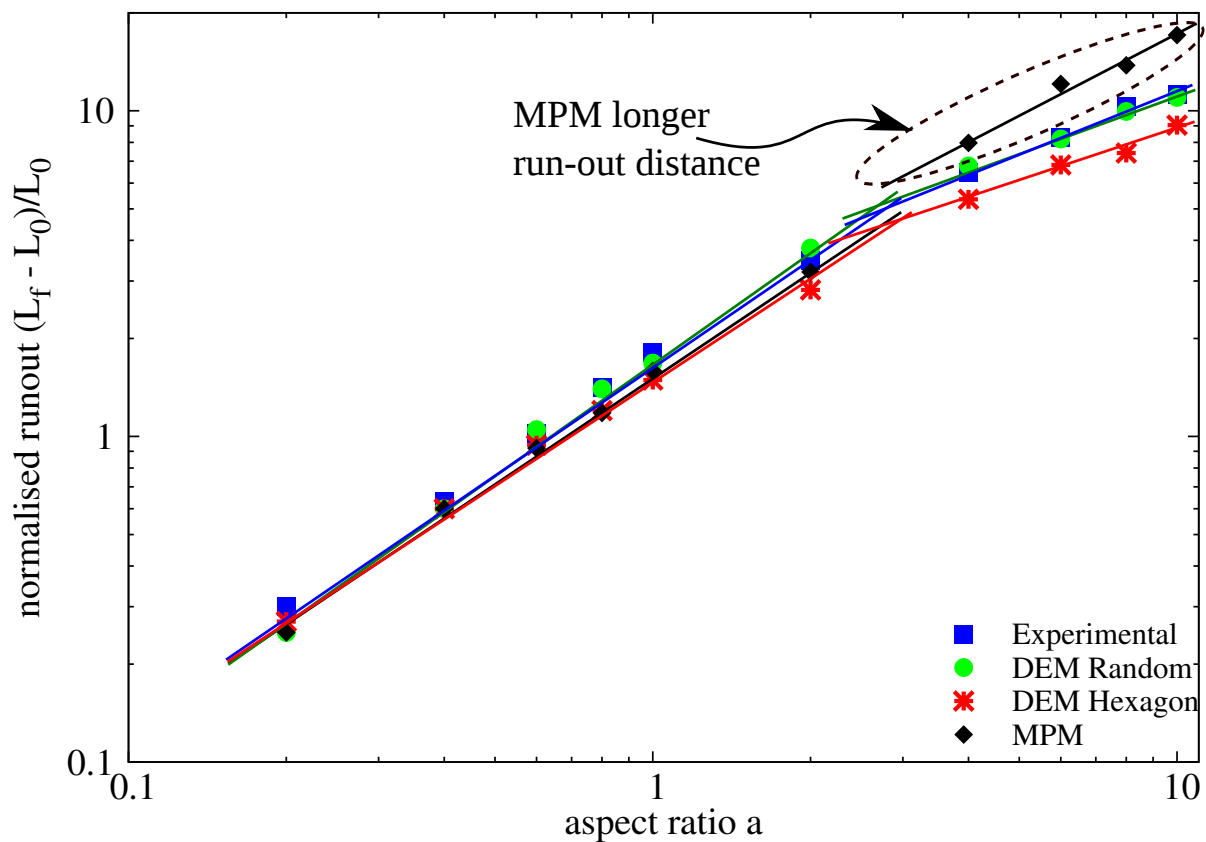


Figure 4.4 Normalised final run-out distance for columns with different initial aspect ratio

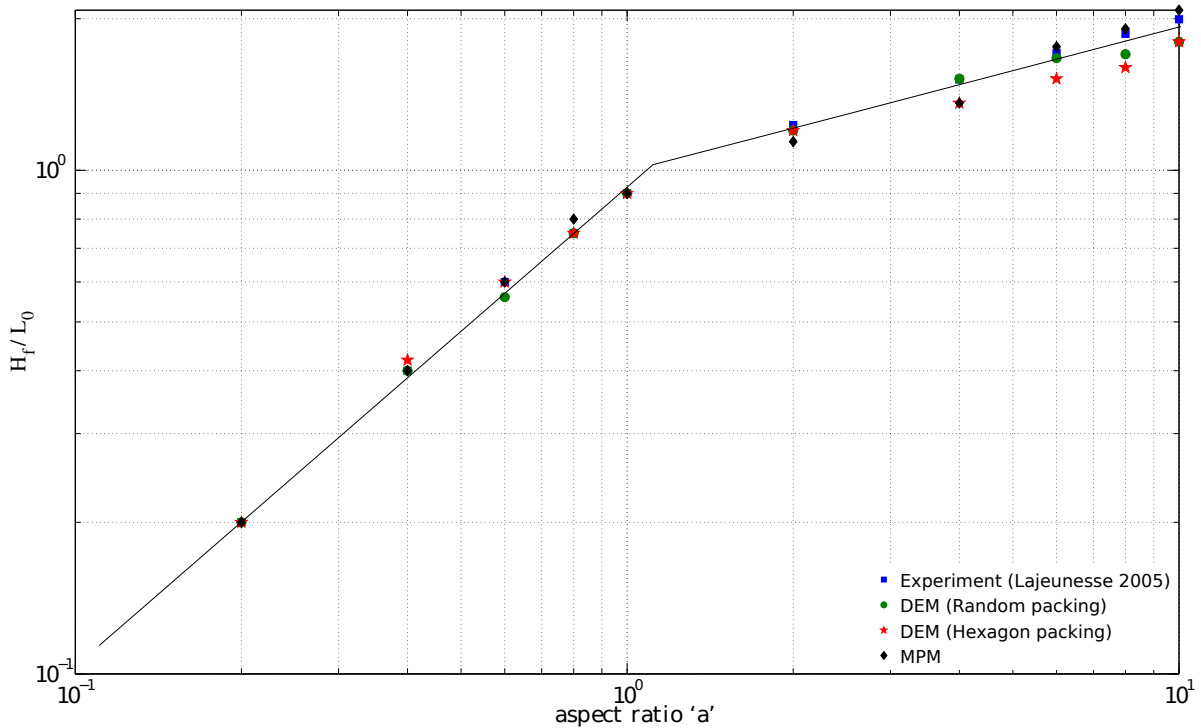


Figure 4.5 Normalised final collapse height for columns with different initial aspect ratio

1 energy. Numerical simulation of the velocity profile of a granular column ('a'=0.4) at critical  
 2 time  $\tau_c$  is presented in figure 4.6. At critical time, the velocity field depends only on the  
 3 position of the grain along the sliding mass. The maximum velocity is observed at the front of  
 4 the flowing mass corresponding to that of a plug flow in horizontal direction. Particulate and  
 5 continuum simulations show similar run-out distance at the critical time. Both approaches show  
 6 similar quantity of material destabilised above the failure surface. However, the crystalline  
 7 arrangement of soil grains in a hexagonal packing results in a different flow mechanics, which  
 8 also shows the effect of jamming at the flow front. The continuum nature of MPM results in a  
 9 slightly different geometry of the material destabilised above the failure surface in comparison  
 10 to DEM simulations. The velocity profile is similar to a steady granular surface flow observed  
 11 by Lajeunesse et al. (2004).

12 For columns with lower initial aspect ratios, the run-out distance is proportional to the mass  
 13 flowing above the failure surface. The spreading results from a Coulomb-like failure of the edges  
 14 and implies no free fall of the column. Daerr and Douady (1999) also observed active Coulomb  
 15 yielding in transient granular surface flows. In this case, the effective friction properties of the  
 16 flow can be simply predicted from the shape of the final deposit. The amount of mass mobilized  
 17 during the collapse is significantly affected by the angle of the failure surface. Figure 4.6  
 18 shows that both numerical techniques predict a distinct failure surface when the flow is fully

developed at critical time  $\tau_c$ . The angle of the failure surface is found to be about  $55^\circ$ . The failure surface begins from the toe of the column and protrudes inwards at an angle of 50 to  $55^\circ$ . The formation of the “truncated conical deposit” or “conical deposit” depends only on the initial length of the column, as the angle of the failure surface is found to be independent of the aspect ratio. The failure angle is consistent with the interpretation in terms of *active Coulomb failure* (Lajeunesse et al., 2004), which leads to a predicted failure angle  $\theta_y = 45^\circ + \delta/2$ , where  $\delta$  is the internal friction angle of the granular material. In the present study, the friction angle of the glass beads is  $22^\circ$ , which leads to  $\theta_y = 45^\circ + 22^\circ/2 = 56^\circ$ , which is in good agreement with the numerical simulations and experimental observations by Lajeunesse et al. (2004). The fracture angle has a direct effect on the transition between the truncated cone and the conical deposit occurring at an aspect ratio of 0.7. Schaefer (1990) observed the onset of instabilities in a narrow wedges of  $56$  to  $65^\circ$  for Cambridge-type constitutive models that describes granular flows, which is in-line with the failure angle observed in the present study.

The final profile of the granular column with an initial aspect ratio of 0.4 is shown in figure 4.7. Both MPM and DEM show similar run-out behaviour. The continuum approach is able to capture the flow dynamics of short columns, wher the failure mechanism is active Coulomb failure. In dense hexagonal packing, the failure surface is steep due to crystallisation effect. The variation in the angle of the failure surface causes a difference in the amount of material destabilised, and in turn in the run-out distance. This crystallisation phenomenon is found to have a significant influence on the final deposit of the granular column. Lacaze and Kerswell (2009) observed that poly-disperse grains have lesser tendency to crystallize especially in the case of tall columns.

For tall columns ( $a' > 2.3$ ), the flow is still initiated by a well defined failure surface as can be seen in figure 4.8. However, in this case the initial granular column is much higher than the top of the failure surface. Due to gravity most of the grains in the column experience free-fall consuming the column along their way. When they reach the vicinity of the failure surface, the flow gets deviated along the horizontal direction releasing a huge amount of kinetic energy gained during the free fall. For larger aspect ratio ( $a > 0.7$ ), the resulting static region is a cone, the final height of the cone, i.e,  $H_f$  lies above the summit of the failure surface. Hence, a different evolution is observed from that of the axis-symmetric geometry (Lube et al., 2005), where the final height coincides with the summit of the failure surface forming a truncated conical deposit. Lajeunesse et al. (2004) observed that the variation in the deposit morphology between the axis-symmetric case and the rectangular collapse to be a geometrical effect rather than as an experimental artefact.

An initial failure surface starting from the toe end of the column at an angle of about  $55^\circ$  can be observed at the critical time  $\tau_c$ . As the collapse of the granular collapse progresses,

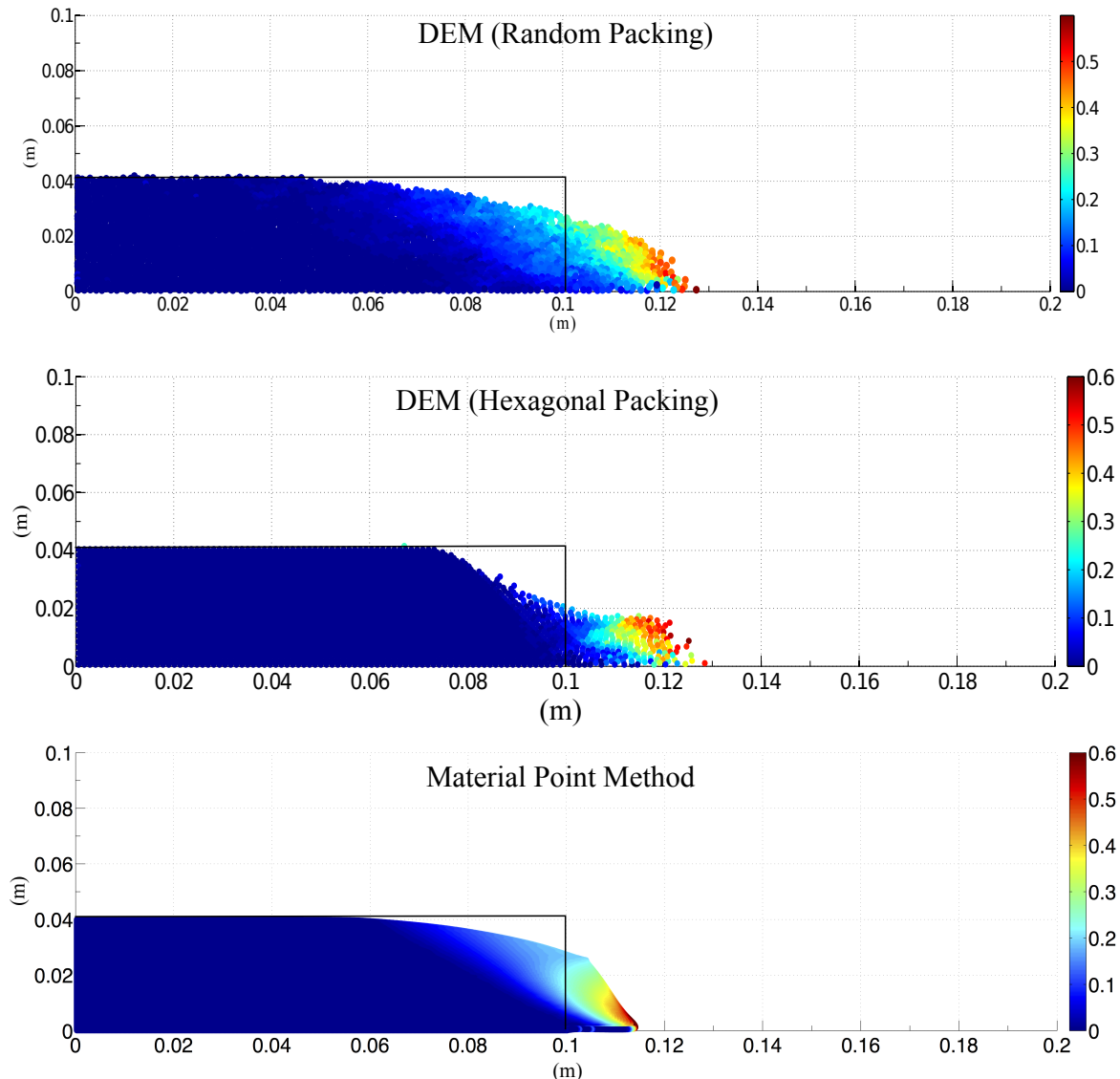


Figure 4.6 Velocity profile of a granular column collapse (' $a' = 0.4 \& t = \tau_c')$

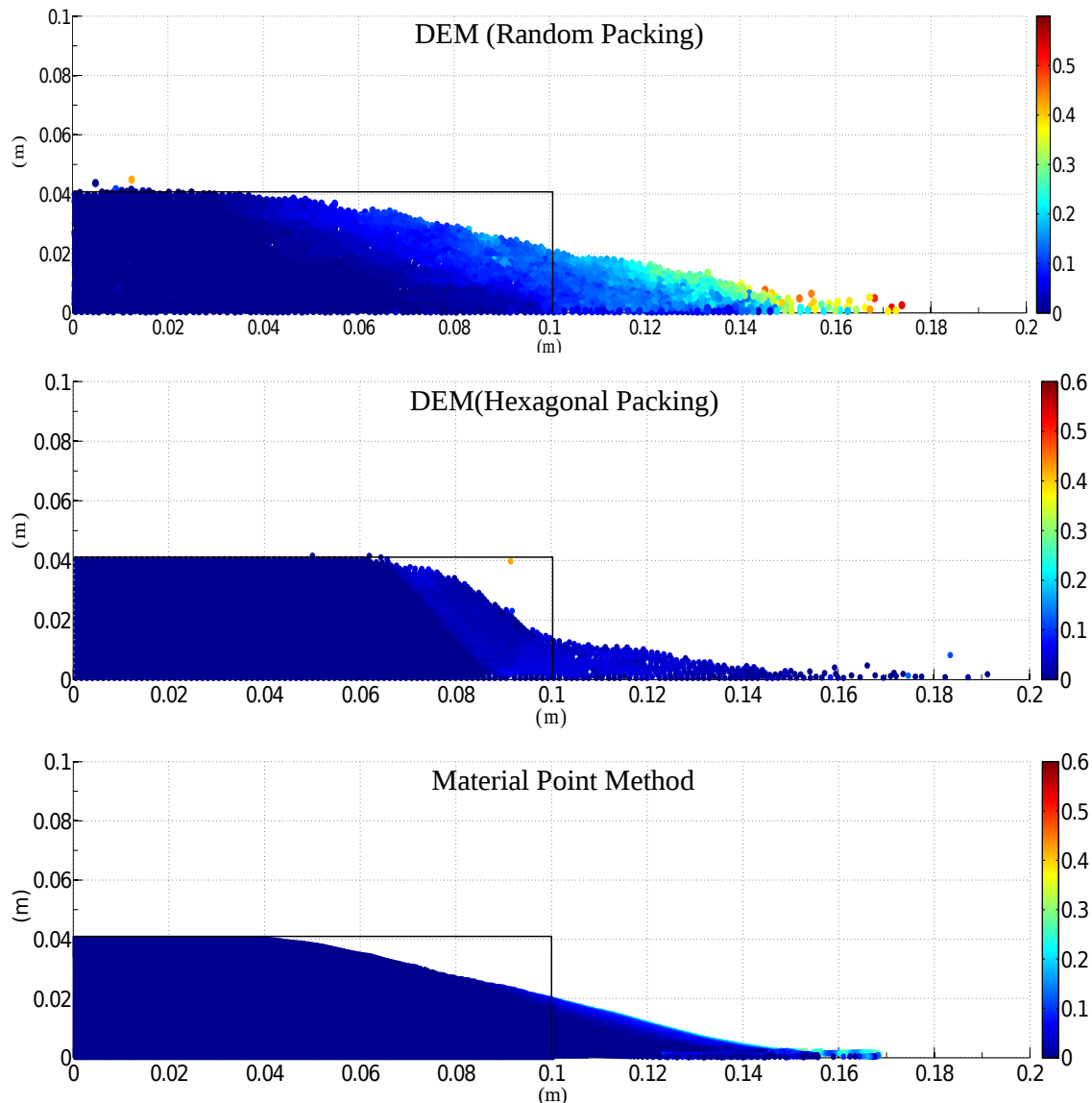


Figure 4.7 Velocity profile of a granular column collapse ( $a' = 0.4$  &  $t = 3 \times \tau_c$ )

1 successive failure planes parallel to the initial failure surface are formed and shear failure occurs  
 2 along these planes. The presence of several shear bands in the final profile of the collapsed  
 3 granular column confirms this hypothesis. Crystallisation in hexagonal packing has a significant  
 4 effect on the run-out distance by forming series of parallel shear bands, resulting in unnatural  
 5 flow kinematics. However, MPM exhibits a single failure surface. This observation throws  
 6 light on the mechanics of propagation of shear bands in massive landslides such as the Storegga  
 7 submarine landslide. The flow behaviour becomes similar to that of columns with lower aspect  
 8 ratio as the flow starts descending along the failure plane. The final profile of the collapsed  
 9 granular column with an initial aspect ratio of 6 is presented in Figure 4.9. For tall columns,  
 10 the dissipation process is more complex due to the free-fall dynamics. The vertical acceleration  
 11 of the grains induces a non-trivial mass distribution in the flow while spreading. This mass  
 12 distribution plays a dominant role in the power-law scaling law obeyed by the run-out ([Staron and Hinch, 2007](#)).  
 13

14 Regardless of the experimental configuration and the initial aspect ratio of the columns, the  
 15 flow is initiated by a well-defined rupture surface, above which the material slides down leaving  
 16 a static region underneath the failure plane. Depending on the aspect ratio of the column, two  
 17 asymptotic behaviours are observed. For smaller aspect ratios, the flow is dominated by friction  
 18 where as large aspect ratio columns are influenced by the pressure gradient.

19 To study the influence of aspect ratio on the flow dynamics of granular columns, the flow  
 20 front  $L(t)$  and the maximum height of column  $H(t)$  are tracked. The evolution of scaled height  
 21 ( $H_f/L_0$ ) and the run-out distance  $(L_f - L_0)/L_0$  with time for granular columns with an initial  
 22 aspect ratio of 0.4 and 6 are presented in figure 4.10. Three distinct regions can be observed  
 23 in the flow evolution of a granular column collapse regardless of the initial aspect ratio of  
 24 the column. An initial transient acceleration phase is observed for a time  $0.8\tau_c$ . This phase  
 25 is followed by a heap movement of granular materials at the foot with a constant spreading  
 26 velocity  $V$  for about  $2\tau_c$ . When time ' $t$ ' >  $\tau_c$ , the velocity varies linearly with depth in the  
 27 flowing layer and decreases exponentially with depth near the static layer. This velocity profile  
 28 is similar to those observed in steady granular surface flows ([Lajeunesse et al., 2004](#)). Most  
 29 of the run-out happens during this phase. The final phase involves deceleration of the flow  
 30 front and the flow comes to rest after about  $0.6\tau_c$ . The spreading of the granular column ceases  
 31 after a time in the order of about  $3\tau_c$ , however some motion still persists along the free surface  
 32 behind the flow front for a much longer time due to internal rearrangement, the duration of  
 33 which can last up to  $t \approx 6\tau_c$ .

34 The critical time is evaluated as the time at which the potential energy available for the flow  
 35 has been converted to the kinetic energy. In short columns, the critical time observed in both  
 36 hexagonal and random packing of grains matches the experimental observations. However, the

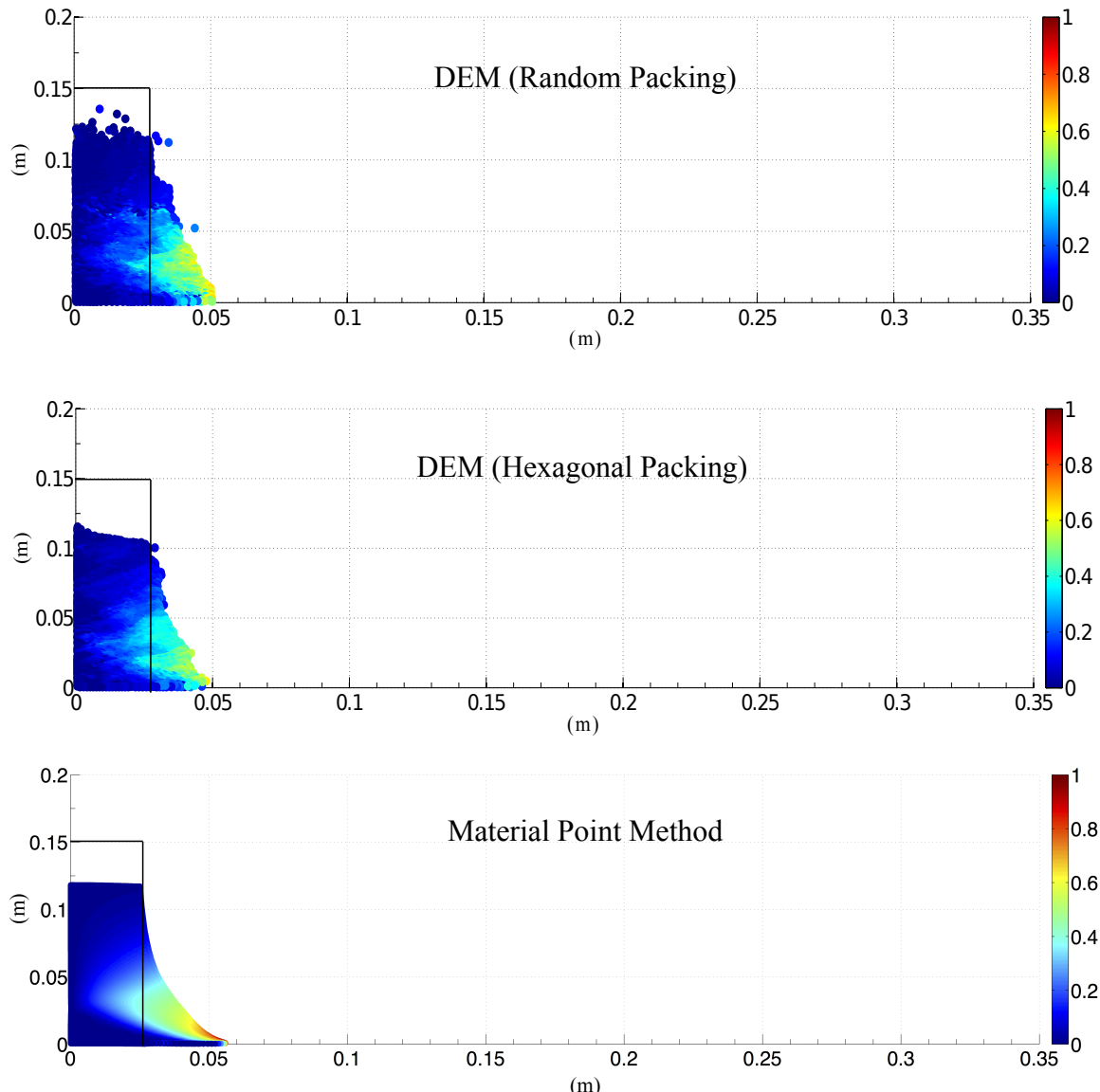


Figure 4.8 Velocity profile of a granular column collapse ( $a' = 6$  &  $t = \tau_c$ )

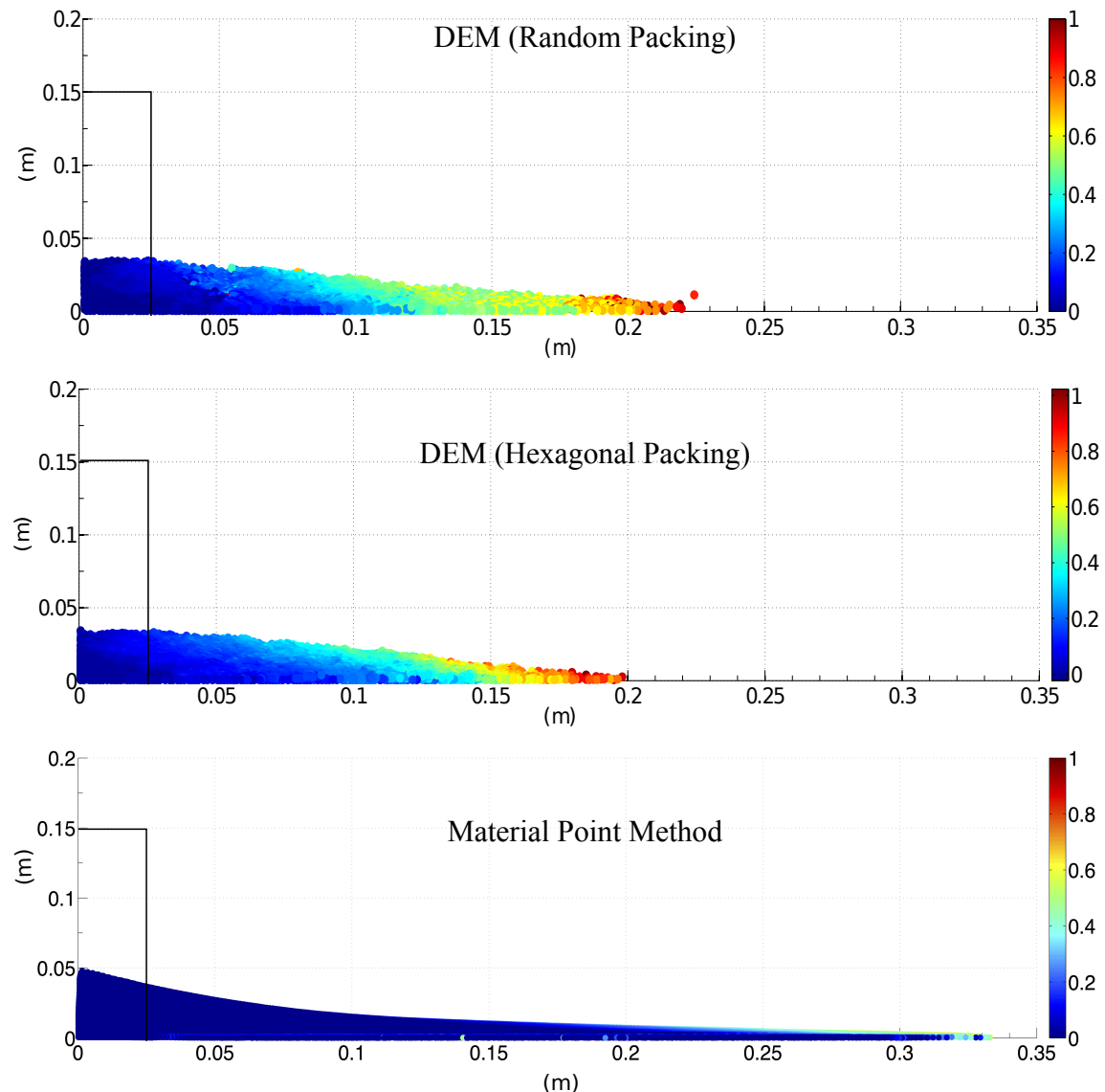


Figure 4.9 Velocity profile of a granular column collapse ( $a' = 6$  &  $t = 3 \times \tau_c$ )

Material Point Method overestimates the critical time by a factor of 1.25, which means that it takes longer for the flow to be fully mobilized. However, the actual run-out duration of the flow is short and the granular mass comes to rest at about  $t = 3\tau_c$ .

For columns with larger aspect ratios, the continuum and particulate approaches simulate similar flow evolution behaviour for times up to  $3\tau_c$ , beyond which particulate simulation decelerates and comes to rest, while the flow continues to evolve in MPM simulations resulting in longer run-out distance. The flow comes to rest at time  $t = 6\tau_c$ . The three phases in a granular flow can be distinctly observed in the flow evolution plot for a granular column with initial aspect ratio of 6 (see figure 4.10b). The flow evolution behaviour observed in the case of DEM simulation matches the experimental observation by Lajeunesse et al. (2004). Hexagonal packing predicts longer time for the flow to evolve, which can be attributed to crystallisation of grains. In MPM simulations, the failure starts at the toe of the column and slowly propagates up to form the failure surface. This results in slower initiation of the flow. It can be observed that MPM overestimates the critical time by 50%. Although, MPM and DEM simulations show the same run-out at time  $t = 3\tau_c$ , the flow evolution between both the approaches is different. MPM simulations continue to accelerate beyond  $3\tau_c$  and ceases to flow at  $6\tau_c$ . In order to understand the difference in the flow dynamics in the case of Material Point Method it is important to study the mechanism of energy dissipation.

#### 4.2.4 Energy dissipation mechanism

The energy dissipation mechanism during the collapse provides useful insight into the flow dynamics. In the case of small aspect ratios, the columns undergo no free fall. The spreading mainly results from the failure of the edges, while the top of the column remains essentially undisturbed in the central area. Staron and Hinch (2007) showed that the amount of energy dissipated during the spreading  $\delta E$  can be easily recovered using the simple shape of the final deposit and volume conservation (see figure 4.11). The difference of potential energy between the initial and the final states gives

$$\delta E = \frac{1}{6}g\rho(L_f - L_0)H_0^2, \quad (4.8)$$

where  $\rho$  is the density of the packing. It is assumed that this energy is dissipated by the work of friction forces  $W_\mu$  over the total distance run by the center of mass G of the spreading material. Staron et al. (2006) considers two regions of dissipation: the amount of mass destabilised  $\frac{1}{4}(L_f - L_0)H_0$  over two thirds of the runout distance  $2(L_f - L_0)/3$  (considering the triangular shape of the final deposit and the initial and final positions of the center of mass).

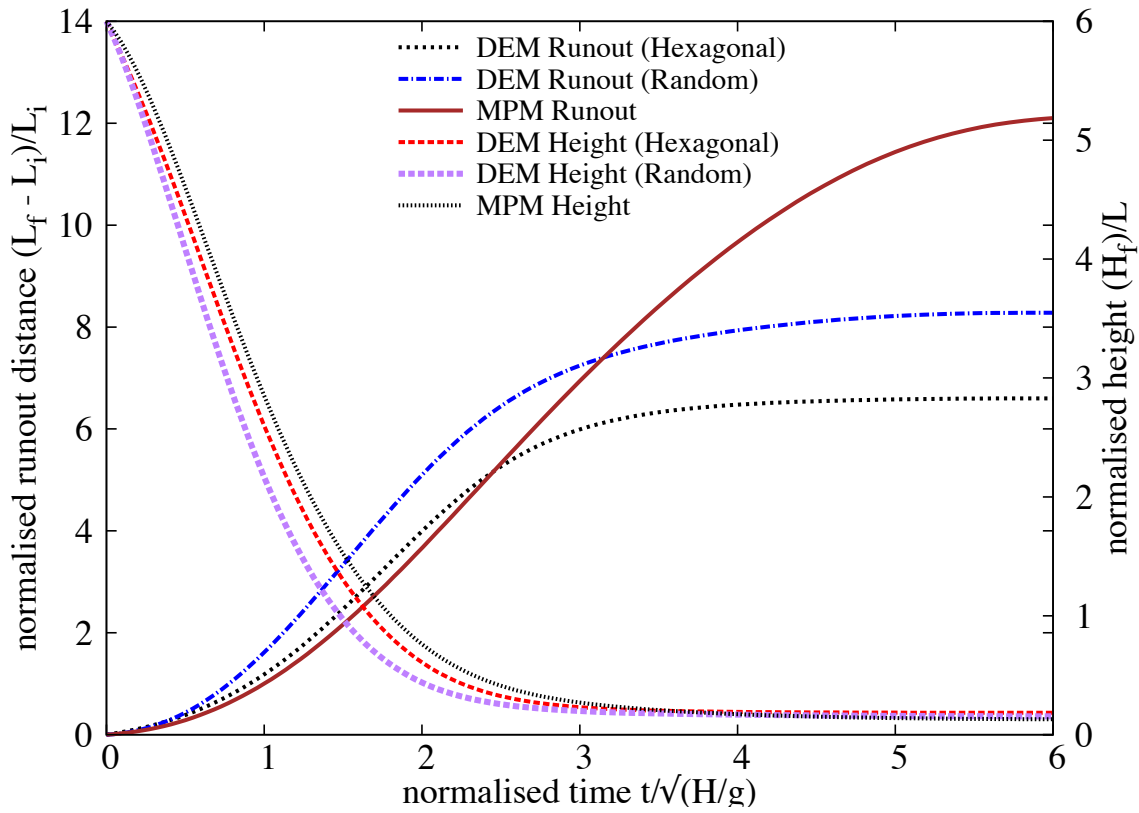
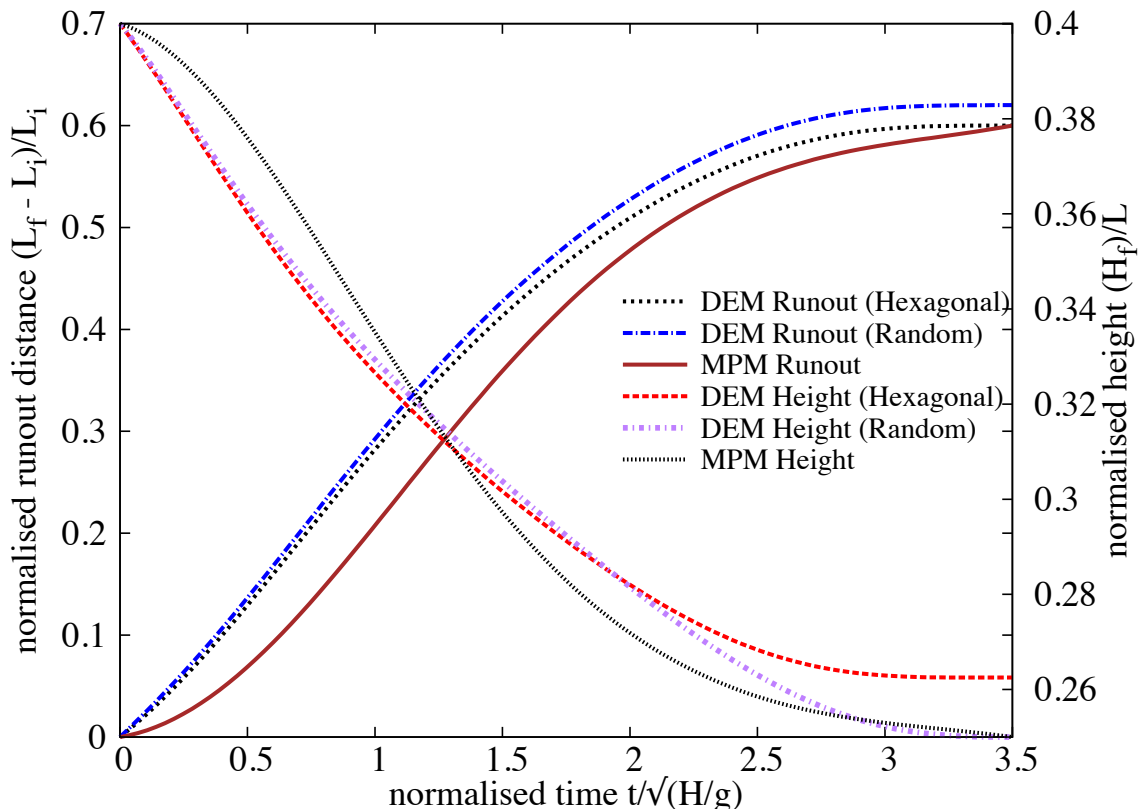


Figure 4.10 Flow evolution of granular column collapse

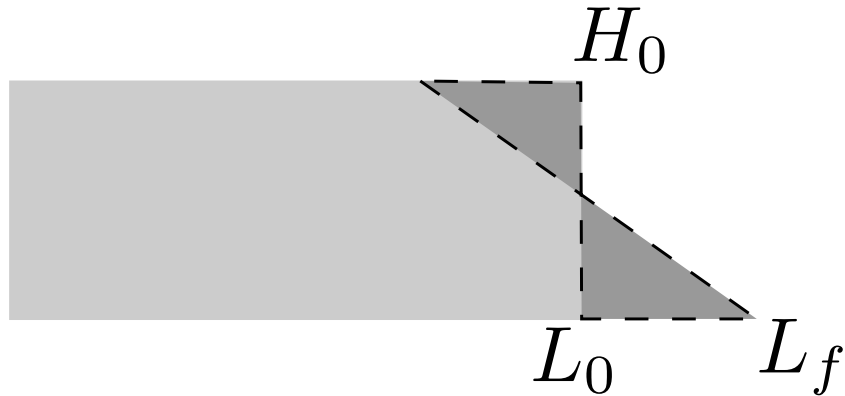


Figure 4.11 Scheme of collapse for small aspect ratio columns. The amount of energy  $\delta E$  lost in the process can be evaluated from the run-out distance  $L_f - L_0$  (after [Staron and Hinch \(2007\)](#)).

The effective coefficient of friction  $\mu_e$  characterizes the mean dissipation in the flow. The work of friction forces is

$$W_\mu = \frac{1}{6} \mu_e g \rho (L_f - L_0) H_0^2, \quad (4.9)$$

Equating  $\delta E$  and  $W_\mu$  gives  $\mu_e (L_f - L_0) = H_0$ . The scaling of the runout leads directly to the relation  $\mu_e = \lambda^{-1}$ , which is the numerical constant in the power law of the run-out that depends on the material properties ([Balmforth and Kerswell, 2005](#)). The amount of energy  $\delta E$  dissipated during the spreading is compared with  $W = N_p g m_p r_p$ , where  $N_p$  is the total number of grains,  $m_p$  is their mass, and  $r_p$  is the total horizontal distance run by each of them. We observe that the dissipation energy  $\delta E$  is proportional to  $W$ . [Staron and Hinch \(2007\)](#) observed that the coefficient of proportionality gives a measure of the effective friction and observed a power law dependence between  $\mu_e$  and internal friction angle  $\mu$ :  $\mu_e = 0.425\mu^{0.2}$ . The effective friction angle  $\mu_e$  of  $21^\circ$  is observed, which is very close to the critical state friction angle of  $22^\circ$  used in MPM simulations. This proves that the energy dissipation mechanism modelled in a continuum sense as a frictional dissipation process captures the flow kinematics observed in DEM and experiments, for short columns.

[??](#) shows the time evolution of the normalised potential energy ( $E_p/E_0$ ) and kinetic energy ( $E_k/E_0$ ) for granular columns with initial aspect ratio ‘a’ = 0.4. The normalised potential and kinetic energy are computed as

$$E_p = \sum_{p=1}^{N_p} m_p g h_p \quad (4.10)$$

$$E_{ki} = \frac{1}{2} \sum_{p=1}^{N_p} m_p v_p^2 \quad (4.11)$$

1 where  $N_p$  is the total number of particles,  $m_p$  is the mass of a particle ‘ $p$ ’,  $h_p$  is the height and  
 2  $v_p$  is the velocity of the particle ‘ $p$ ’. The cumulative dissipation energy is computed as

$$3 \quad \frac{E_d}{E_0} = 1 - \frac{E_k}{E_0} - \frac{E_p}{E_0}. \quad (4.12)$$

5 It can be observed that both MPM and DEM show similar energy dissipation mechanism.  
 6 The DEM simulation shows 3% more potential energy dissipation in comparison with MPM  
 7 simulations. This small difference in the potential energy is due to grain rearrangements. This  
 8 shows the ability of continuum approach in capturing the flow kinematics of columns with  
 9 small aspect ratios (‘ $a' \leq 2.3$ ).

10 The evolution of normalised kinetic and potential energy of a tall column collapse (‘ $a'$  of  
 11 6) is shown in figure 4.12b. It can be observed from the figure that the initial potential energy  
 12 stored in the particle is converted to kinetic energy which is dissipated as the granular material  
 13 flows down. Three successive stages can be identified in the granular column collapse. The  
 14 flow is still initiated by a well defined failure surface. However, the centre of gravity of the  
 15 granular column is much higher than the top of the failure surface, which results in free fall of  
 16 grains under gravity consuming the column along their way. In this stage ( $t < 0.8\tau_c$ ), the initial  
 17 potential energy stored in the grains is converted into vertical motion. In the second stage, when  
 18 the grains reach the vicinity of the failure surface, they undergo collisions with the bottom plane  
 19 and the neighbouring grains, thus causing the flow to deviate along the horizontal direction  
 20 releasing a large amount of kinetic energy gained during the free fall (see figure 4.9). In the third  
 21 stage, the grains eventually leave the base area of the column and flow sideways (Lajeunesse  
 22 et al., 2004). As the process involves collective dynamics of all the grains, it is difficult to  
 23 predict the exact trajectory of a grain, however, the overall dynamics can be explained.

24 DEM simulations model both collisional and frictional dissipation process during the  
 25 collapse of tall columns. However, MPM simulations assume that the total initial potential  
 26 energy stored in the system is completely dissipated through friction over the entire run-out  
 27 distance, this results in longer run-out distance. Figure 4.12b shows the evolution of energy  
 28 with time. At the initial stage of collapse, characterised by free fall of grains under gravity,  
 29 DEM simulation due its particulate nature shows a rapid reduction in the potential energy in  
 30 comparison with MPM, where the failure begins from the toe of the column. The continuum  
 31 nature of MPM simulations results in slower initiation of collapse (see figure 4.10b). It can  
 32 be also observed from figure 4.12b that dissipation energy in MPM is 25% less than DEM  
 33 simulations. In order to understand the mechanism of energy dissipation, it is important to  
 34 understand the contribution from the cumulative frictional and collisional parts. The frictional  
 35 dissipation (basal and internal friction) observed in DEM is almost identical to the frictional

dissipation observed in MPM. The difference in the dissipation energy is due to the collisional regime, which occurs at  $0.8\tau_c$ . The total and frictional dissipation curves diverge around  $0.8\tau_c$  where the grains near the vicinity of the failure surface undergo collisions with the bottom plane and the neighbouring grains resulting in collisional dissipation of the stored potential energy. DEM simulation show drop in the peak kinetic energy at  $\approx 0.8\tau_c$ , which is at the beginning collisional dissipate stage. MPM lacks this collision dissipation mechanism, which results in longer run-out distances for columns with large aspect ratios.

$\mu(I)$  rheology, discussed in ??, describes the granular behaviour using a dimensionless number, called the *inertial number I*, which is the ratio of inertia to pressure forces. Small values of I corresponds to critical state of soil mechanics and large values of I corresponds to the fully collisional regime of kinetic theory.  $\mu(I)$  rheology is adopted in MPM simulations to understand the characteristics of the flow regime. Mohr-Coulomb model was used along with  $\mu(I)$  rheology. Friction angle is changed according to the value obtained by [Da Cruz et al. \(2005\)](#) friction law that is dependent on the inertial number I as  $\mu = \mu_{min} + bI$  where  $\mu_{min} = 0.22$  and  $b = 1$ . Figure 4.13 shows the flow evolution of granular column collapse for aspect ratio ‘a’ of 0.4 and 6 using  $\mu(I)$  rheology. For short columns, the evolution of flow based on  $\mu(I)$  rheology is identical to the MPM simulation using Mohr-Coloumb model. However, for tall columns,  $\mu(I)$  rheology evolves at the same rate as the DEM simulations up to  $t = 0.8\tau_c$ , after which MPM simulation continues to accelerate due to lack of collisional dissipation, while the DEM simulation decelerates with time.

Figure 4.23b shows that the short column attains a maximum inertial number of 0.012, which is in the dense granular flow regime, inertial number  $I \approx 10^{-3}$  to 0.1 ([Da Cruz et al., 2005](#)). However, the maximum inertial number  $I \approx 0.04$ , for tall is still within the dense granular flow regime. DEM simulations, however, showed a collisional regime that has inertial number higher than 0.1. This shows that continuum approach using frictional laws are able to capture the flow kinematics at small aspect ratios, however are unable to precisely describe the flow behaviour for tall columns, which is characterised by an initial collisional regime.

#### 4.2.5 Role of initial grain properties

[Lube et al. \(2005\)](#) observed that the run-out distance scales with the initial aspect ratio of the column, independent of the material properties. The run-out evolution after the initial transition regime is a frictional dissipation process, and the lack of influence of material properties on the run-out behaviour is inconsistent with continuum modelling of granular flow behaviour. [Balmforth and Kerswell \(2005\)](#) observed that the material properties have almost no influence on the exponent of the normalised run-out as a function of the initial aspect ratio. The numerical constant of proportionality, however, showed clear material dependence. This corroborates the

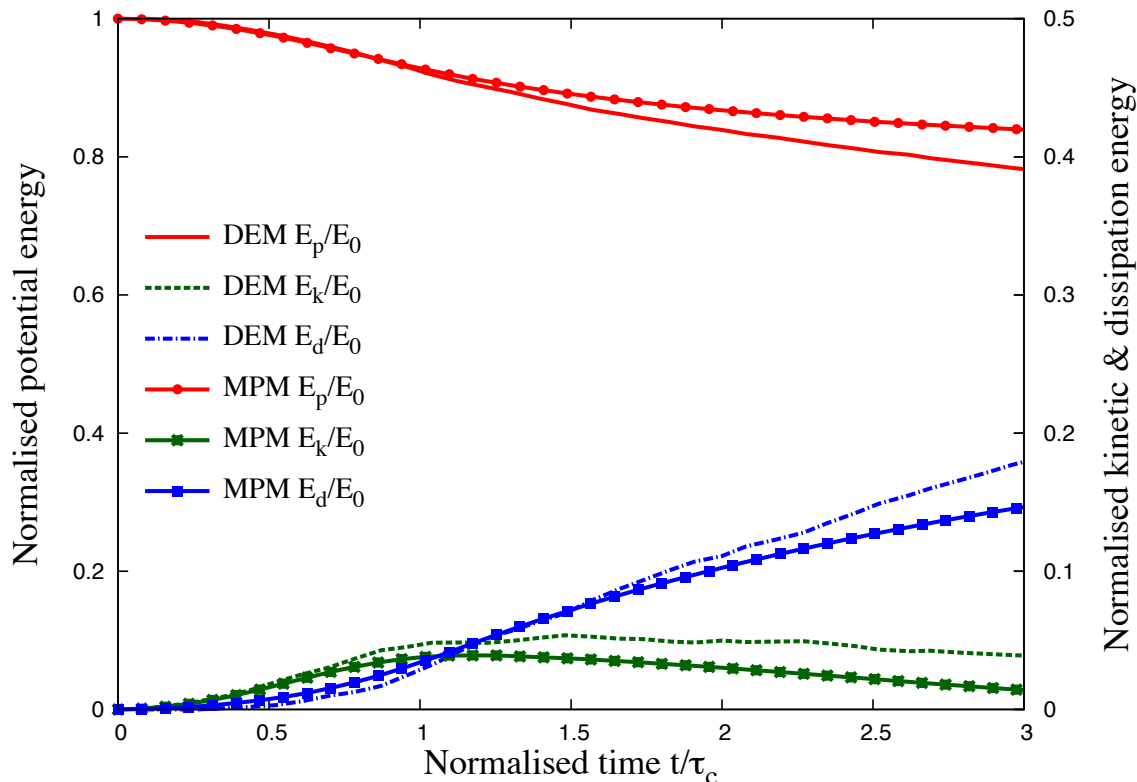
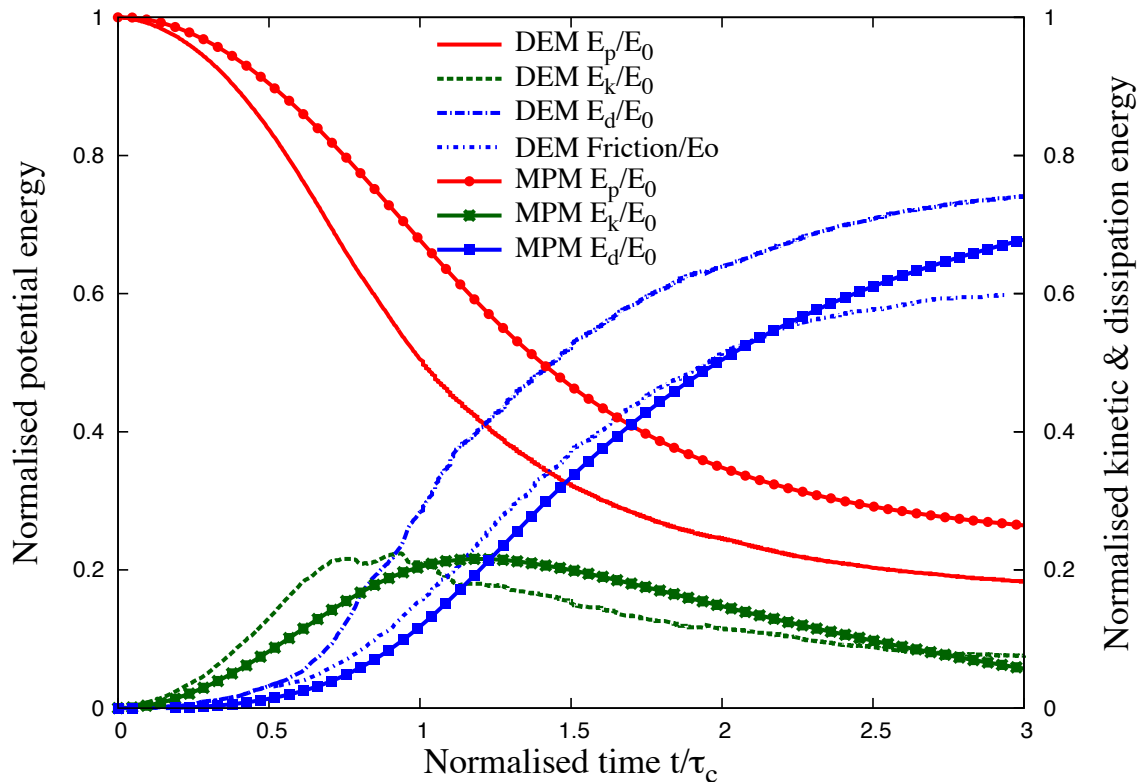
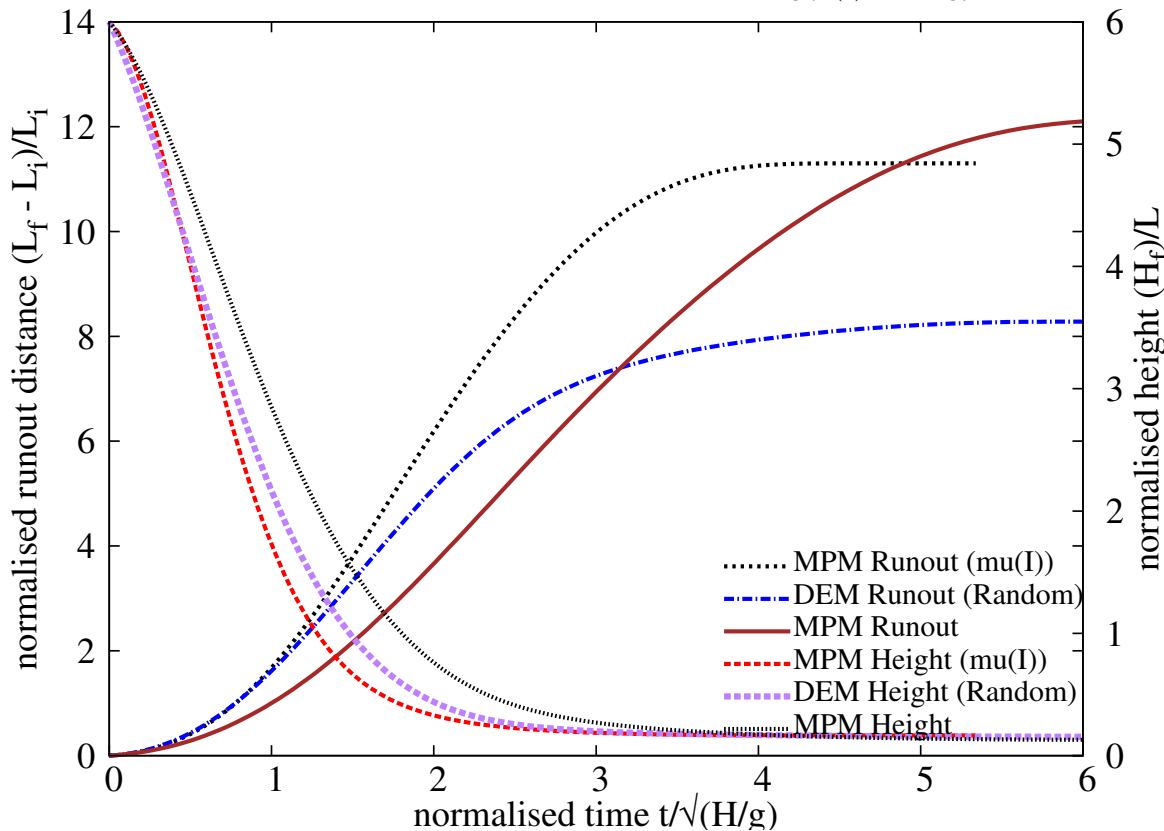
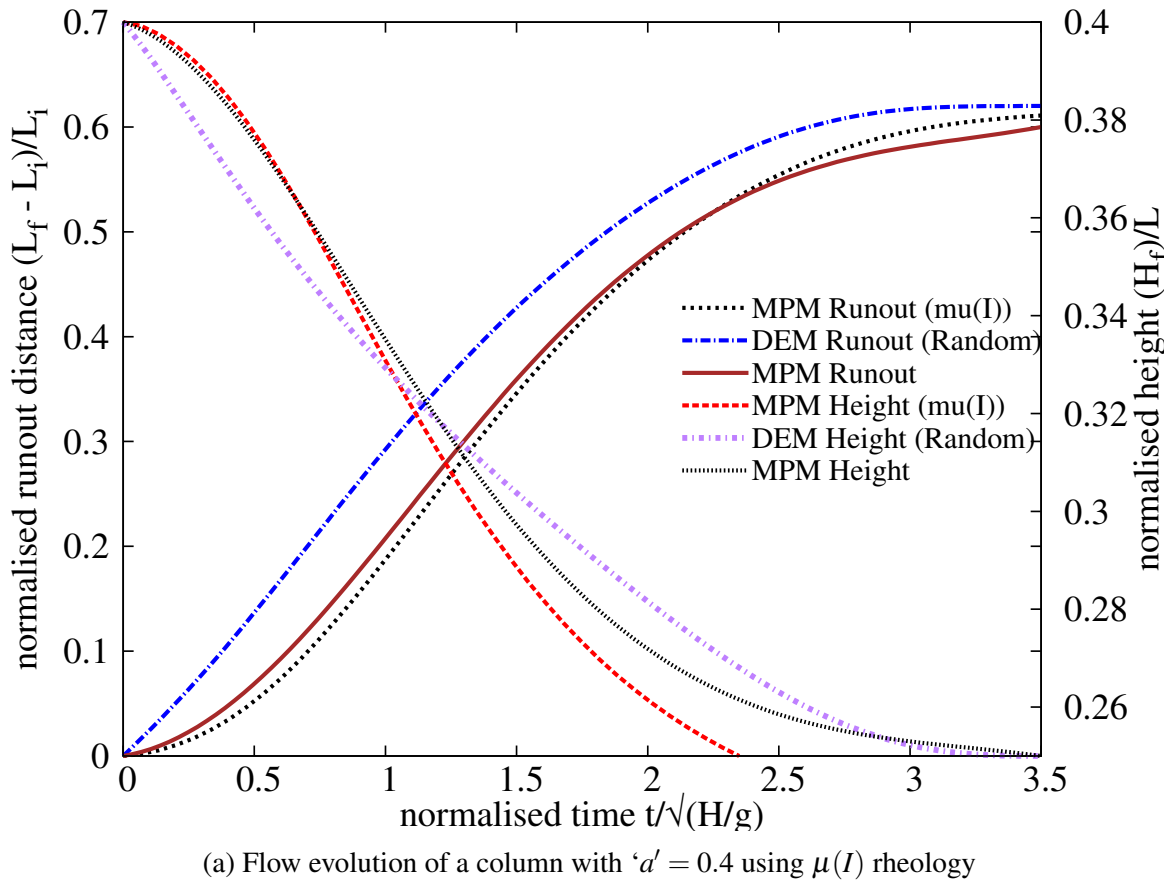
(a) Energy evolution of a column with ' $a'$  = 0.4(b) Energy evolution of a column with ' $a'$  = 6

Figure 4.12 Energy evolution of granular column collapse

## 4.2 Granular column collapse

Figure 4.13 Flow evolution of granular column collapse using  $\mu(I)$  rheology

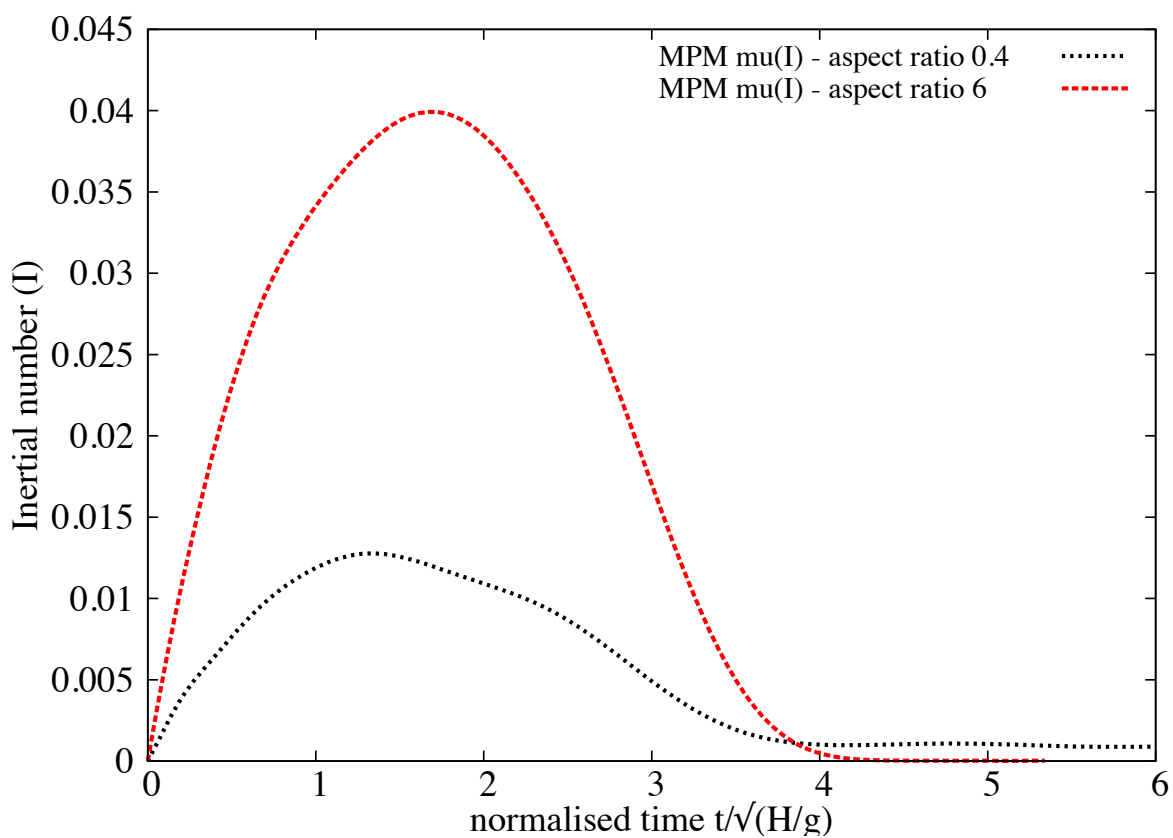


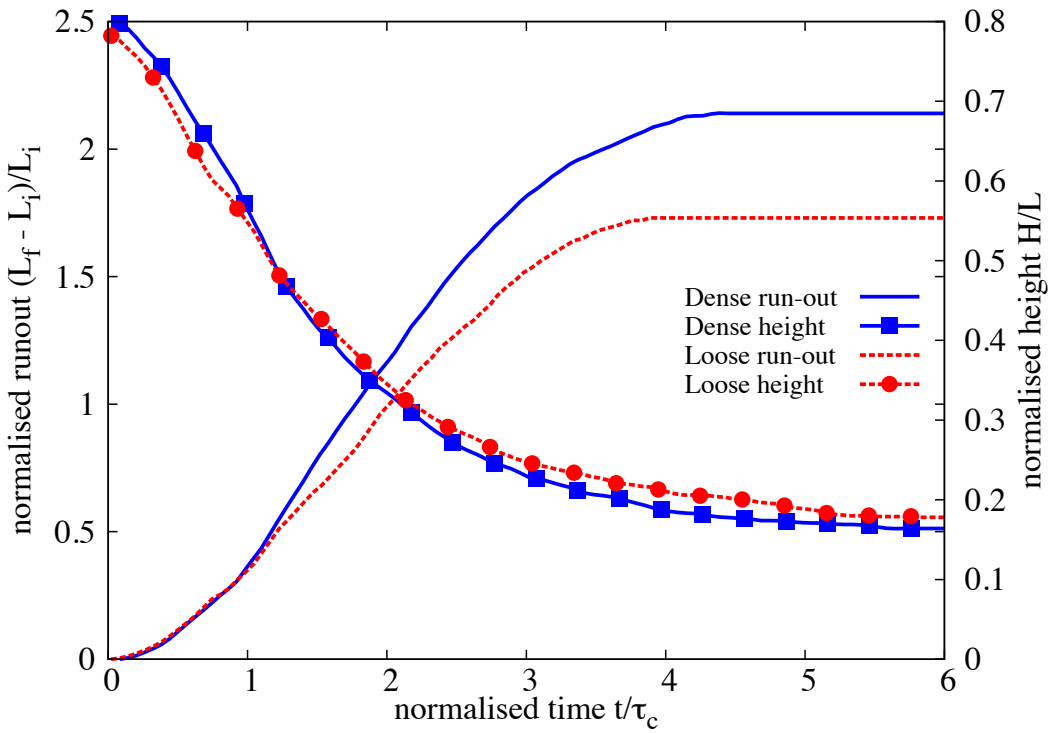
Figure 4.14 Evolution of inertial number with time for columns with ' $a' = 0.4$  and ' $a' = 6$

conclusions of Lajeunesse et al. (2004) and softens that of Lube et al. (2005). Daerr and Douady (1999) also observed strong influence of initial packing density and the internal structure on the behaviour of granular flows.

It should be noted that the collapse experiment is highly transient and no clear stationary regime is observed. On the contrary, the acceleration and the deceleration phases cover nearly the whole duration of the spreading. This makes it difficult to analyse the flow structure and its relation with other characteristic of the system. The knowledge of the final run-out is not a sufficient characterization of the deposit: one also needs to know how the mass is distributed during the flow to understand the dynamics and the dissipation process. This is expected to be true in natural contexts as well as in experiments. While the inter-grain friction does not affect the early vertical dynamics, nor the power-law dependence, it controls the effective frictional properties of the flow, and its internal structure (Staron and Hinch, 2007). It is interesting to note that the details of the structure of the flow do not influence the final run-out dependence, and thus seem to play a marginal role in the overall behaviour of the spreading. This could explain why simple continuum model with a frictional dissipation could reproduce the run-out scaling for columns with small aspect ratios.

The run-out behaviour of a loose (79% packing fraction) and a dense (83% packing) granular column ( $a = 0.8$ ) is studied to understand the influence of material properties. The evolution of normalised run-out with time for two different initial packing densities are presented in figure 4.15. At the initial stage of collapse  $t = \tau_c$ , the flow behaviour is identical in both dense and loose conditions. However, the dense column flows 30% longer than the loose condition. Both the columns come to rest at around  $t = 4\tau_c$ . The columns, however, show similar evolution of the normalised height. This shows that only a part of the column is destabilised during the collapse.

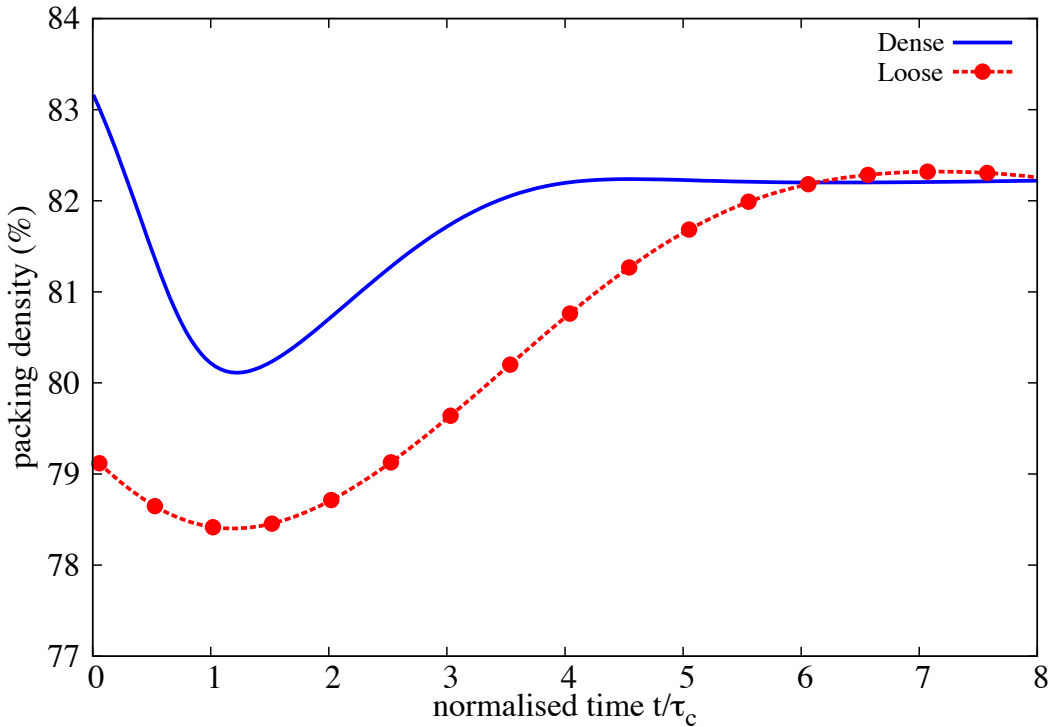
Figure 4.17 show the evolution of potential and kinetic energy with time. Similar potential energy evolution in both dense and loose conditions reveals that there is no change in the overall mechanism of collapse. The dense condition has slightly higher peak kinetic energy than the loose column. In the free-fall phase, the dense column shows a steeper increase in the horizontal kinetic energy in comparison with the loose column. This indicates that dense granular mass is pushed farther away more quickly than the loose column. Loose column exhibits higher vertical kinetic energy which may be due to particle rearrangement resulting in densification of the granular mass. figure 4.16 shows that the loose sample densifies as the flow evolves. Both dense and loose granular columns dilate during the initial stage of collapse, this is due to grains failing by shear along the fracture surface. In both cases, the granular mass attains similar packing density at the end of the flow. Dense granular column dilates, while the loose column compacts to achieve the same critical density. Lajeunesse et al. (2004) observed

Figure 4.15 Effect of density on run-out evolution ‘ $a'$  = 0.8

that the flow comes to rest at around  $3\tau_c$ , but the grains continue to re-arrange until  $6\tau_c$ , similar behaviour is observed in DEM simulations. The dense condition has higher mobilised potential energy at the start of the flow, which yields higher horizontal kinetic energy for the flow. A higher proportion of kinetic energy is lost during compaction, in comparison to the dense granular column. This behaviour in addition to higher mobilised potential results in longer run-out distance in dense granular column.

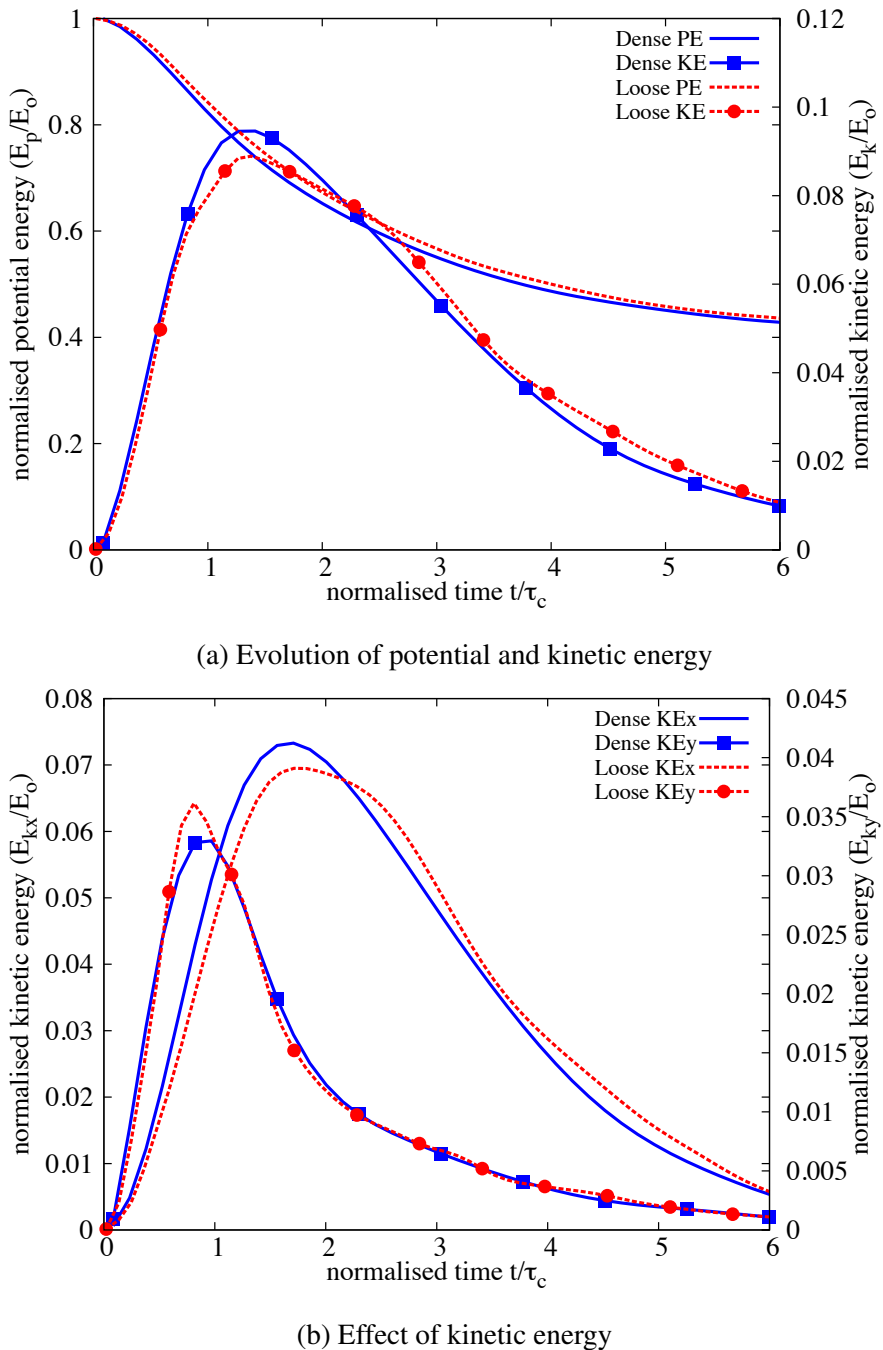
In order to remove the effect of crystallisation on the run-out behaviour, a highly polydisperse sample ( $r = d_{max}/d_{min} = 6$ ) is used. The flow kinematics of a dense (relative density  $D_r = 74\%$ ) and a loose ( $D_r = 22\%$ ) granular column with aspect ratio of 0.8 is studied. Similar to the previous case, the dense granular column exhibits longer run-out distance (see figure 4.18). Due to compaction of grains in loose condition, almost 20% of the initial potential energy available for collapse is lost in densification due to grain rearrangements in comparison to dense condition (see figure 4.20). The compaction of grains in loose column and the dilation in dense column results in significantly different flow structure, especially at the flow front (Figure 4.19). As the loose column densifies, more granular mass is pushed to the flow front resulting in higher vertical effective stress. The loose column exhibits a more parabolic final deposit profile in comparison to the dense column, which shows a triangular deposit at the front.

## 4.2 Granular column collapse

Figure 4.16 Evolution of local packing density ' $a'$  = 0.8

In short column, only a part of the granular column above the failure surface participates in the flow. However, it appears that the collapse for large aspect ratios mixes two very different dynamics: while the second stage consists of a “conventional” horizontal granular flows, the first stage implies a large vertical acceleration. It shows how the initial condition can influence the overall behaviour of a granular system. The effect of density on the run-out behaviour of tall columns is investigated. Similar to short columns, the dense granular column with aspect ratio of 6 shows higher run-out distance in comparison to the loose condition. The dense granular flows almost twice as much as that of the loose granular column. Unlike short columns, the evolution of run-out is different even at the initial stage of the collapse. The dense granular column, which has higher initial potential energy show a rapid increase in the run-out due to free-fall and higher mobilised potential energy. During the stage of collapse, the dense granular column has 15 % higher normalised kinetic energy available for the horizontal push. This results in longer run-out distance for dense granular column in comparison with initially loose granular column.

The initial packing fraction has a significant influence on the flow kinematics and the run-out behaviour, this suggests that triggering mechanisms play a crucial role in the case of natural flows. This stresses the necessity of accounting for initiation mechanisms while

Figure 4.17 Effect of density on energy evolution  $a = 0.8$

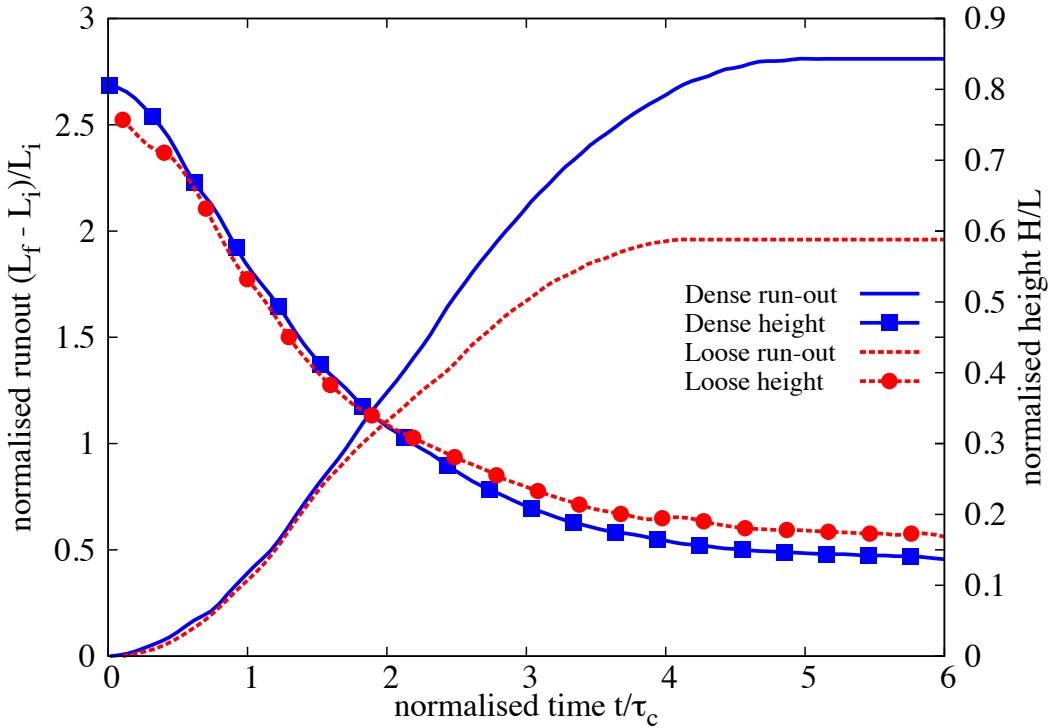
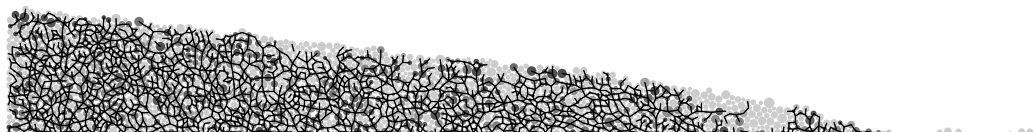


Figure 4.18 Effect of density on run-out evolution ' $a'$  = 0.8 (poly-dispersity ' $r$ ' = 6)

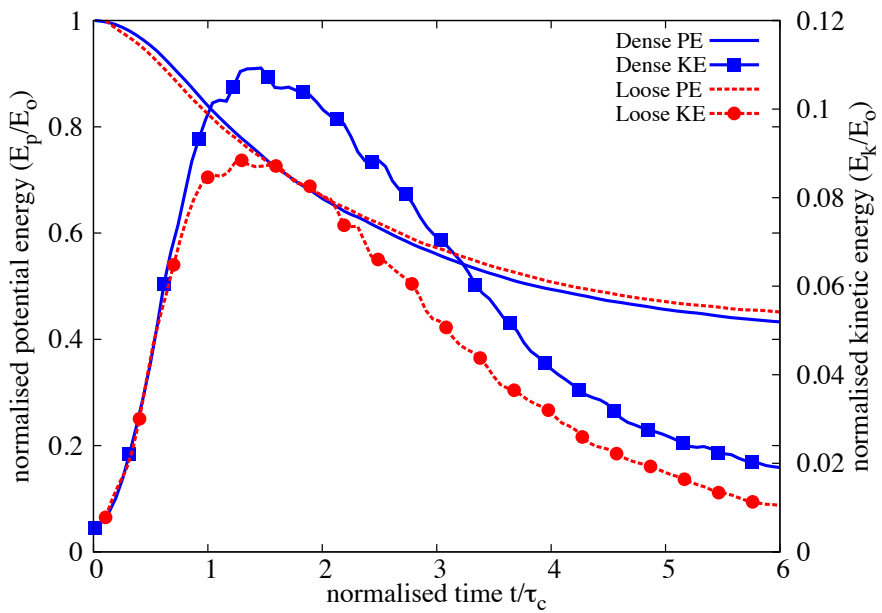


(a) Dense initial packing

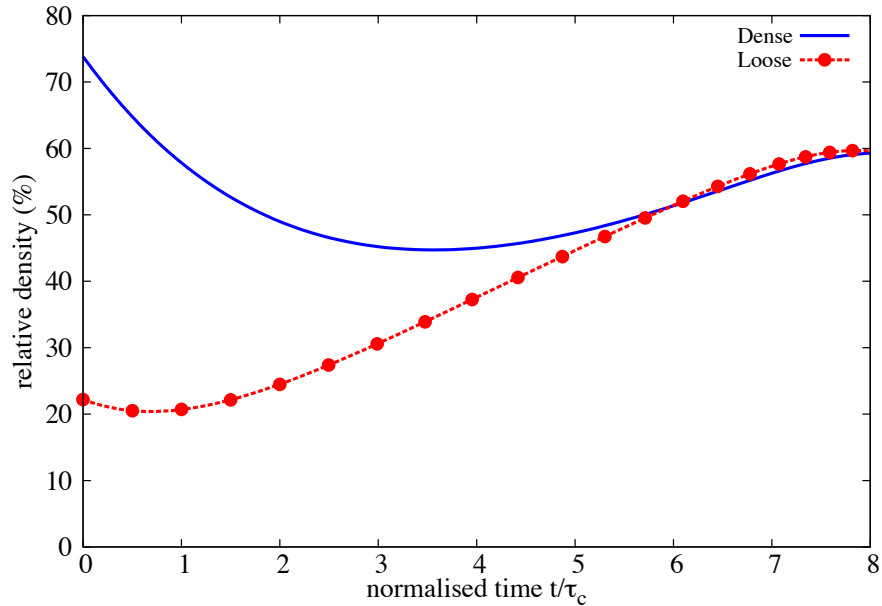


(b) Loose initial packing

Figure 4.19 Snapshots of granular column collapse  $t = 6\tau_c$

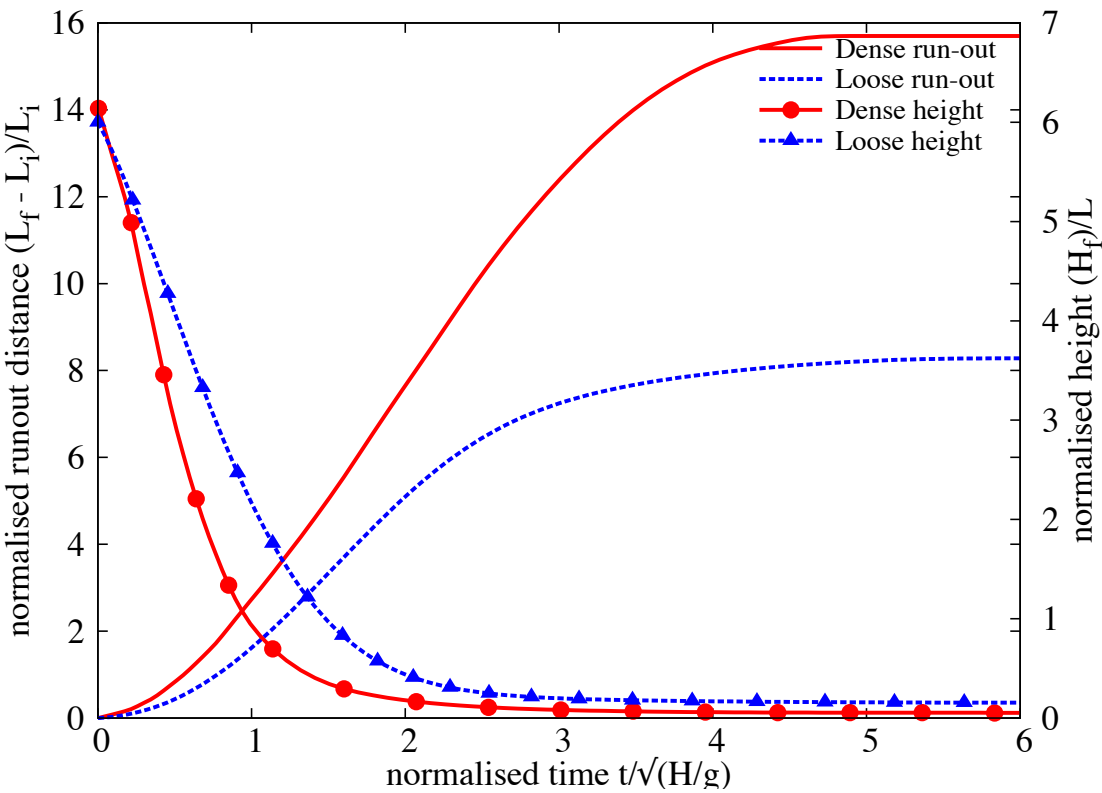


(a) Evolution of potential and kinetic energy

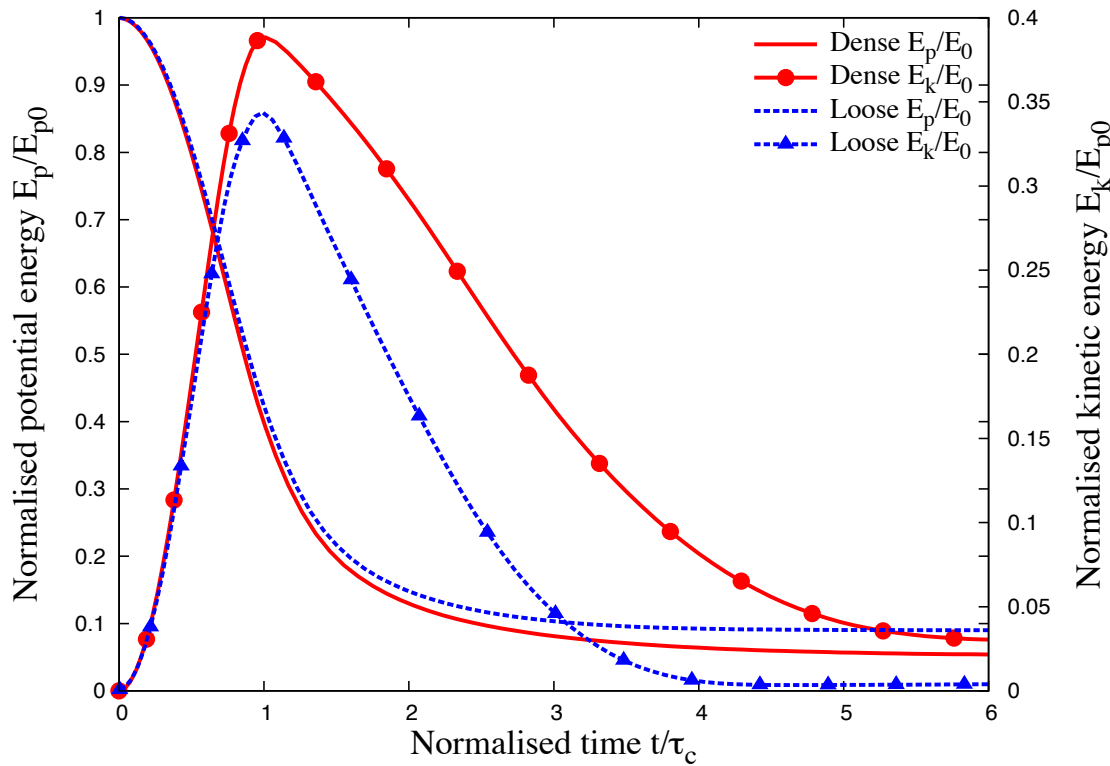


(b) Evolution of packing density

Figure 4.20 Effect of density on energy and packing fraction evolution ' $a'$  = 0.8 (poly-dispersity ' $r$ ' = 6)



(a) Effect of density on run-out evolution



(b) Effect of density on energy evolution

Figure 4.21 Effect of density on run-out behaviour and energy evolution ' $a'$  = 0.6

- <sup>1</sup> modelling the run-out behaviour using continuum approaches to predict realistic granular flow  
<sup>2</sup> behaviour.

### <sup>3</sup> 4.3 Slopes subjected to impact loading

<sup>4</sup> Transient granular flows occur very often in nature. Well-known examples are rockfalls,  
<sup>5</sup> debris flows, and aerial and submarine avalanches. In the geotechnical context, transient  
<sup>6</sup> movements of large granular slopes is a substantial factor of risk due to their destructive force  
<sup>7</sup> and the transformations they may produce in the landscape. Natural granular flows may be  
<sup>8</sup> triggered as a result of different processes such as gradual degradation, induced by weathering  
<sup>9</sup> or chemical reactions, liquefaction and external forces such as earthquakes. Most contemporary  
<sup>10</sup> research on granular materials deals with the steady-state flow. Transients and inhomogeneous  
<sup>11</sup> boundary conditions are much less amenable to observation and analysis, and have thus been  
<sup>12</sup> less extensively studied despite their primary importance in engineering practice. In all cases,  
<sup>13</sup> an initially static pile of grains is disturbed by external forces, it then undergoes an abrupt  
<sup>14</sup> accelerated motion and spreads over long distances before relaxing to a new equilibrium state  
<sup>15</sup> when the whole kinetic energy acquired during destabilisation is dissipated by friction and  
<sup>16</sup> inelastic collisions.

<sup>17</sup> This section investigates the ability of MPM, as a continuum approach, to reproduce  
<sup>18</sup> the evolution of a granular pile destabilised by an external energy source. In particular, a  
<sup>19</sup> central issue is whether power-law dependence of the run-out distance and time observed with  
<sup>20</sup> respect to the initial geometry or energy can be reproduced by a simple Mohr-Coulomb plastic  
<sup>21</sup> behaviour for granular slopes subjected an impact energy. Effect of different input parameters,  
<sup>22</sup> such as the distribution of energy and base friction, on the run-out kinematics are studied by  
<sup>23</sup> comparing the data obtained from DEM and MPM simulations. As we shall see, MPM is  
<sup>24</sup> successfully able to simulate the transient evolution with a single input parameter, the internal  
<sup>25</sup> angle of friction. This opens the way to the simulation of geological-scale flows on complex  
<sup>26</sup> topographies.

#### <sup>27</sup> 4.3.1 Numerical set-up

<sup>28</sup> The DEM sample is composed of  $\sim 13000$  disks with a uniform distribution of diameters by  
<sup>29</sup> volume fractions ( $d_{max} = 1.5d_{min}$ ). The mean grain diameter and mass are  $d \simeq 2.455$  mm and  
<sup>30</sup>  $m \simeq 0.0123$  kg, respectively. The grains are first poured uniformly into a rectangular box of  
<sup>31</sup> given width and then the right-hand side wall is shifted further to the right to allow the grain to  
<sup>32</sup> spread. A talus is obtained when all grains come to rest; see figure 4.22. This procedure leads

to a mean packing fraction  $\simeq 0.82$ . Soil grains with mean density of  $2600 \text{ kg m}^{-3}$  and internal friction coefficient of 0.4 between grains is adopted.

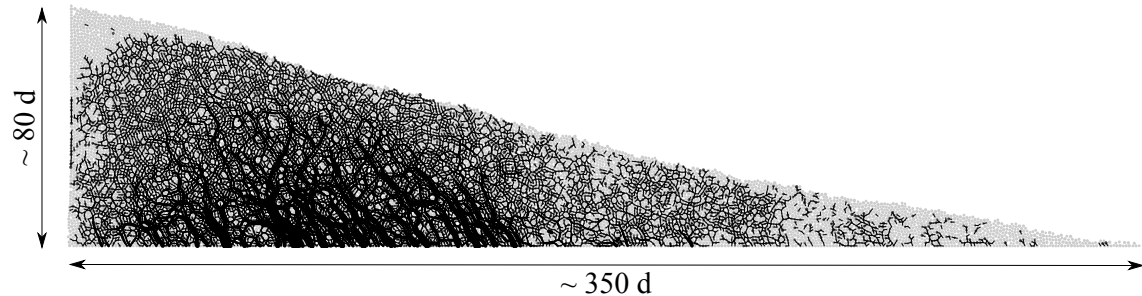


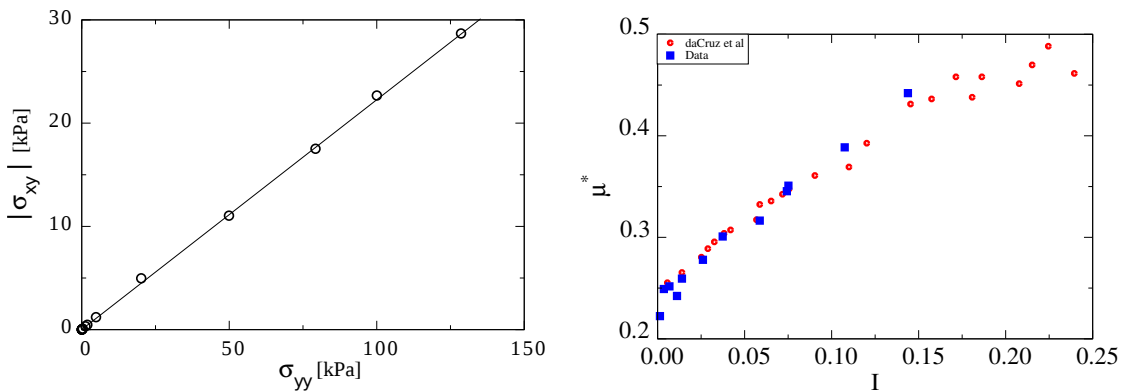
Figure 4.22 Initial geometry and dimensions of the pile

The initial static pile is set into motion by applying a constant horizontal gradient  $v_{0x}(y) = k(y_{max} - y)$  with  $k > 0$ . Such a configuration mimics the energy transfer mechanism of a horizontal quake along the bottom of the pile. The evolution of pile geometry and the total kinetic energy as a function of the initial input energy  $E_0$  is studied. The run-out distance  $L_f$  is the distance of the rightmost grain, which is still in contact with the main mass when the pile comes to rest. The run-out will be normalized by the initial length  $L_0$  of the pile, as in the experiments of collapsing columns. The total run-out duration  $t_f$  is the time taken by the pile to reach its final run-out distance  $L_f$ .

For grain scale simulations, classical DEM and Contact Dynamics approach are used. This research is done in collaboration with Patrick Mutabaruka, University of Montpellier, who performed Contact Dynamics (CD) simulations that are presented in this section. A detailed description of the Contact Dynamics method can be found in [Jean \(1999\)](#); [Moreau \(1993\)](#); [Radjai and Dubois \(2011\)](#); [Radjai and Richefeu \(2009\)](#). The CD method is based on implicit time integration of the equations of motion and a nonsmooth formulation of mutual exclusion and dry friction between particles. The CD method requires no elastic repulsive potential and no smoothing of the Coulomb friction law for the determination of forces. For this reason, the simulations can be performed with large time steps compared to discrete element simulations. The unknown variables are particle velocities and contact forces, which are calculated at each time step by taking into account the conservation of momenta and the constraints due to mutual exclusion between particles and the Coulomb friction. An iterative research algorithm based on a non-linear Gauss-Seidel scheme is used. The only contact parameters within the CD method are the friction coefficient  $\mu$ , the normal restitution coefficient  $\varepsilon_n$  and the tangential restitution coefficient  $\varepsilon_t$  between particles.

The natural units of the system are the mean grain diameter  $d$ , mean grain mass  $m$  and gravity  $g$ . For this reason, the length scales are normalised by  $d$ , time by  $(d/g)^{1/2}$ , velocities by

<sup>1</sup>  $(gd)^{1/2}$  and energies by  $mgd$ . In MPM simulations the material point spacing is kept the same  
<sup>2</sup> as the mean grain diameter. A mesh size of 0.0125m is adopted with 25 material points per cell.  
<sup>3</sup> The effect of mesh size and the number of material points per cell is investigated in section 4.3.5.  
<sup>4</sup> A Mohr-Coulomb model with no dilation is used to simulate the continuum behaviour of the  
<sup>5</sup> granular pile. Periodic shear tests using CD, see figure 4.23a, reveals a macroscopic friction  
<sup>6</sup> coefficient of 0.22. The evolution of inertial number with friction is presented in figure 4.23b.



(a) Evaluating the critical state friction angle from periodic shear test. (b) Evolution of Inertial number with friction  $\mu^*$

Figure 4.23 Periodic shear test using CD (Mutabaruka, 2013).

### 4.3.2 Evolution of pile geometry and run-out

<sup>8</sup> Figure 4.24 shows the initial evolution of granular slope subjected to an initial impact energy  
<sup>9</sup>  $E_0 = 61$  (in dimensionless units) using MPM. As the granular slope is sheared along the bottom,  
<sup>10</sup> the shear propagates to the top leaving a cavity in the vicinity of the left wall. This cavity gets  
<sup>11</sup> partially filled as the granular mass at the top collapse behind the flowing mass due to inertia.  
<sup>12</sup> Similar behaviour is observed during the initial stages of the flow evolution using DE and CD  
<sup>13</sup> techniques (see figure 4.25). Due to inertia, the grains at the top of the granular heap roll down  
<sup>14</sup> to fill the cavity, while the pile continues to spread.

<sup>15</sup> The flow involves a transient with a sharp change in the geometry of the pile followed  
<sup>16</sup> by continuous spreading. The gradient input energy applied to the granular slope mimics  
<sup>17</sup> a horizontal quake from the bottom. Despite the creation of a cavity behind the flowing  
<sup>18</sup> mass, the granular heap always remains in contact with the left wall irrespective of the input  
<sup>19</sup> energy. Figure 4.26a shows the normalized run-out distance  $(L_f - L_0)/L_0$  and total run-out time  
<sup>20</sup>  $t_f$  as a function of the input energy  $E_0$ . Two regimes characterized by power-law relationship  
<sup>21</sup> between the run-out distance and time as a function of  $E_0$  can be observed. In the first  
<sup>22</sup> regime, corresponding to the range of low input energies  $E_0 < 40 mgd$ , the run-out distance

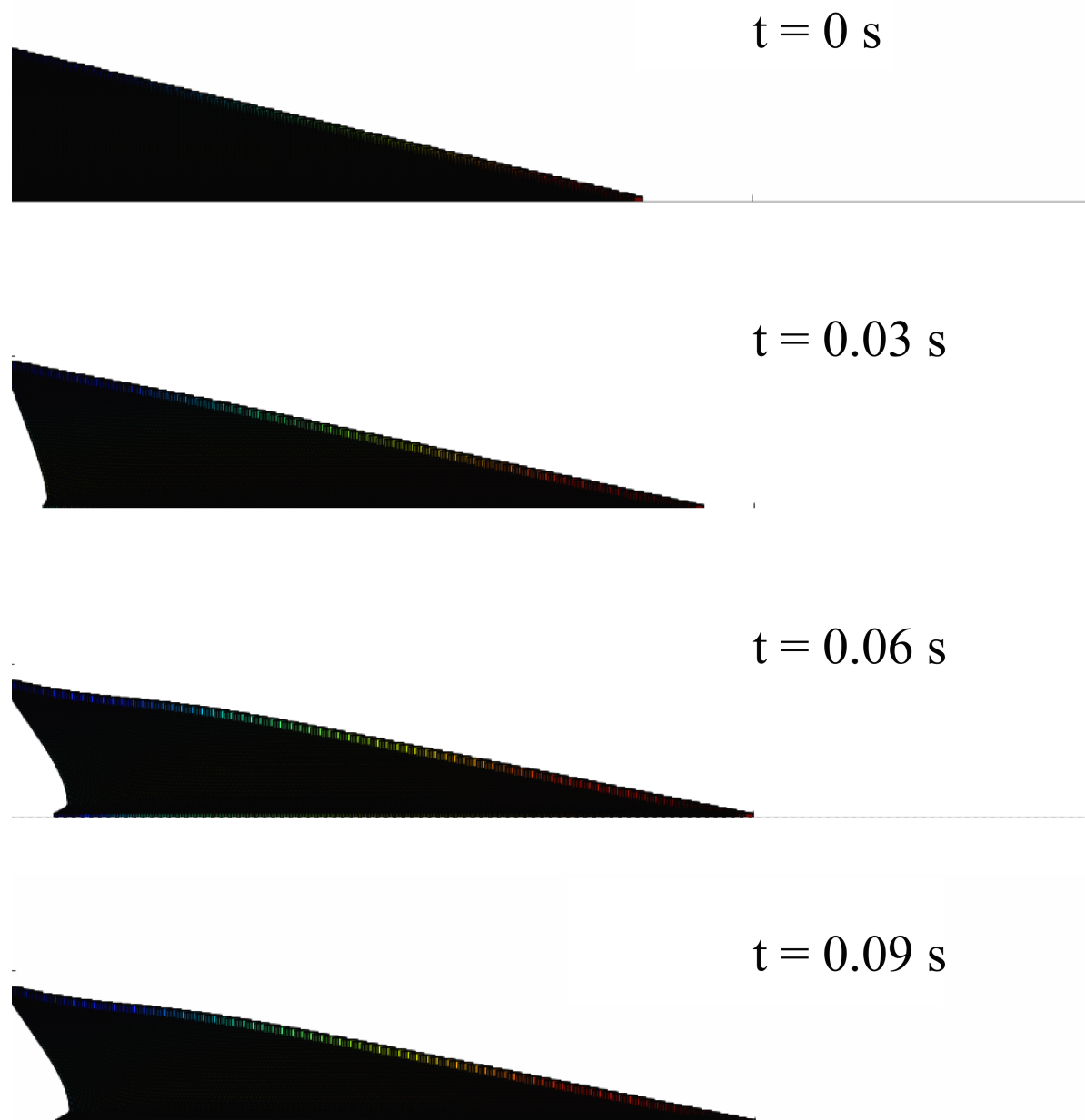


Figure 4.24 MPM simulation of the initial stages of granular pile subjected to a gradient impact energy.

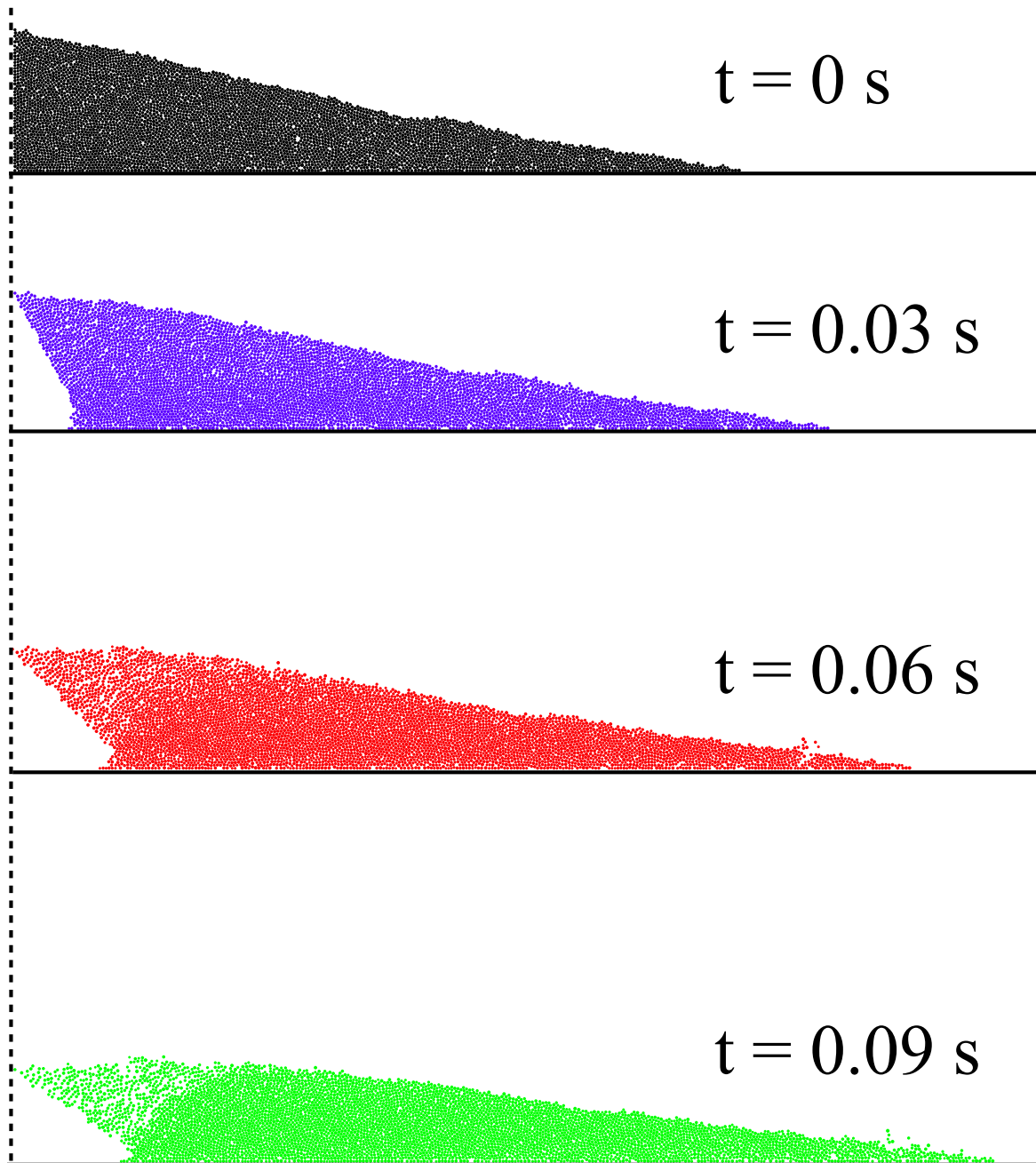


Figure 4.25 CD simulation of the initial stages of granular pile subjected to a gradient impact energy. ([Mutabaruka, 2013](#)).

observed varies as  $L_f \propto (E_0)^\alpha$  with  $\alpha \simeq 0.206 \pm 0.012$  over nearly one decade. Overall, the run-out distance predicted by the continuum approach matches the DEM simulations. At very low energies, DEM simulations show longer run-out distance due to local fluidisation. The difference in the run-out between DEM and CD arise mainly from the scales of description and the inelastic nature of Contact Dynamics. Similar behaviour between DEM and CD approaches was observed by Radjai et al. (1997).

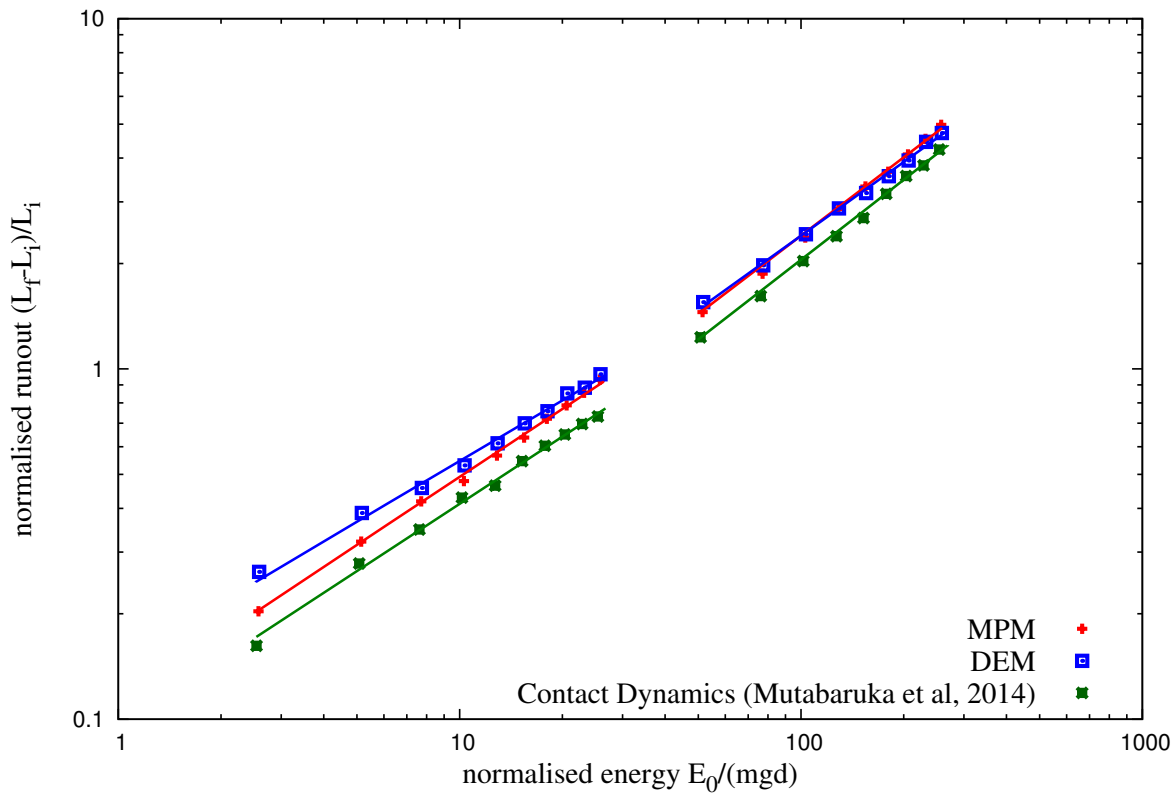
While the run-out exhibits a power-law relation with the initial input energy, DEM simulations show that the flow duration remains constant at a value  $t_f \simeq 60 (d/g)^{0.5}$  irrespective of the value of  $E_0$ . The constant run-out time, in grain-scale simulations, indicates the collapse of grain into the cavity left behind the pile. An average run-out speed can be defined as  $v_s = (L_f - L_0)/t_f$ . According to the data,  $v_s \propto (E_0)^{0.52 \pm 0.012}$ . The error on the exponent represents the confidence interval of linear fits on the logarithmic scale. Since the initial average velocity varies as  $v_0 \propto (E_0)^{0.5}$ , this difference between the values of the exponents suggests that the mobilized mass during run-out declines when the input energy is increased.

In the second regime, corresponding to the range of high input energies  $E_0 > 40 \text{ mgd}$ , the run-out distance varies as  $L_f \propto (E_0)^{\alpha'}$  over one decade with  $\alpha' \simeq 0.56 \pm 0.04$  while the duration increases as  $t_f \propto (E_0)^{\beta'}$  with  $\beta' \simeq 0.33 \pm 0.02$ . Hence, in this regime the average run-out speed varies as  $v_s \propto (E_0)^{0.498 \pm 0.01}$ . This exponent is close to the value 0.5 in  $v_0 \propto (E_0)^{0.5}$ , and hence, within the confidence interval of the exponents, in the second regime we may assume  $\beta' \simeq \alpha' - 0.5$  and  $v_s \propto v_0$ . In the second regime, both DEM and MPM predict almost the same run-out behaviour. However, MPM predicts longer duration with increase in input energy.

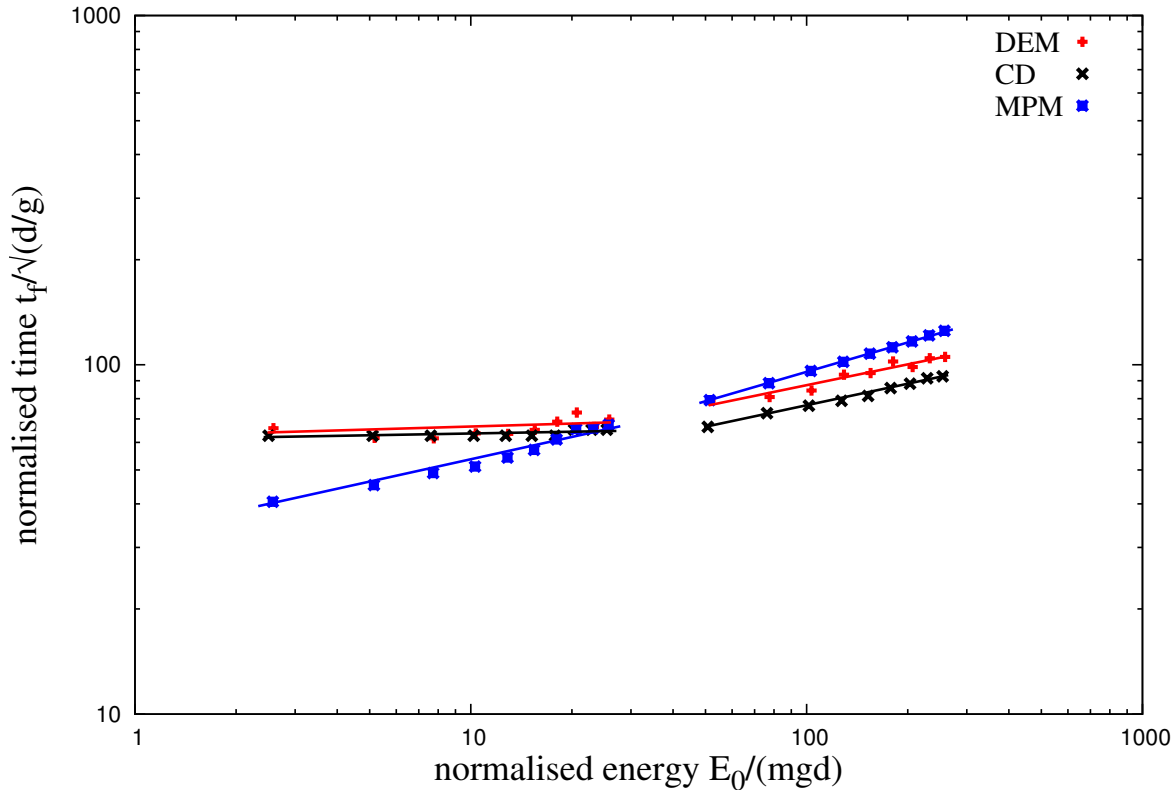
It is worth noting that a similar power-law dependence of the run-out distance and time were found in the case of granular column collapse with respect to the initial aspect ratio. In the column geometry, the grains spread away owing to the kinetic energy acquired during gravitational collapse of the column. Topin et al. (2012) found that the run-out distance varies as a power-law of the available peak kinetic energy at the end of the free-fall stage with an exponent  $\simeq 0.5$ . This value of exponent is lower than the run-out evolution observed in the second regime. This is, however, physically plausible since the distribution of particle kinetic energies at the end of the collapse is more chaotic than in this case where the energy is supplied from the very beginning in a well-defined shear mode. As pointed out by Staron et al. (2005), the distribution of kinetic energies is an essential factor for the run-out distance.

### 4.3.3 Decay of kinetic energy

The non-trivial evolution of the pile geometry in two regimes suggests that the energy supplied to the pile is not simply dissipated by shear and friction along the bottom plane. It is important to split the kinetic energy into the vertical and horizontal components ( $K_{Ex}$  and  $K_{Ey}$ ) of the



(a) Run-out distance as a function of normalised input kinetic energy



(b) Duration of run-out as a function of normalised input kinetic energy

Figure 4.26 Run-out behaviour of a pile subjected a gradient impact energy

velocity field. The input energy is in the  $x$  component, but due to the creation of a cavity next to the left wall and the rolling of the grains down the free surface of the pile and between grains, a fraction of the energy is first transferred to the vertical component of the velocity field and dissipated during the transient phase. The evolution of kinetic energy is studied to understand the behaviour of granular flow that is consistent with the evolution of pile shape.

The evolution of total kinetic energies  $E_k$  with time for different values of the input energy  $E_{ki}$  based on MPM simulations are shown in figure 4.27. MPM simulations shows two distinct regimes in the normalised kinetic energy plot as a function of normalised time figure 4.27b. However, DEM simulations (see figure 4.28) show that the energy evolution corresponding to low energy regime collapse nearly on to a single time evolution. This is consistent with the observation of run-out time  $t_f$  independent of the input energy. In contrast, MPM simulations predict a power law relation between the run-out duration and input energy. However, the plots corresponding to high energy regime collapse only at the beginning of the run-out i.e. for  $t < t_1 \simeq 7.5 (d/g)^{0.5}$ . Although MPM simulations show higher duration of run-out (figure 4.27), the total kinetic energy is completely dissipated at  $t = 60\sqrt{d/g}$ . DEM simulations predict  $t = 80\sqrt{d/g}$  for the kinetic energy to be completely dissipated. This is due particle rearrangement at the free surface (figure 4.29). The granular pile shows some dilation behaviour initially, which is due to grains rolling down to fill the cavity.

Figure 4.30 displays the evolution of kinetic energy in the translational ( $E_x$  and  $E_y$ ) degrees of freedom.  $E_x$  decays similar to the total energy dissipation, but  $E_y$  increases and passes through a peak before decaying rapidly to a negligible level. The transient is best observed for  $E_y$ , which has significant values only for  $t < t_1$ . This energy represents the proportion of kinetic energy transferred to the  $y$  component of the velocity field due to the destabilisation of the pile and collapse of grains in the cavity behind the pile. Higher proportion of vertical acceleration  $E_{ky}/E_0$  is observed for lower values of input energy  $E_0$ . This means that, at lower input energies a larger fraction of the energy is consumed in the destabilisation process. Whereas at a higher input energies, most of the energy is dissipated in the spreading phase. For this reason, the total duration  $t_1$  of this destabilisation phase is nearly the same in both regimes and its value is controlled by the gravity rather than the input energy. The height of the pile being of the order of  $80 d$ , the total free-fall time for a particle located at this height is  $\simeq 12 (d/g)^{0.5}$ , which is of the same order as  $t_1$ . The contribution of the rotational energy during the transient stage and the spreading stage is negligible.

To analyse the second phase for higher input energies, the kinetic energy  $E'_{kx0}$  available at the end of the transient phase is considered. This energy is responsible for most of the run-out and hence it is expected to control the run-out distance and time. Figure 4.31 shows the evolution of  $E_{kx}$  normalized by  $E'_{kx0}$  as a function of time. The plots have seemingly the

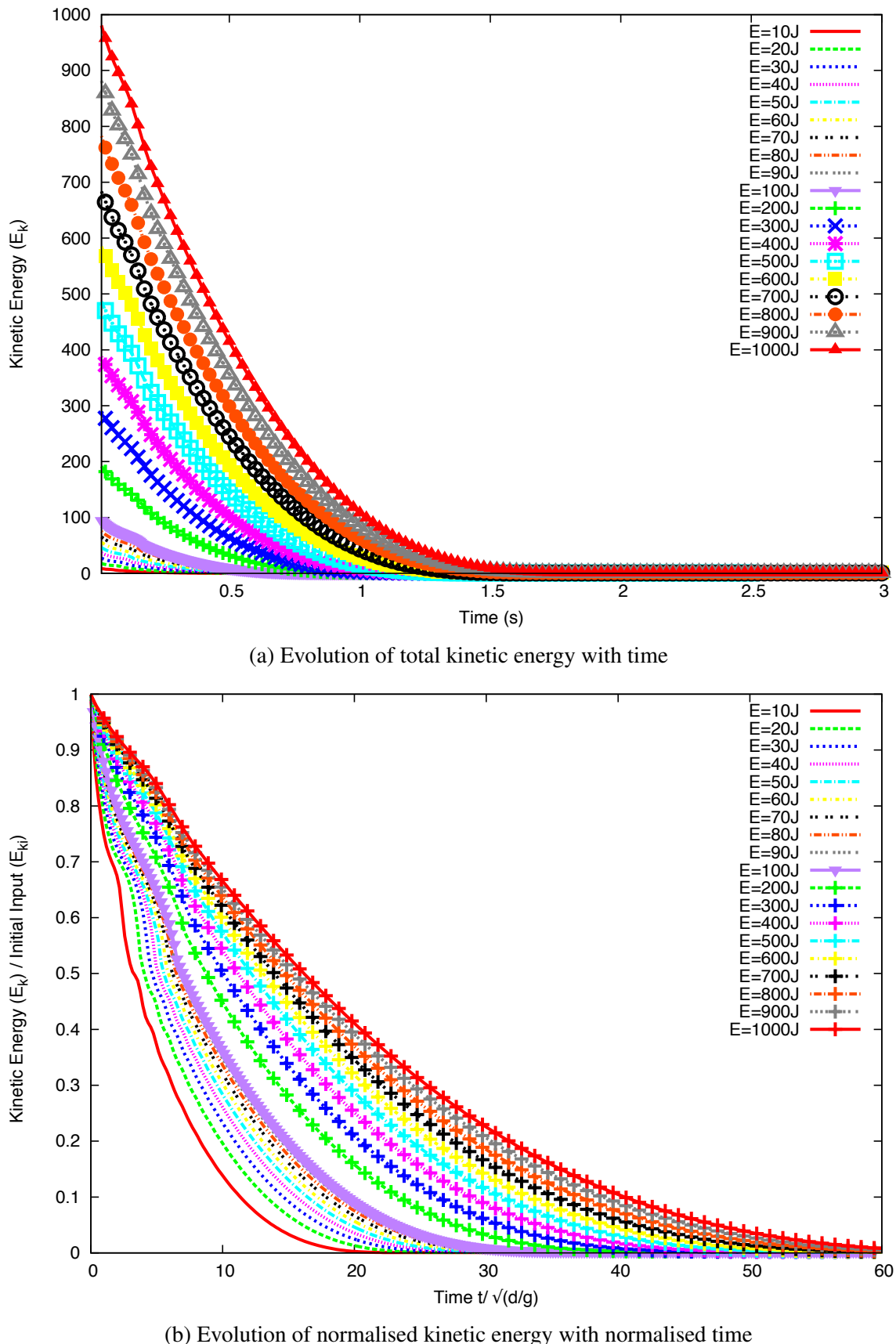


Figure 4.27 Evolution of kinetic energy with time (MPM)

## 4.3 Slopes subjected to impact loading

43

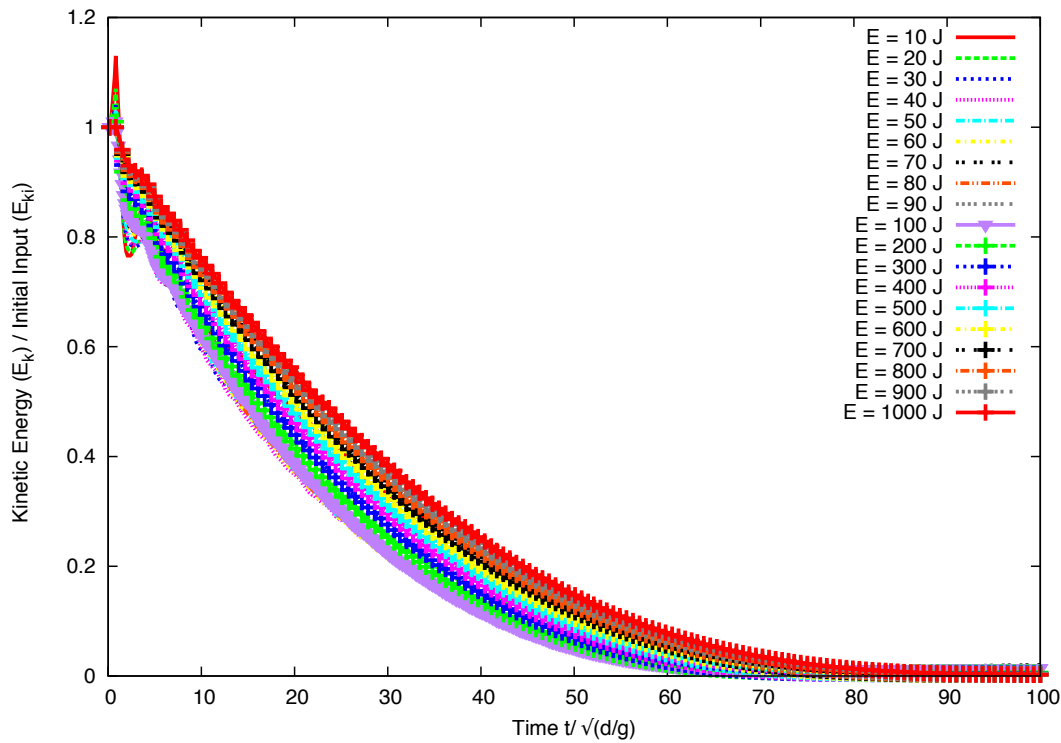
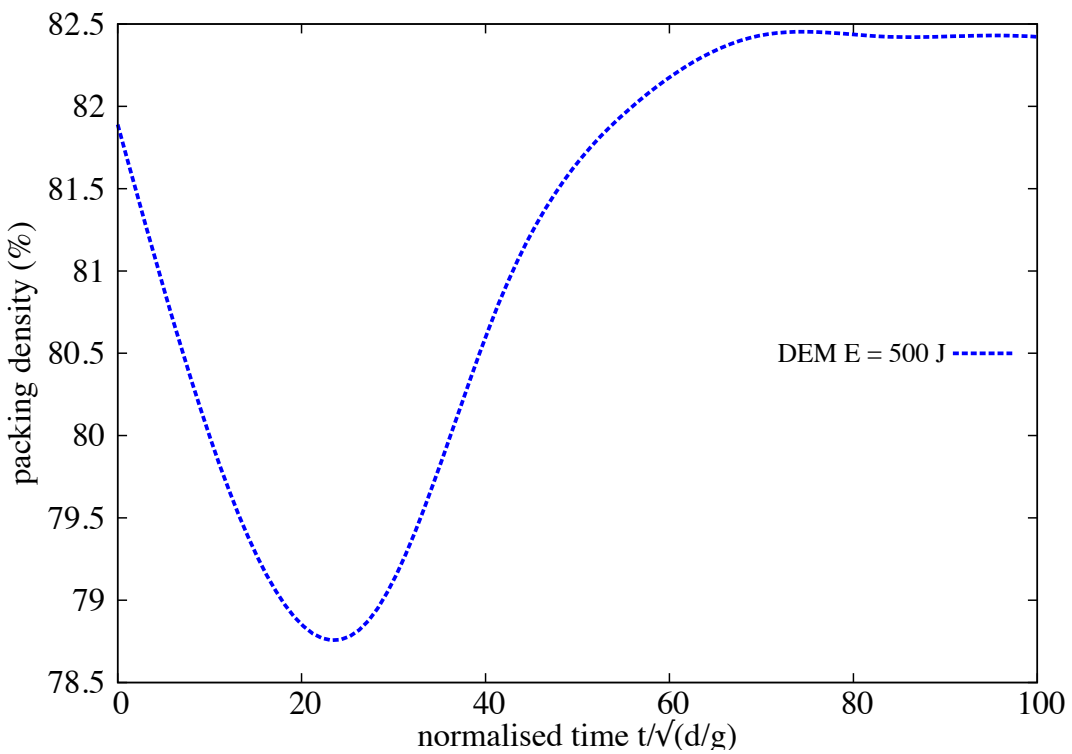
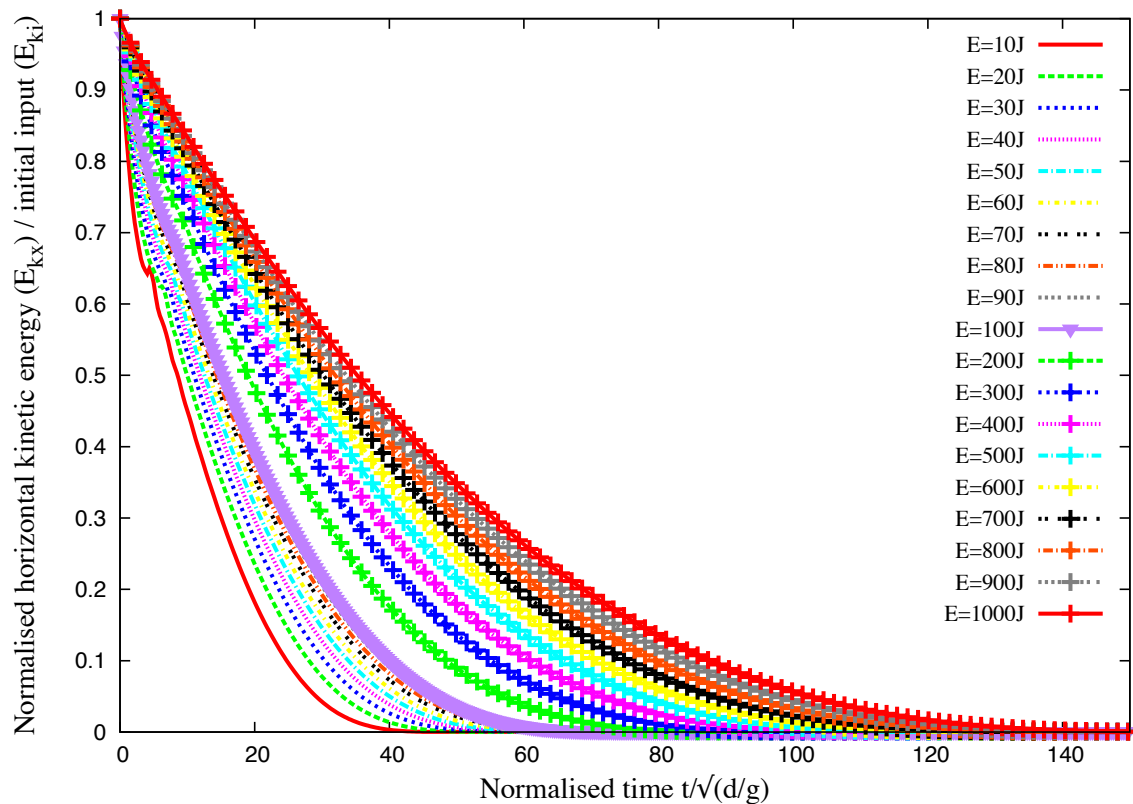
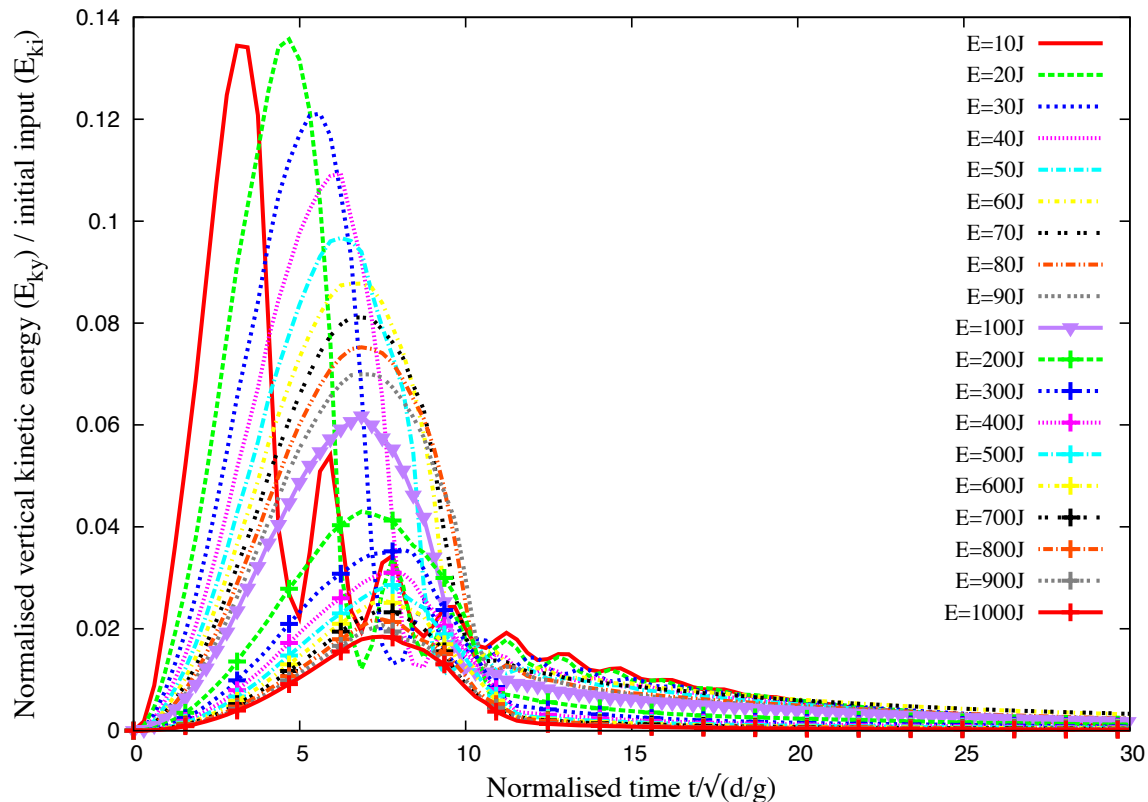


Figure 4.28 Evolution of normalised kinetic energy with normalised time

Figure 4.29 Evolution of packing density with time  $E_0 = 152mgd$  (DEM)



(a) Evolution of normalised horizontal kinetic energy with time



(b) Evolution of normalised vertical kinetic energy with time

Figure 4.30 Evolution of vertical and horizontal kinetic energy with time (MPM)

## 4.3 Slopes subjected to impact loading

45

same aspect but they show different decay times. A decay time  $\tau$  can be defined as the time required for  $E_{kx}$  to decline by a factor 1/2. Figure 4.32 shows the same data in which the time  $t'$  elapsed since  $t_1$  is normalized by  $\tau$ . Interestingly, now all the data nicely collapse on to a single curve. However, this curve can not be fitted by simple functional forms such as variants of exponential decay. This means that the spreading of the pile is not a self-similar process in agreement with the fact that the energy fades away in a finite time  $t'_f$ .

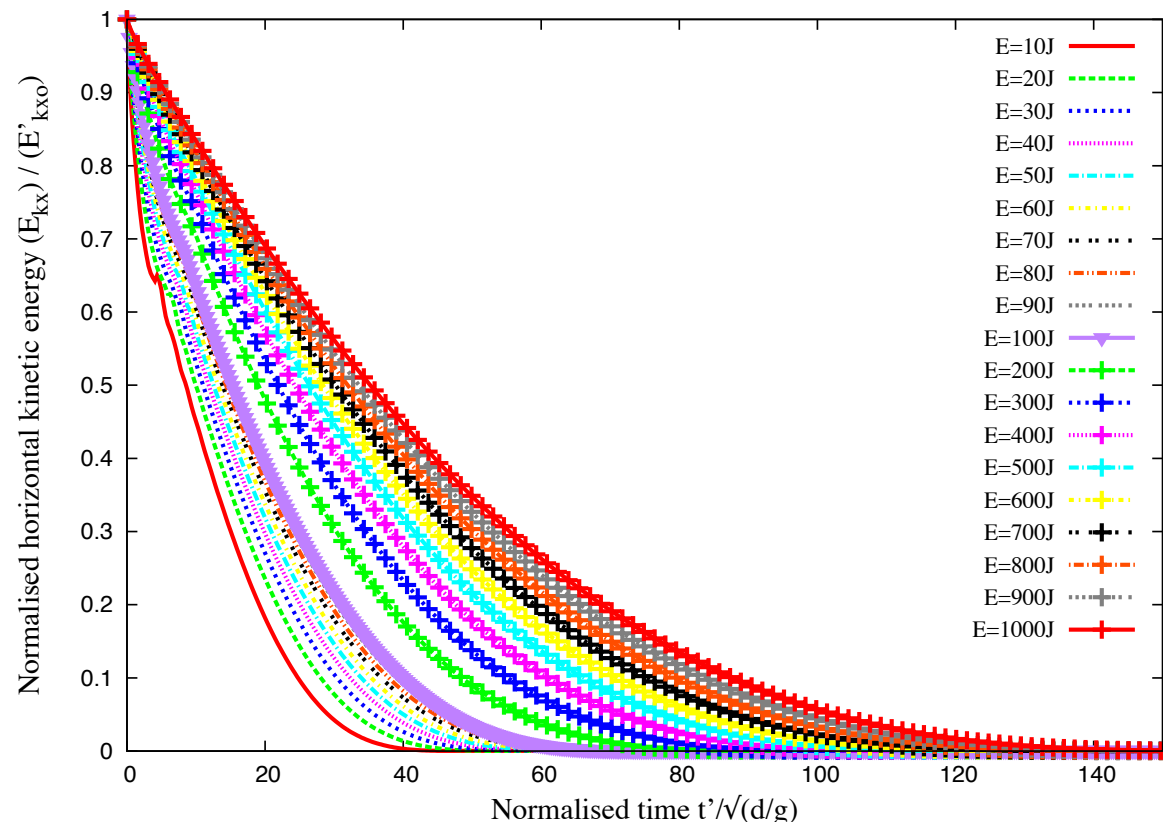


Figure 4.31 Evolution of kinetic energy in the  $x$  component of the velocity field normalized by the available kinetic energy at the end of the transient as a function of time elapsed since the same instant (MPM).

The scaling of the data with the decay time  $\tau$  suggests that the run-out time  $t'_f$ , since the beginning of the second phase, might be a simple function of  $\tau$ . Figure 4.33a shows both  $t'_f$  and  $\tau$  as a function of  $E'_{x0}$ , where a power-law relation can be observed for both time scales. The run-out time  $t'_f \propto (E'_{x0})^{\beta'}$  has the same exponent  $\beta' \simeq 0.33 \pm 0.02$  as  $t_f$  as a function of  $E_0$ . For the decay time we have  $\tau \propto (E'_{x0})^{\beta''}$  with  $\beta'' \simeq 0.38 \pm 0.03$ . The relation between the two times can thus be expressed as (see figure 4.33b)

$$t'_f = k \tau (E'_{x0})^{\beta'' - \beta'}, \quad (4.13)$$

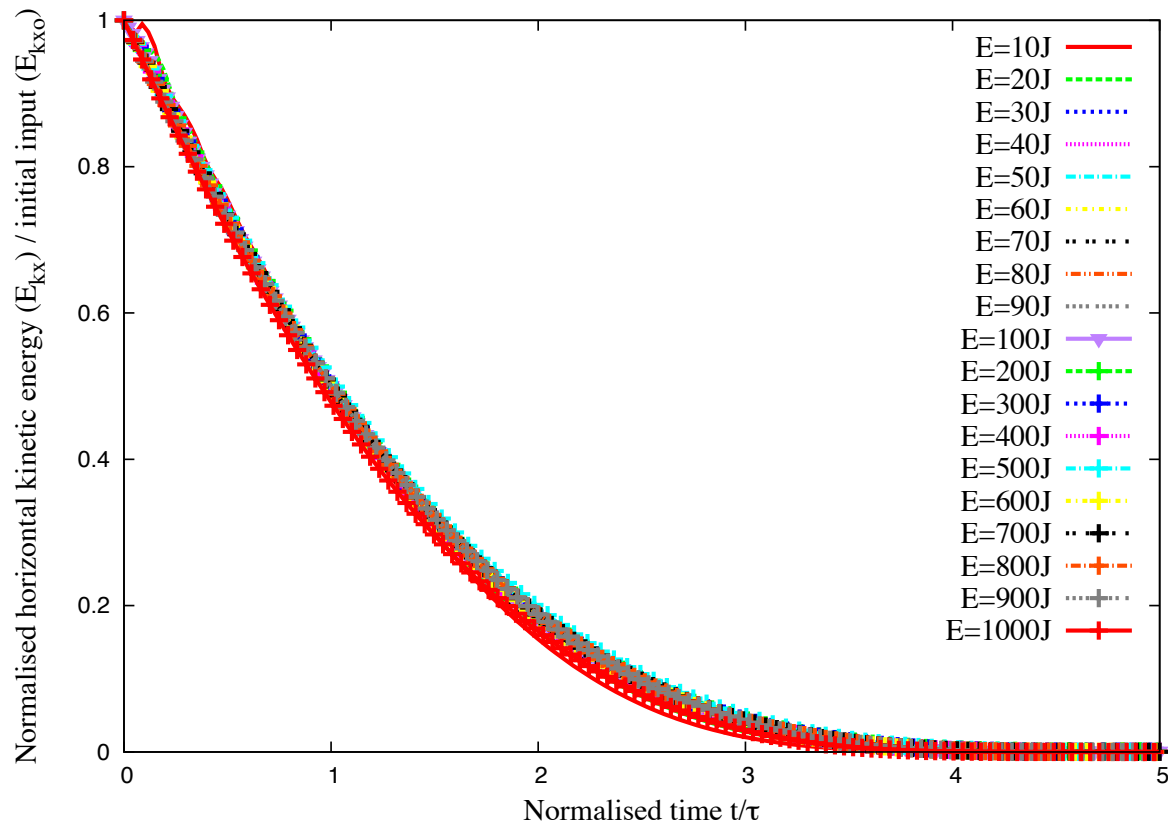


Figure 4.32 Evolution of kinetic energy in the  $x$  component of the velocity field normalized by the available kinetic energy at the end of the transient as a function of normalized time (MPM).

where  $k \simeq 5 \pm 0.4$  and  $\beta'' - \beta' \simeq -0.06 \pm 0.05$ . This value is small enough to be neglected within the confidence interval of the data. It is therefore plausible to assume that the run-out time is a multiple of the decay time and the spreading process is controlled by a single time. A weak dependence on the energy  $E'_{kx0}$  is consistent with the fact that the energy available at the beginning of the second phase is not dissipated in the spreading process (calculated from the position of the tip of the pile) since the pile keeps deforming by the movements of the grains at the free surface even when the tip comes to rest. This can explain the small difference between the two exponents as observed here.

#### 4.3.4 Effect of friction

The run-out distance, duration of flow, and the dissipation of kinetic energy are controlled by the input energy and collective dynamics of the whole pile. However, the run-out behaviour is expected to also depend on the base friction. A series of simulations with different values of base friction was performed using MPM to analyse the influence of friction on the run-out behaviour. The influence of friction on the run-out behaviour is shown in figure 4.34a. The exponent of the power-law relation between the run-out and input energy has a weak dependence on the base friction, the proportionality constant, however, is affected by the change in the base friction. This behaviour is similar to that observed in granular column collapse with varying initial properties (Balmforth and Kerswell, 2005; Lajeunesse et al., 2005).

CD simulations using different values of coefficient of restitution show no difference in the run-out behaviour. At large input energies, the pile remains in a dense state so that multiple collisions inside the pile occur at small time scales compared to the deformation time. When the restitution coefficients are increased, more collisions occur during a longer time interval but the overall energy dissipation rate by collisions remains the same. This effect is a seminal example of collective effects which erase the influence of local parameters at the macroscopic scale.

In contrast with the restitution coefficients, the effect of friction coefficient, however, is quite important for the run-out. MPM simulations with varying friction coefficient shows that, both the run-out distance and the decay time decrease as the friction coefficient is increased. This effect is much more pronounced at low values of the friction coefficient. Similar behaviour was observed in CD simulations. The run-out time, for example, is reduced by a factor of  $\approx 4$  as  $\mu_s$  is increased from 0.1 to 0.2 while the change in the run-out and duration is less effected with increase in friction coefficient. This “saturation effect” can be observed in a systematic way in simple shear tests. The dissipation rate may reach a saturation point where the dilation of granular materials and rolling of the grains change in response to increase in friction coefficient Estrada et al. (2008).

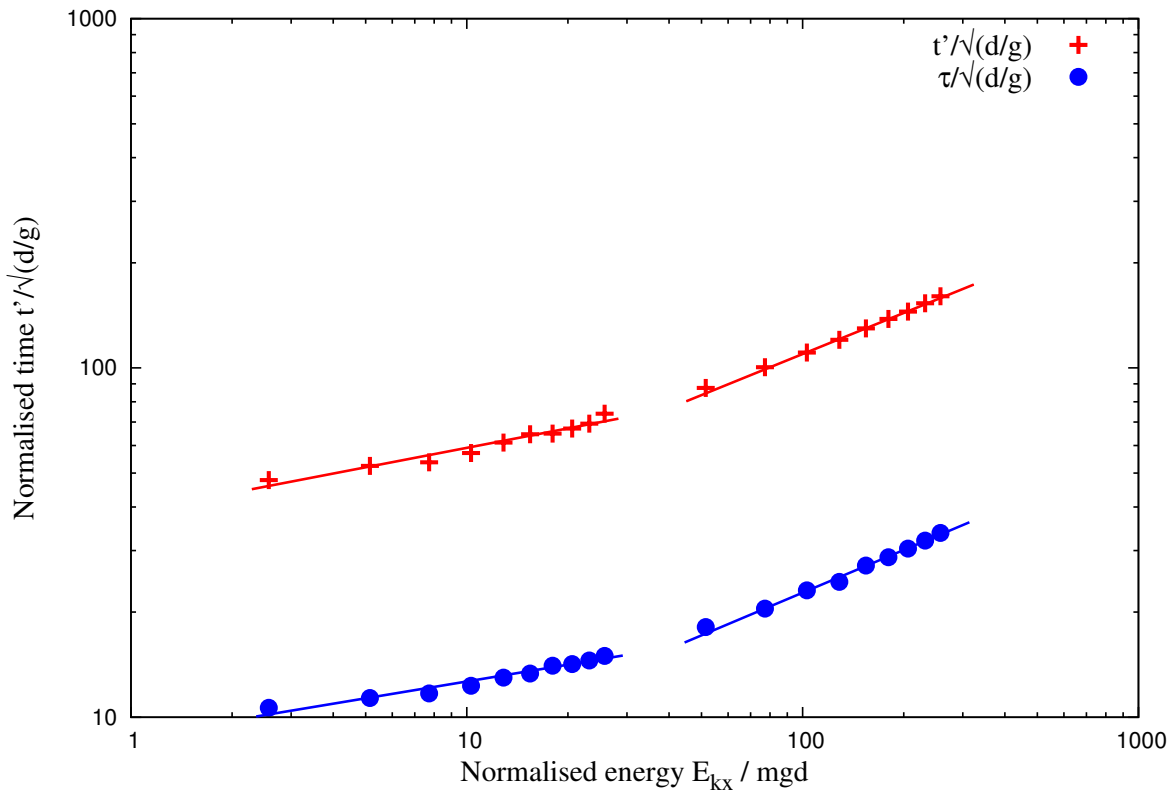
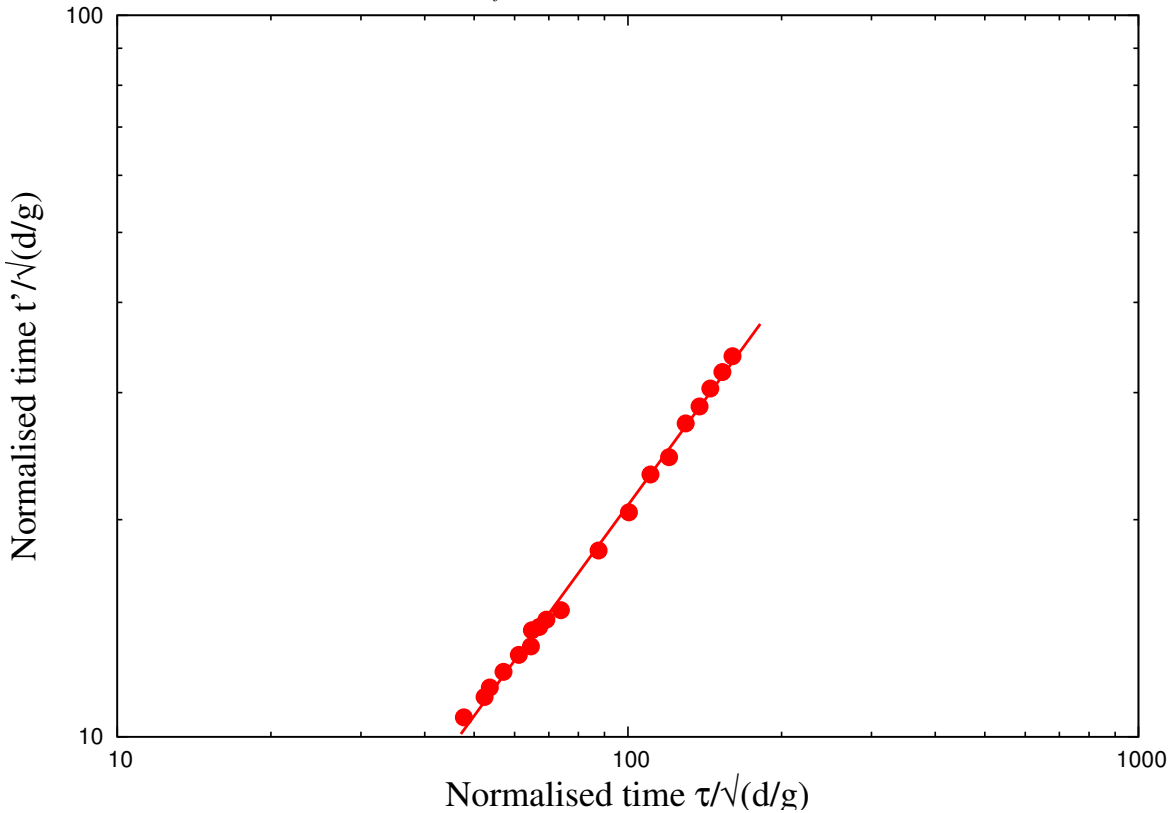
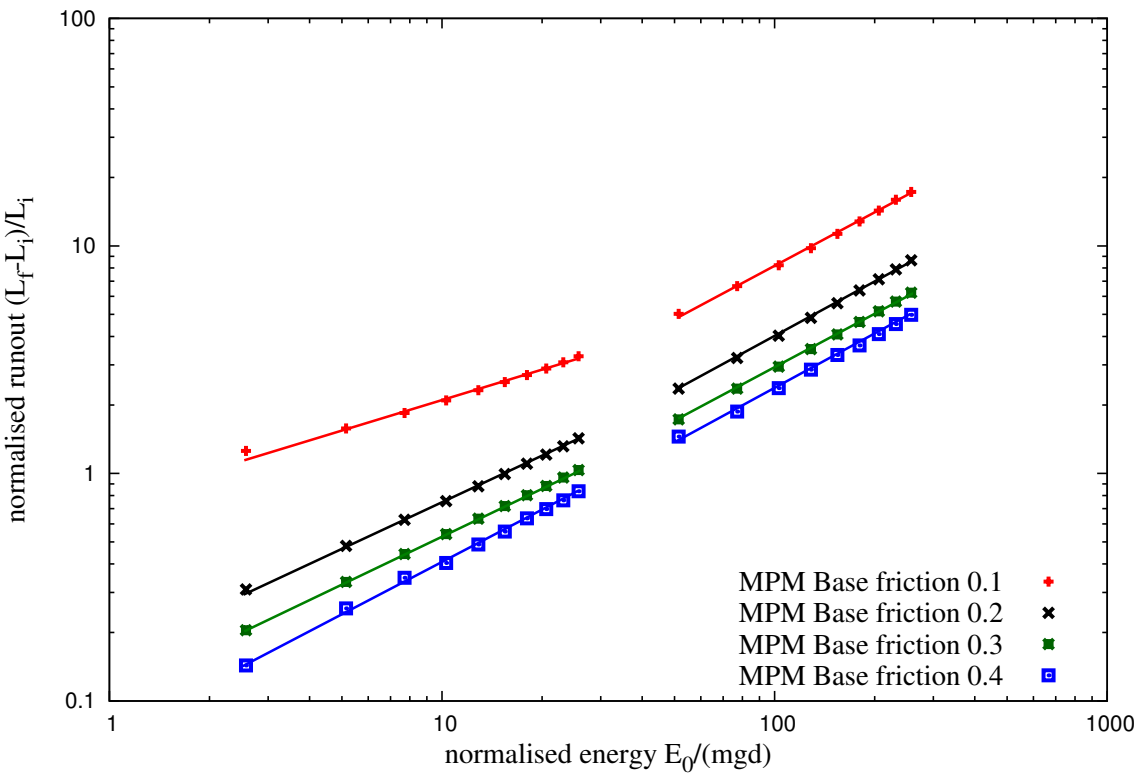
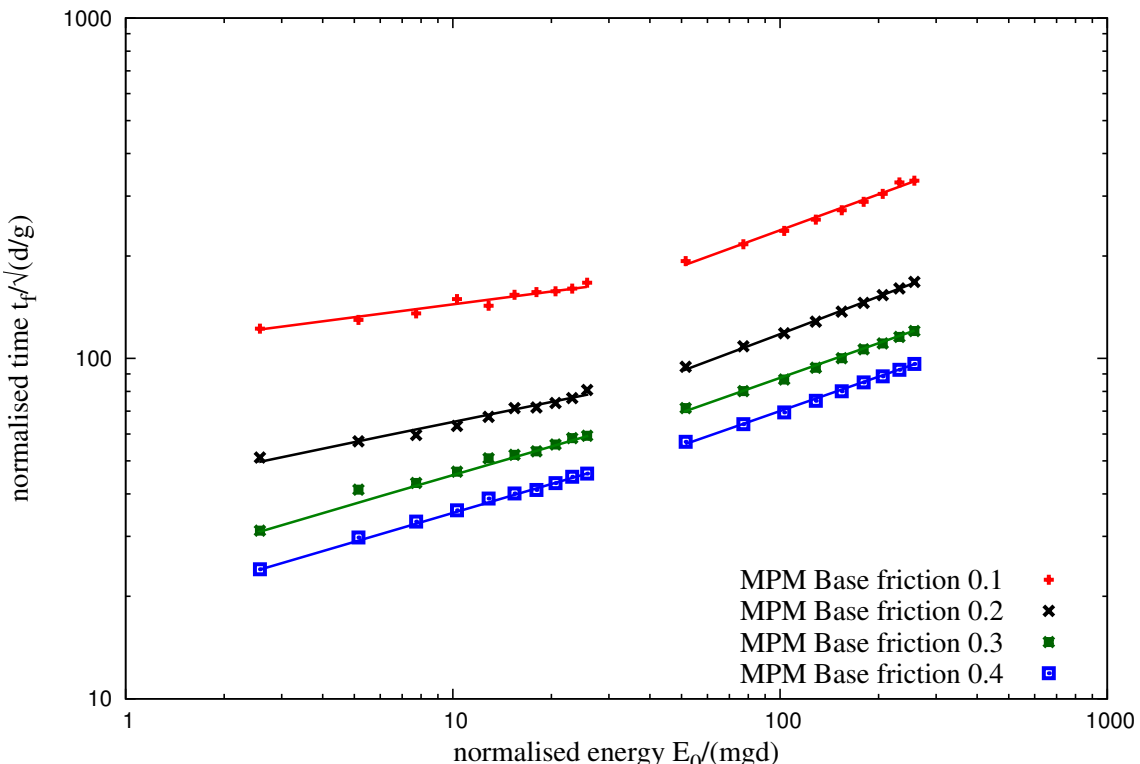
(a) Power law evolution of  $t'_f$  and  $\tau$  as a function of kinetic energy  $E'_{kx0}$ .(b) Linear relationship between decay time and run-out time after the transient as a function of the normalised kinetic energy  $E_{kx0}$ .

Figure 4.33 Decay time and run-out time as a function of the normalised kinetic energy  $E_{kx0}$ .

## 4.3 Slopes subjected to impact loading



(a) Effect of friction on the run-out distance



(b) Effect of friction on the duration of run-out.

Figure 4.34 Effect of friction on the run-out behaviour

**<sup>1</sup> 4.3.1 Effect kinetic energy distribution**

<sup>2</sup> [Staron et al. \(2005\)](#) observed that the distribution of kinetic energies is an essential factor for  
<sup>3</sup> the run-out distance. In order to understand the influence of energy distribution on the run-out  
<sup>4</sup> behaviour, granular pile subjected to two different velocity fields was studied. A uniform  
<sup>5</sup> velocity  $V_{xo}(y) = V_0$  is applied to the entire pile, in contrast to the gradient impact velocity.  
<sup>6</sup> Snapshots of flow kinematics at initial stages are shown in figure [4.35](#) (MPM simulations)  
<sup>7</sup> and figure [4.36](#) (DEM). It can be observed from the figures that the continuum behaviour is  
<sup>8</sup> identical to that of grain-scale simulations. As each grain experiences the same velocity, grains  
<sup>9</sup> located at the top of the slope are pushed farther away and unlike the gradient input velocity,  
<sup>10</sup> the cavity left behind the granular mass is not filled by the soil grains at the top.

<sup>11</sup> Figure [4.37a](#) shows the influence of velocity distribution on the run-out behaviour. At low  
<sup>12</sup> input energy, the gradient velocity distribution shows significantly longer run-out in comparison  
<sup>13</sup> to uniform velocity distribution. Section [4.3.3](#) showed that at lower input energies a larger  
<sup>14</sup> fraction of the energy is consumed in the destabilisation process. Which means that the amount  
<sup>15</sup> energy available for flow is less, in uniform velocity distribution, this energy is even smaller  
<sup>16</sup> due to the uniform distribution of the initial impact velocity. However at higher input energy,  
<sup>17</sup> where most of the energy is dissipated during the spreading phase, the run-out distance has a  
<sup>18</sup> weak dependence on the distribution of velocity in the granular mass. The duration of the flow  
<sup>19</sup> shows similar behaviour to the run-out, however, the slope subjected a gradient velocity flows  
<sup>20</sup> quicker than the uniform velocity distribution. Gradient velocity distribution provides more  
<sup>21</sup> input energy at the initial stage to overcome the frictional resistance at the base. Hence, it can  
<sup>22</sup> be observed that the material property and the distribution of kinetic energy in the system has a  
<sup>23</sup> non-trivial influence on the flow kinematics and the internal flow structure.

**<sup>24</sup> 4.3.5 Effect of mesh size and number of material points per cell**

<sup>25</sup> [Abe et al. \(2013\)](#) observed that for a coarse mesh, the numerical error decreases with increase  
<sup>26</sup> in the number of material points per cell. In contrast, they observed an opposite trend for the  
<sup>27</sup> fine meshes (0.01 ). The influence of numerical noise due to particles crossing the background  
<sup>28</sup> mesh was not observed when the mesh size is greater than 0.05 m. [Coetzee et al. \(2005\)](#) also  
<sup>29</sup> found that the numerical error decreases with increase in mesh refinement.

<sup>30</sup> In the present study, the effect of mesh size and the number of material points per cell on  
<sup>31</sup> the run-out behaviour is investigated. For a mesh size of 0.0125 m, the number of material  
<sup>32</sup> points per cell (PPC) is varied as 4, 16, 25, 36, 64, 81 and 100. The effect of number of material  
<sup>33</sup> points on the run-out behaviour is presented in figure [4.38](#). At low input energy of 50 J, 4  
<sup>34</sup> and 16 material points per cell result in longer run-out distance, where as the run-out distance

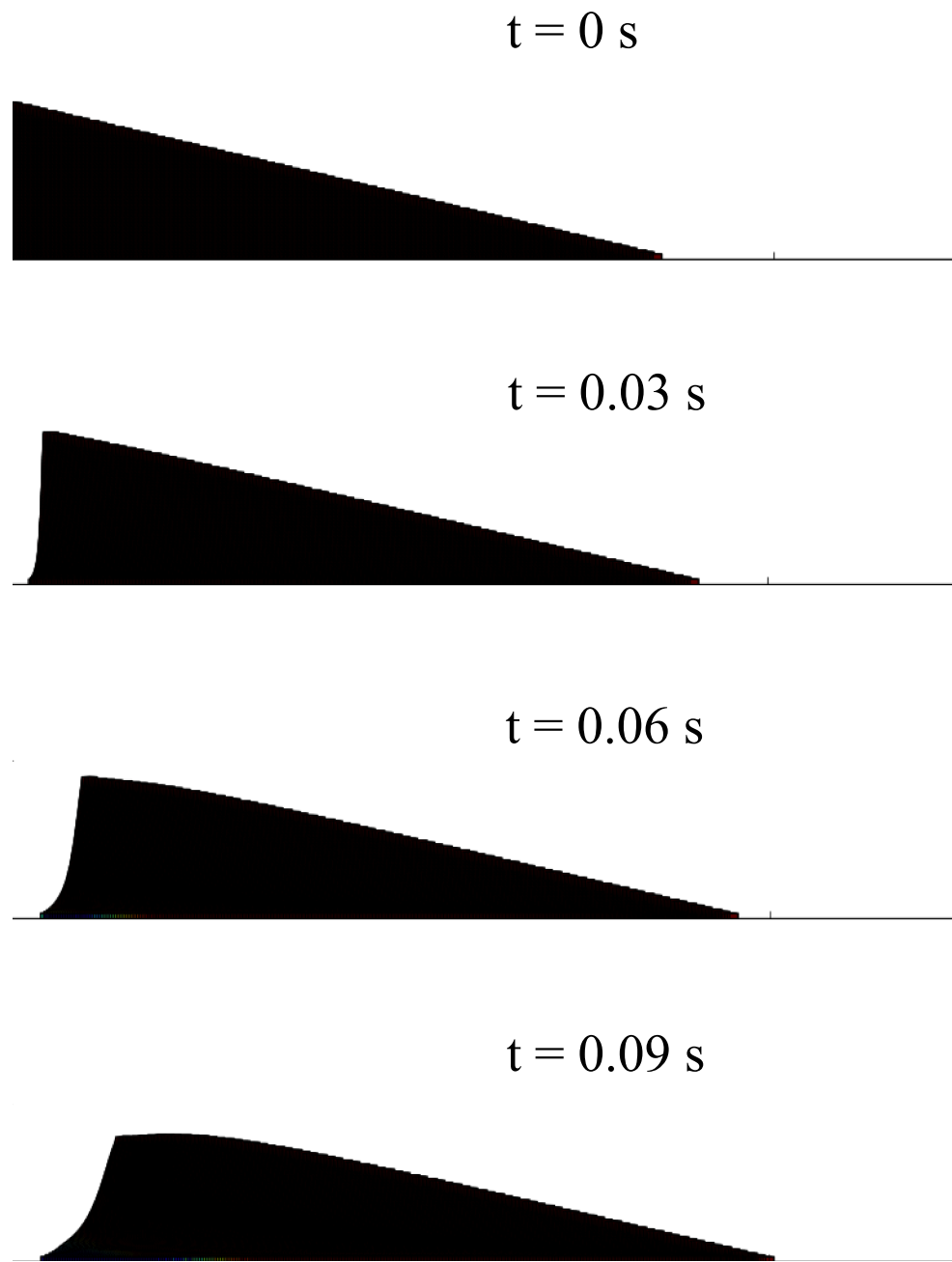


Figure 4.35 Snapshots of MPM simulations of the evolution of granular pile subjected to a gradient impact energy  $E_0 = 61 \text{ mgd}$ .

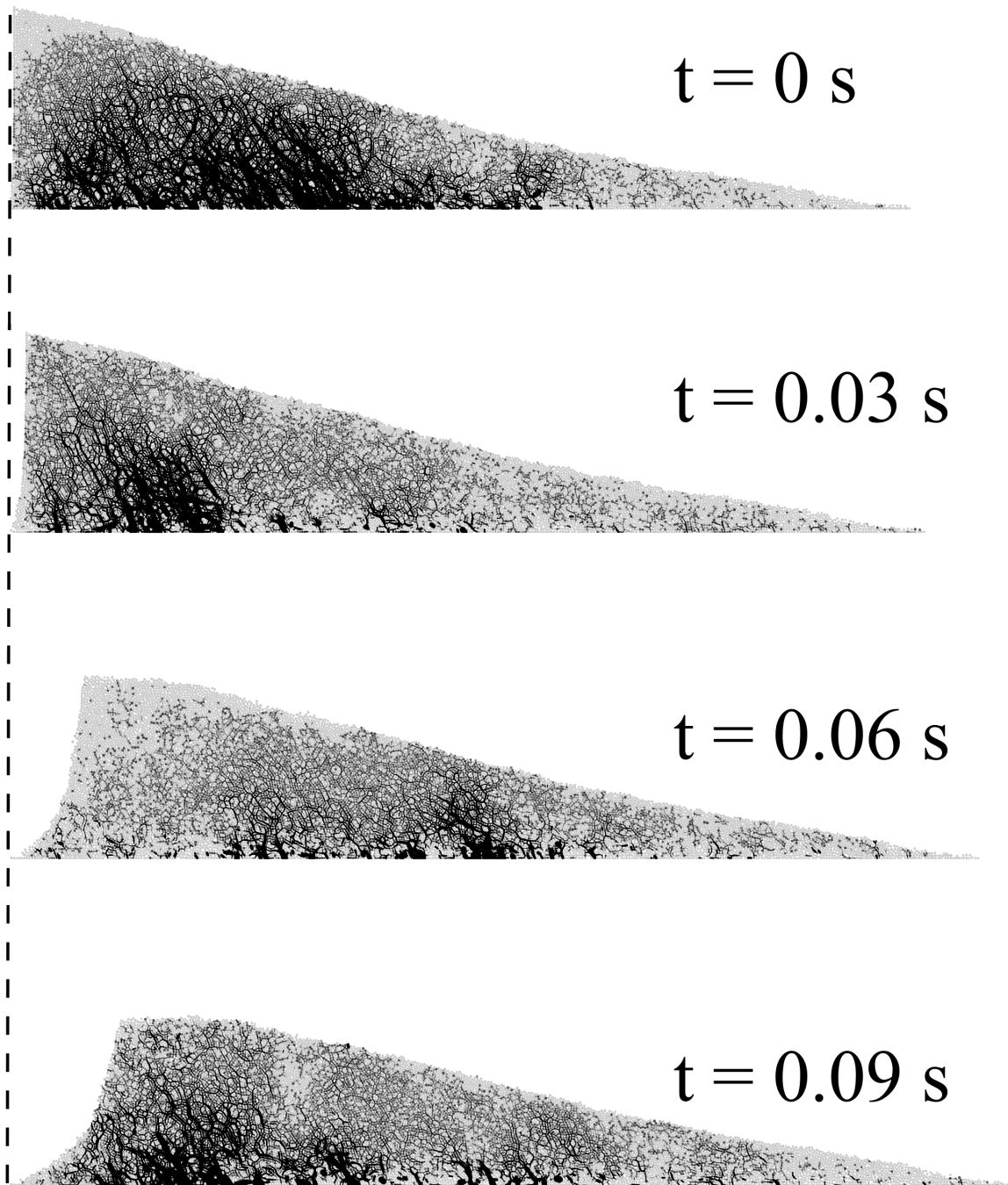
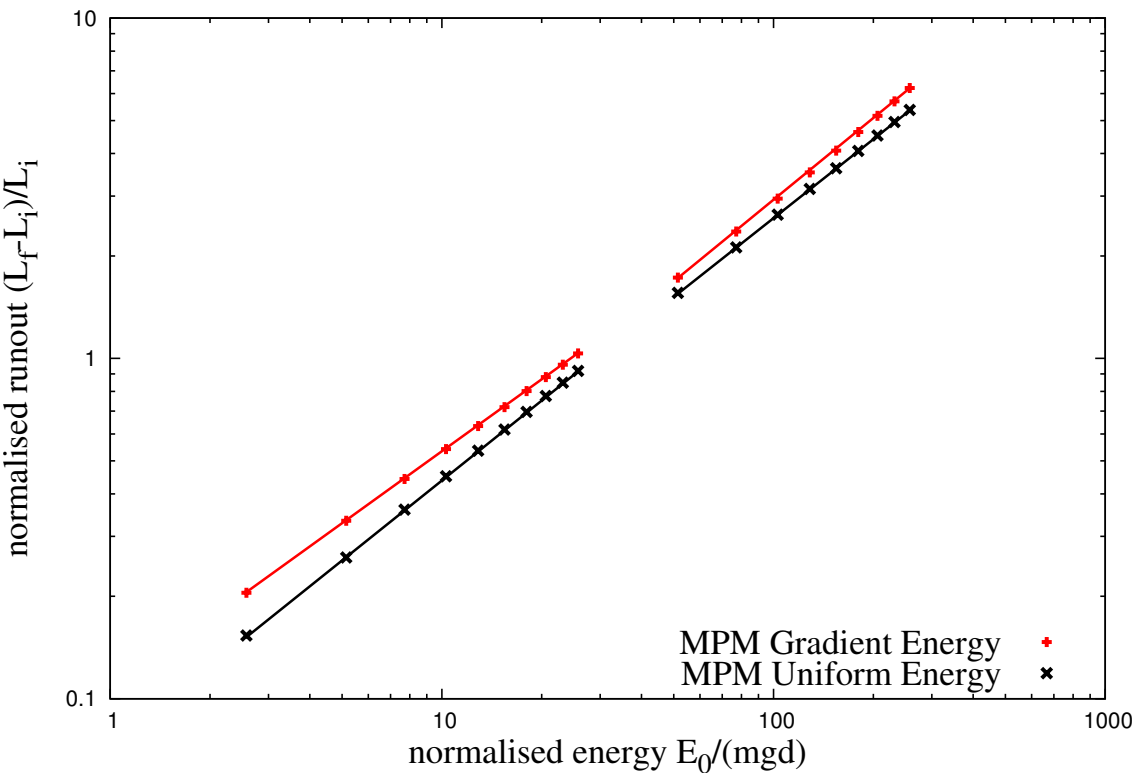
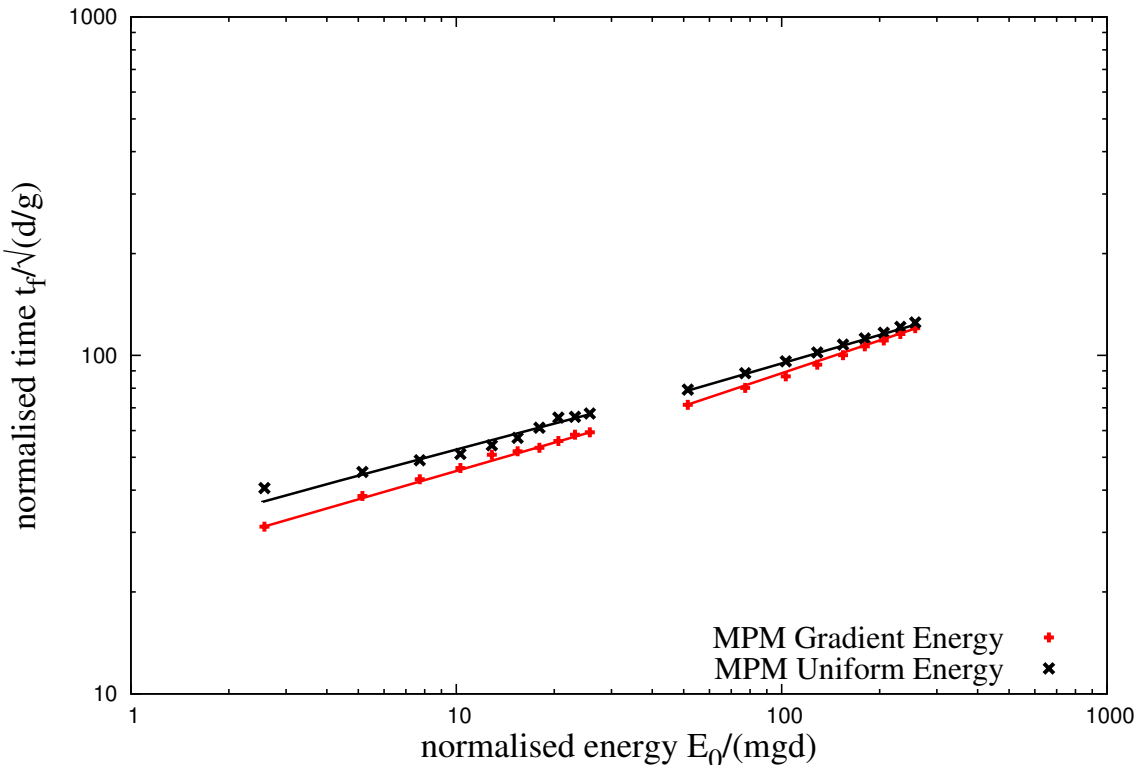


Figure 4.36 Snapshots of DEM simulations of the evolution of granular pile subjected to a gradient impact energy  $E_0 = 61 \text{ mgd}$ .

## 4.3 Slopes subjected to impact loading



(a) Run-out distance as a function of normalised input kinetic energy



(b) Duration of run-out as a function of normalised input kinetic energy

Figure 4.37 Effect of input velocity distribution on the run-out behaviour

<sup>1</sup> converges when the number of PPC is more than 25. While at higher input energy (500 J),  
<sup>2</sup> both 4 and 16 PPC results in almost the same run-out distance, but is higher than the run-out  
<sup>3</sup> predicted with more than 25 points per cell.

<sup>4</sup> The evolution of the granular pile during the initial stage of flow is show in figure 4.39  
<sup>5</sup> for different number of material points per cell. At low input energy, fewer material points  
<sup>6</sup> per cell result in larger separation from the left wall. Distinct shear bands can be observed for  
<sup>7</sup> more than 16 PPC. The flow structure is similar for more than 25 PPC. At higher input energy  
<sup>8</sup> (see figure 4.40), almost all cases predict similar flow structure, except 4 PPC.

<sup>9</sup> Figure 4.41 shows the evolution of kinetic energy with time for varying number of material  
<sup>10</sup> points per cell. At low input energy, the horizontal kinetic energy evolution is identical for all  
<sup>11</sup> cases. A slightly quicker run-out evolution during the spreading phase can be observed for the  
<sup>12</sup> case of 4 material points per cell. However, increase in material points per cell significantly  
<sup>13</sup> affects the evolution of the vertical kinetic energy  $KE_y$ . At low energy, a large proportion of the  
<sup>14</sup> input energy is dissipated in the destabilisation process. This results in material points falling  
<sup>15</sup> behind the spreading mass to the fill the cavity. Fewer number of material points per cell results  
<sup>16</sup> in cell crossing noise as the material points filling the cavity experience free-fall due to gravity.  
<sup>17</sup> The effect of cell-crossing noise can be seen in the oscillation of vertical kinetic energy for  
<sup>18</sup> fewer material points per cell. However, at high input energy, most of the input velocity is  
<sup>19</sup> dissipated during the spreading process. This means that only a small fraction of energy is  
<sup>20</sup> available in the vertical component resulting in almost similar behaviour for all cases. Four  
<sup>21</sup> material points per cell results in a higher peak vertical kinetic energy than other cases, unlike  
<sup>22</sup> low energy case, no oscillations were observed at high input energy.

<sup>23</sup> The effect of mesh size on the flow kinematics is studied by comparing two mesh sizes:  
<sup>24</sup> 0.01 m and 0.0125 m (see figure 4.42). It can be observed that the run-out distance converges  
<sup>25</sup> with increase in the number of material points per cell in both cases. Less than 1% difference  
<sup>26</sup> in the run-out distance was observed between a mesh size of 0.0125 m and 0.01 m. The final  
<sup>27</sup> run-out duration is almost unaffected by the increase in the number of material points per cell.

<sup>28</sup> This shows that the run-out distance is affected by the number of material points per cell.  
<sup>29</sup> However, the duration of the run-out is independent of the number of material points per cell.  
<sup>30</sup> The computation time increases with increase in material points per cell and for finer mesh.  
<sup>31</sup> However, the run-out distance converges with increase in number of material points per cell.  
<sup>32</sup> Hence, an optimum number of 25 material points per cell was adopted in this case. In summary,  
<sup>33</sup> for conducting a successful MPM analysis, a careful selection of the mesh size and the number  
<sup>34</sup> of particles is necessary.

## 4.3 Slopes subjected to impact loading

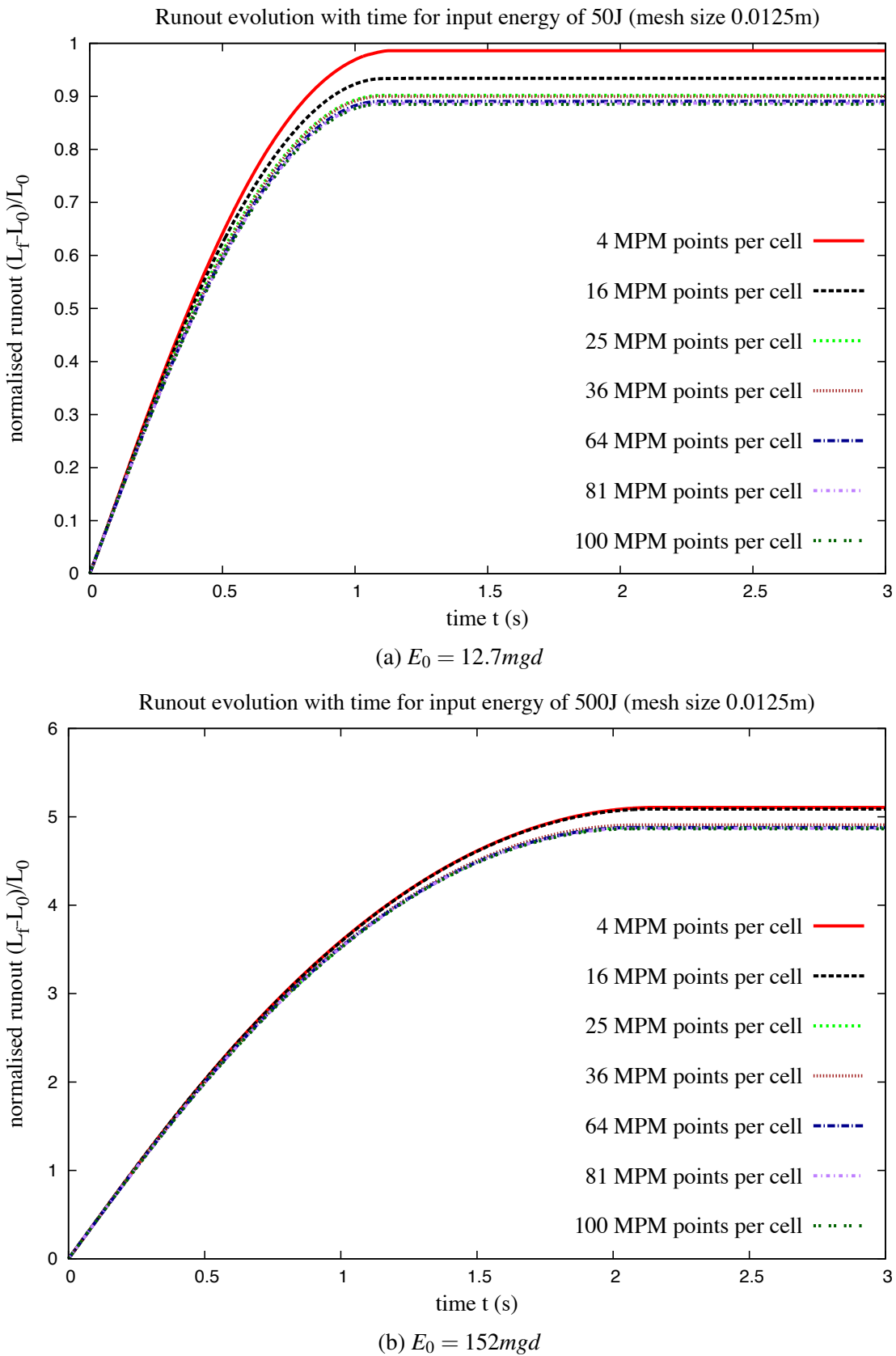


Figure 4.38 Evolution of run-out with time for varying material points per cell.

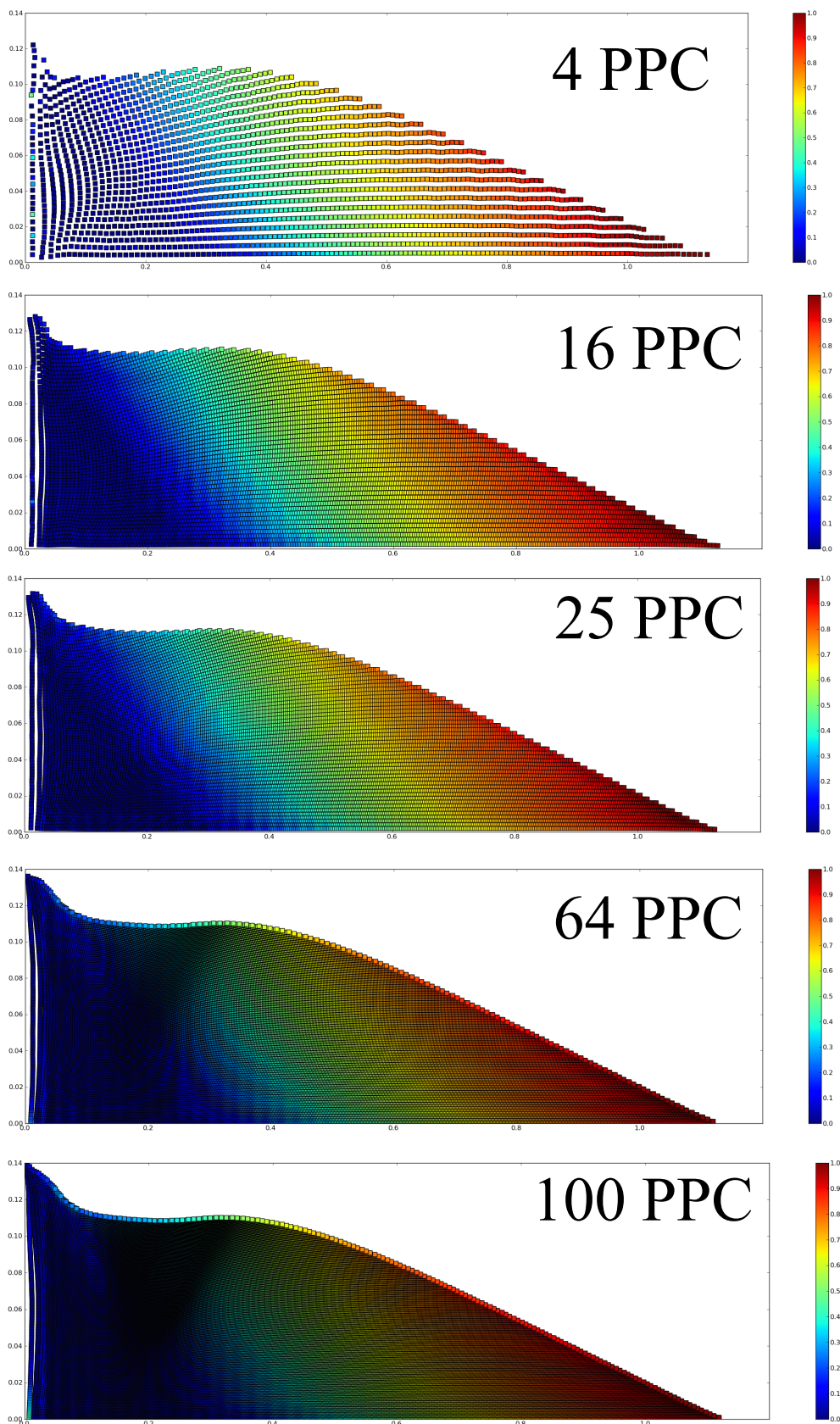


Figure 4.39 Effect of number of material points on cell on the run-out behaviour  $E_0 = 12.7mgd$ . Velocity profile (m/s) of granular pile subjected to gradient impact loading.

## 4.3 Slopes subjected to impact loading

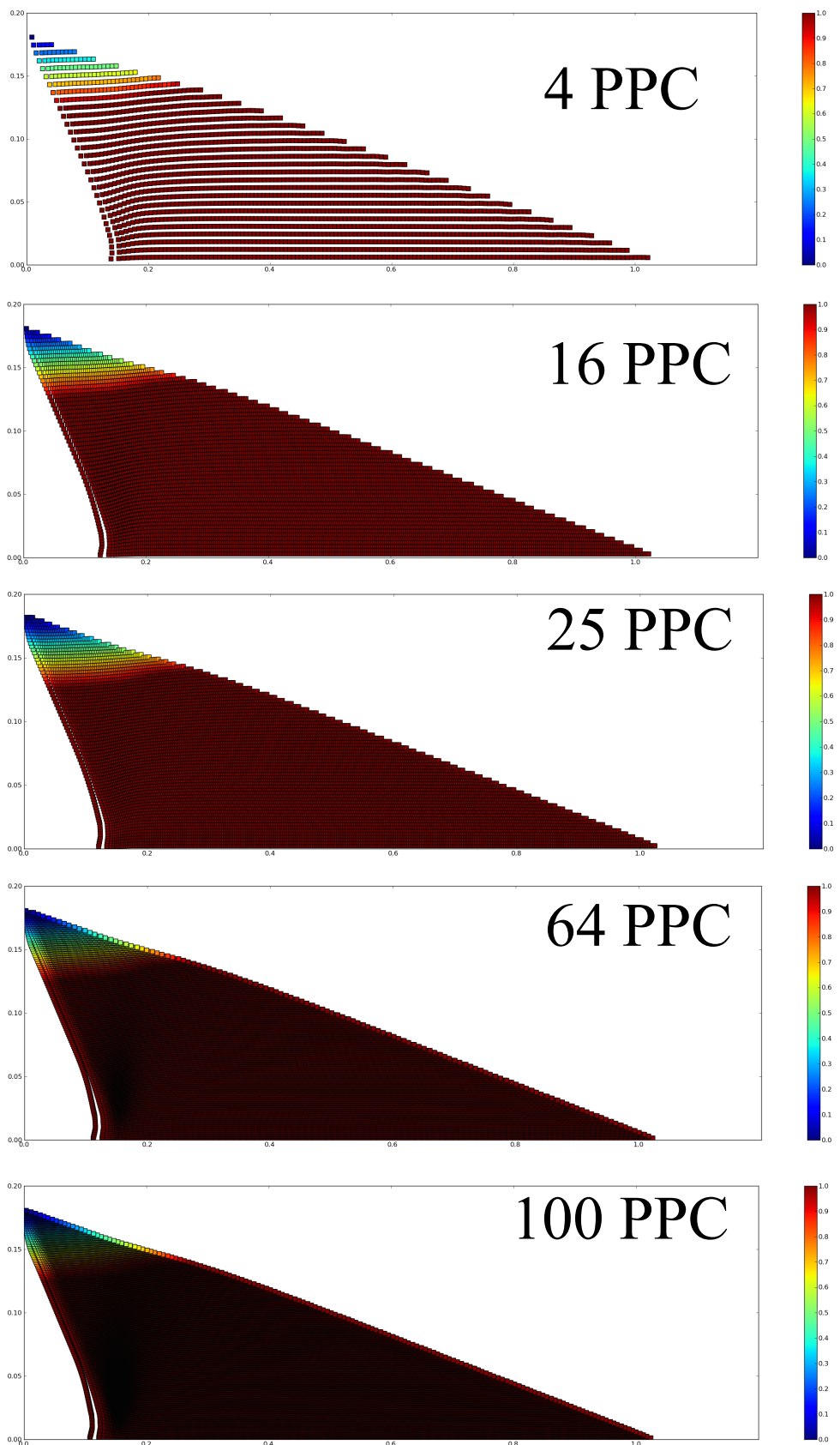


Figure 4.40 Effect of number of material points on cell on the run-out behaviour  $E_0 = 152mgd$ . Velocity profile (m/s) of granular pile subjected to gradient impact loading.

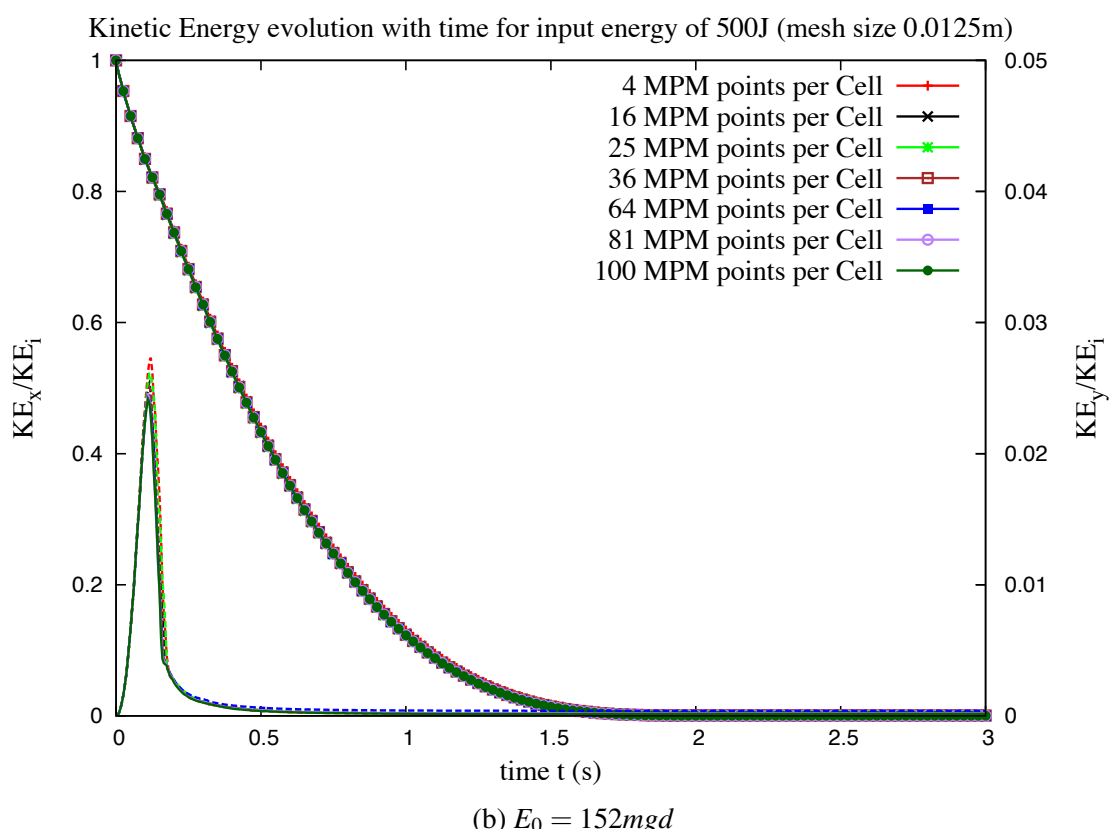
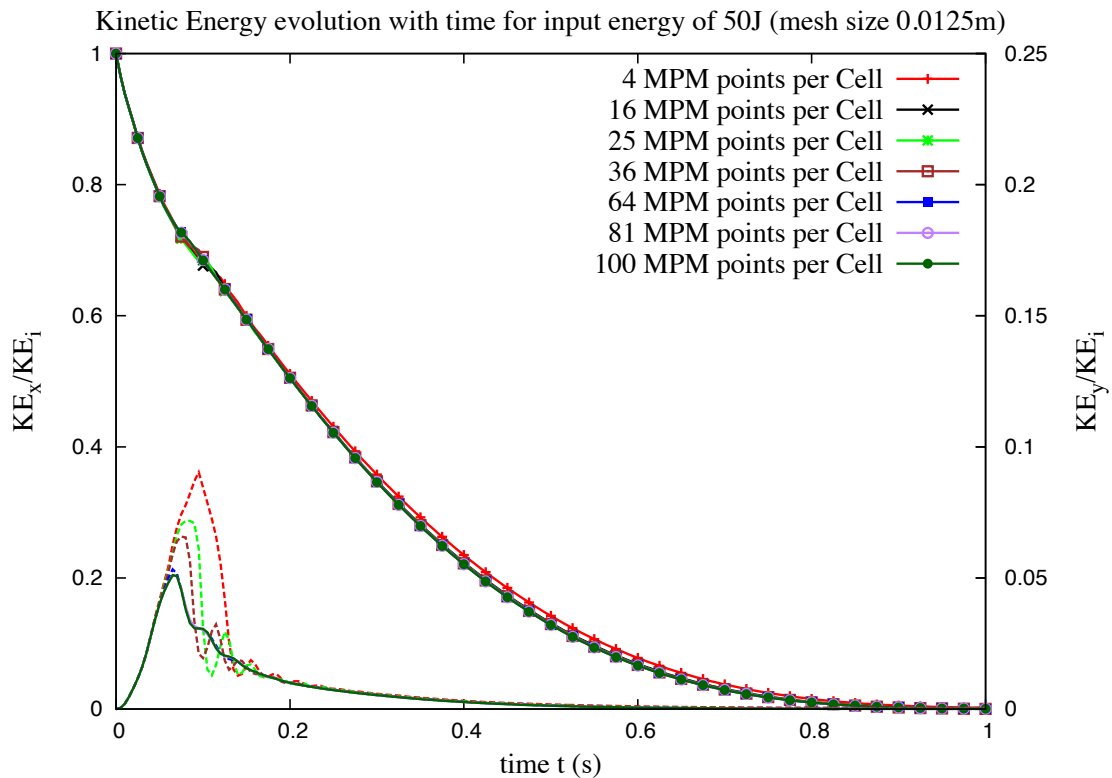


Figure 4.41 Evolution of kinetic with time for varying material points per cell

## 4.3 Slopes subjected to impact loading

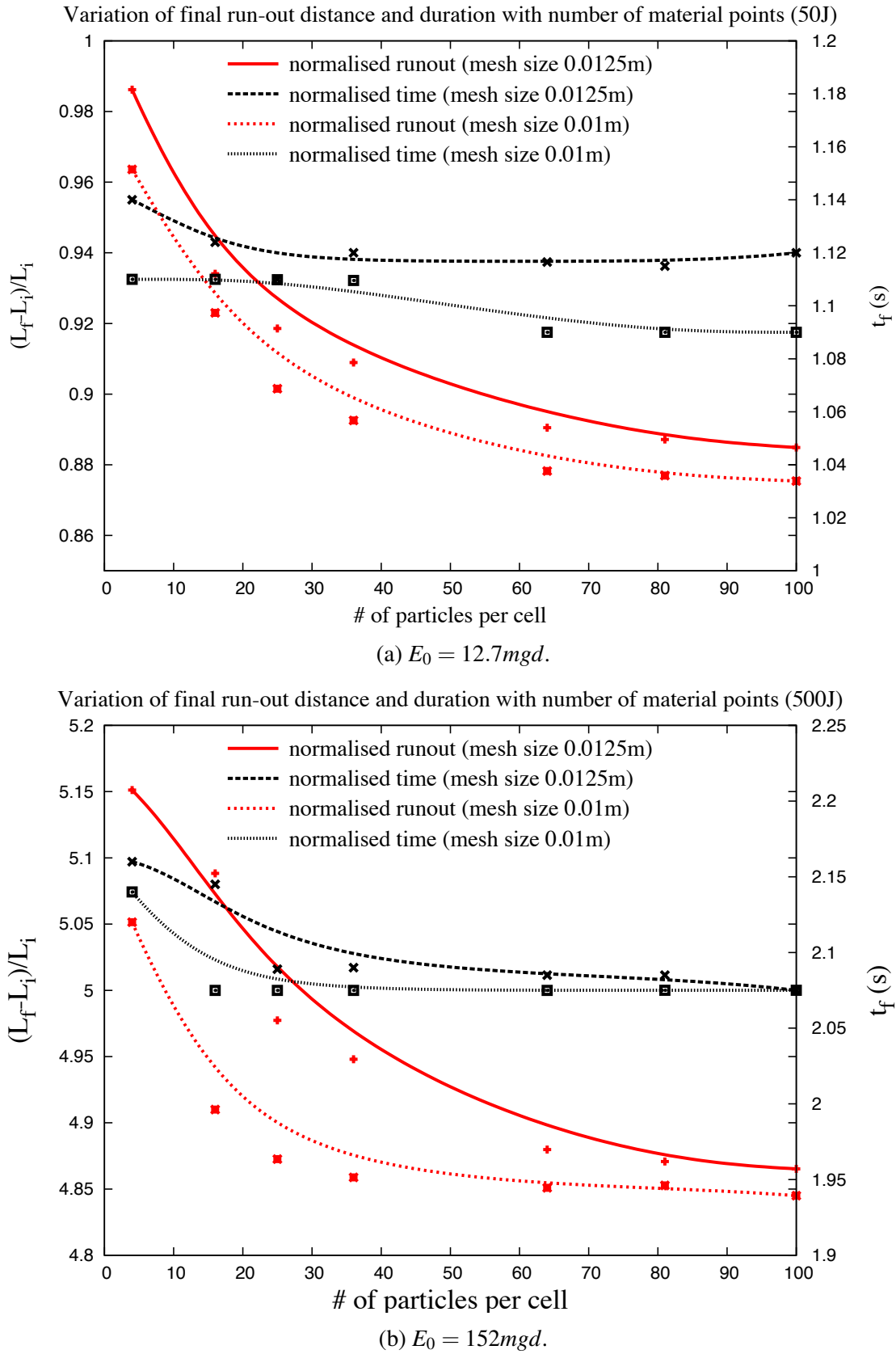


Figure 4.42 Evolution of run-out and duration of flow for varying material points per cell.

### **4.3.6 Comparison with granular column collapse**

Figure 4.43 shows the run-out behaviour of granular column collapse and the slope subjected to impact velocities as a function of normalise energy. In the case of column collapse, the peak energy at  $\tau_c$  is used as the energy available for the flow. It can be observed that MPM and DEM predict similar run-out behaviour for low energy regime (short columns), which undergo frictional failure along the flanks. However MPM predicts longer run-out for high energy regime (corresponding to a  $> 2.3$ ), where the granular column experiences significant collisional dissipation. The lack of a collisional energy dissipation mechanism in MPM results in over prediction of run-out distances. In the case of granular column subjected to impact velocity, the dissipation is friction and MPM is able to predict the run-out response in good agreement with DEM simulations. At very low energy, DEM simulations show longer run-out in the case of slope subjected to impact due to local destabilisation at the flow front.

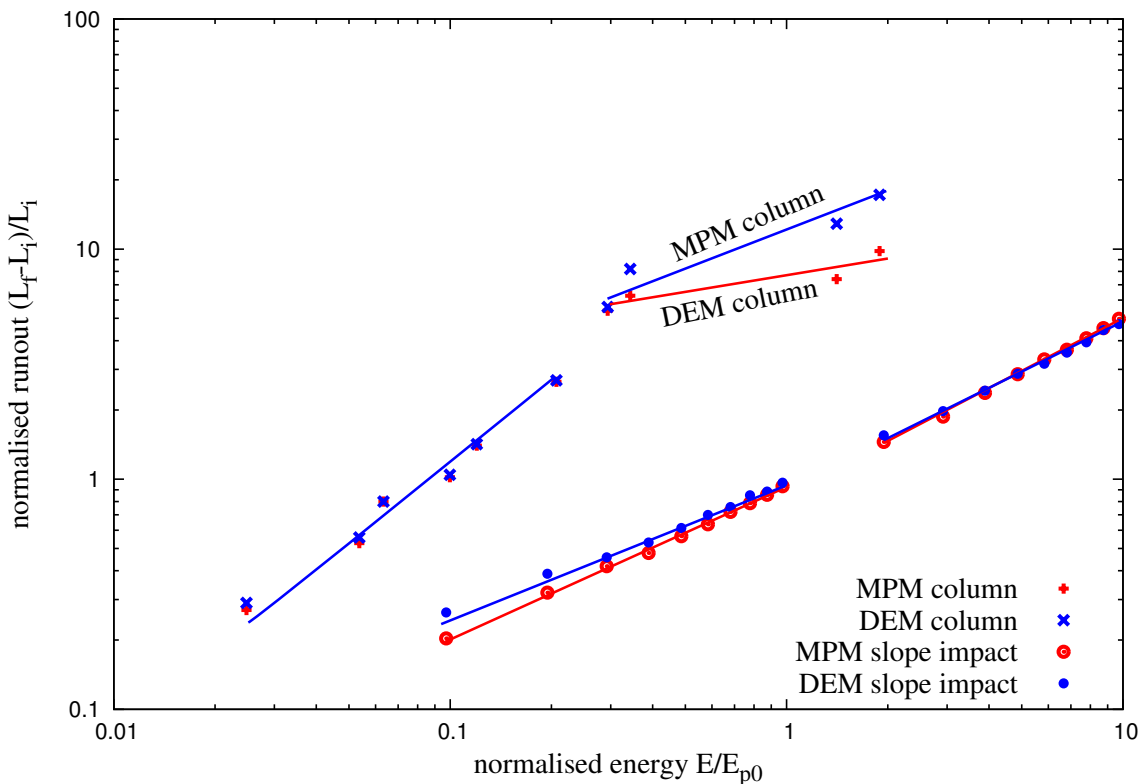


Figure 4.43 Comparison of column collapse with slope subjected to impact loading.

## 4.4 Summary

Multi-scale simulation of dry granular flows were performed to capture the local rheology, which causes complex flow dynamics, and to understand the capability of limitations of continuum models in capturing granular flow dynamics. MPM with a simple frictional dissipation model is able to capture the flow kinematics of dry granular flows. However, the lack of collisional dissipation in MPM is a limitation in capturing collapse of tall columns. Both DEM and MPM simulations show a power-law dependence of the run-out and time with the initial aspect ratio of the column. The initial configuration and material properties shows a significant influence on the run-out behaviour.

Natural granular flows are triggered by different mechanisms. The distribution of kinetic energy in the granular mass is found to have an effect on the flow kinematics. A multi-scale analyses of granular slope subjected to impact velocity reveals a power-law dependence of the run-out distance and time as a function of the input energy with non-trivial exponents. This reveals that the power-law behaviour is a generic feature of granular dynamics. The values of the exponents are not simple functions of the geometry.

We also observe two regimes with different values of the exponents: a low-energy regime and a high-energy regime. The low energy regime reflects mainly the destabilisation of the pile, with a run-out time independent of the input energy. Whereas, the second regime is governed by the spreading dynamics induced by higher input energy. The evolution of granular slope in the high-energy regime can be described by a characteristic decay time and the energy available at the end of the first stage, where the pile is destabilised. MPM is successfully able to simulate the transient evolution with a single input parameter, the macroscopic friction angle. This study exemplifies the ability of MPM, a continuum approach, in modelling complex granular flow dynamics and opens the possibility of realistic simulation of geological-scale flows on complex topographies.



# References

- Abe, K., Soga, K., and Bandara, S. (2013). Material Point Method for Coupled Hydromechanical Problems. *Journal of Geotechnical and Geoenvironmental Engineering*, page 04013033. 1  
2  
3  
4
- Balmforth, N. J. and Kerswell, R. R. (2005). Granular collapse in two dimensions. *Journal of Fluid Mechanics*, 538:399–428. 5  
6
- Bandara, S. (2013). *Material Point Method to simulate Large Deformation Problems in Fluid-saturated Granular Medium*. PhD thesis, University of Cambridge. 7  
8
- Bardenhagen, S. and Kober, E. (2004). The generalized interpolation material point method. *Computer Modeling in Engineering and Sciences*, 5(6):477–496. 9  
10
- Cambou, B., Jean, M., and Radjaï, F. (2009). *Micromechanics of granular materials*. Wiley-ISTE. 11  
12
- Coetzee, C. J., Vermeer, P. A., and Basson, A. H. (2005). The modelling of anchors using the material point method. *International Journal for Numerical and Analytical Methods in Geomechanics*, 29(9):879–895. 13  
14  
15
- Crosta, G. B., Imposimato, S., and Roddeman, D. (2009). Numerical modeling of 2-D granular step collapse on erodible and nonerodible surface. *J. Geophys. Res.*, 114(F3):F03020. 16  
17
- Da Cruz, F., Emam, S., Prochnow, M., Roux, J. N., and Chevoir, F. (2005). Rheophysics of dense granular materials: Discrete simulation of plane shear flows. *Physical Review E - Statistical, Nonlinear, and Soft Matter Physics*, 72(2):1–17. 18  
19  
20
- Daerr, A. and Douady, S. (1999). Two types of avalanche behaviour in granular media. *Nature*, 399(6733):241–243. 21  
22
- Estrada, N., Taboada, A., and Radjai, F. (2008). Shear strength and force transmission in granular media with rolling resistance. *Physical Review E*, 78(2):021301. 23  
24
- Girolami, L., Hergault, V., Vinay, G., and Wachs, A. (2012). A three-dimensional discrete-grain model for the simulation of dam-break rectangular collapses: comparison between numerical results and experiments. *Granular Matter*, pages 1–12. 25  
26  
27
- Guilkey, J., Harman, T., Xia, A., Kashiwa, B., and McMurtry, P. (2003). An Eulerian-Lagrangian approach for large deformation fluid structure interaction problems, Part 1: algorithm development. *Advances in Fluid Mechanics*, 36:143–156. 28  
29  
30
- Hogg, A. J. (2007). Two-dimensional granular slumps down slopes. *Physics of Fluids*, 19(9):9. 31

- <sup>1</sup> Iverson, R. M. (1997). The physics of debris flows. *Rev. Geophys.*, 35(3):245–296.
- <sup>2</sup> Jean, M. (1999). The non-smooth contact dynamics method. *Computer Methods in Applied Mechanics and Engineering*, 177(3-4):235–257.
- <sup>4</sup> Kerswell, R. (2005). Dam break with Coulomb friction: A model for granular slumping? *Physics of Fluids*, 17:057101.
- <sup>6</sup> Lacaze, L. and Kerswell, R. R. (2009). Axisymmetric Granular Collapse: A Transient 3D Flow Test of Viscoplasticity. *Physical Review Letters*, 102(10):108305.
- <sup>8</sup> Lajeunesse, E., Mangeney-Castelnau, A., and Villette, J. P. (2004). Spreading of a granular mass on a horizontal plane. *Physics of Fluids*, 16(7):2371.
- <sup>10</sup> Lajeunesse, E., Monnier, J. B., and Homsy, G. M. (2005). Granular slumping on a horizontal surface. *Physics of Fluids*, 17(10).
- <sup>12</sup> Larrieu, E., Staron, L., and Hinch, E. J. (2006). Raining into shallow water as a description of the collapse of a column of grains. *Journal of Fluid Mechanics*, 554:259–270.
- <sup>14</sup> Lo, C. Y., Bolton, M., and Cheng, Y. P. (2009). Discrete element simulation of granular column collapse. In *AIP Conf. Proc. Powders and Grains 2009*, volume 1145 of *6th International Conference on Micromechanics of Granular Media, Powders and Grains 2009*, pages 627–630.
- <sup>18</sup> Lube, G., Huppert, H. E., Sparks, R. S. J., and Freundt, A. (2005). Collapses of two-dimensional granular columns. *Physical Review E - Statistical, Nonlinear, and Soft Matter Physics*, 72(4):1–10.
- <sup>21</sup> Mitchell, J. K. and Soga, K. (2005). *Fundamentals of soil behavior*. John Wiley & Sons.
- <sup>22</sup> Moreau, J. J. (1993). New computation methods in granular dynamics. In Thornton, C., editor, *Powders and Grains*, page 227. A. A. Balkema.
- <sup>24</sup> Mutabaruka, P. (2013). *Modelisation numerique des milieux granulaires immergés : initiation et propagation des avalanches dans un fluide*. Phd thesis, University of Montpellier 2.
- <sup>26</sup> Radjai, F. and Dubois, F. (2011). *Discrete-element modeling of granular materials*. ISTE Wiley, London; Hoboken, N.J.
- <sup>28</sup> Radjai, F. and Richefeu, V. (2009). Contact dynamics as a nonsmooth discrete element method. *Mechanics of Materials*, 41(6):715–728.
- <sup>30</sup> Radjai, F., Schafer, J., Dipple, S., and Wolf, D. (1997). Collective Friction of an Array of Particles: A Crucial Test for Numerical Algorithms. *Journal de Physique I*, 7(9):1053–1070.
- <sup>32</sup> Rondon, L., Pouliquen, O., and Aussillous, P. (2011). Granular collapse in a fluid: Role of the initial volume fraction. *Physics of Fluids*, 23(7):073301–073301–7.
- <sup>34</sup> Rycroft, C. H., Orpe, A. V., and Kudrolli, A. (2009). Physical test of a particle simulation model in a sheared granular system. *Physical Review E*, 80(3):031305.

- Schaefer, D. G. (1990). Instability and ill-posedness in the deformation of granular materials. *International Journal for Numerical and Analytical Methods in Geomechanics*, 14(4):253–278. 1  
2  
3
- Staron, L. and Hinch, E. J. (2005). Study of the collapse of granular columns using two-dimensional discrete-grain simulation. *Journal of Fluid Mechanics*, 545:1–27. 4  
5
- Staron, L. and Hinch, E. J. (2007). The spreading of a granular mass: Role of grain properties and initial conditions. *Granular Matter*, 9(3-4):205–217. 6  
7
- Staron, L., Radjai, F., and Vilotte, J. P. (2005). Multi-scale analysis of the stress state in a granular slope in transition to failure. *The European physical journal. E, Soft matter*, 18(3):311–20. 8  
9  
10
- Staron, L., Radjai, F., and Vilotte, J.-P. (2006). Granular micro-structure and avalanche precursors. *Journal of Statistical Mechanics: Theory and Experiment*, 2006(07):P07014–P07014. 11  
12  
13
- Topin, V., Monerie, Y., Perales, F., and Radjai, F. (2012). Collapse Dynamics and Runout of Dense Granular Materials in a Fluid. *Physical Review Letters*, 109(18):188001. 14  
15
- Utili, S., Zhao, T., and Houlsby, G. (2014). 3D DEM investigation of granular column collapse: Evaluation of debris motion and its destructive power. *Engineering Geology*. 16  
17
- Warnett, J. M., Denissenko, P., Thomas, P. J., Kiraci, E., and Williams, M. A. (2013). Scalings of axisymmetric granular column collapse. *Granular Matter*, 16(1):115–124. 18  
19
- Zenit, R. (2005). Computer simulations of the collapse of a granular column. *Physics of Fluids*, 17(Compendex):031703–1–031703–4. 20  
21